CrossMark

Scaling K2. V. Statistical Validation of 60 New Exoplanets From K2 Campaigns 2–18

Jessie L. Christiansen[1], Sakhee Bhure[1], Jon K. Zink[2,44], Kevin K. Hardegree-Ullman[3], Britt Duffy Adkins[4], Christina Hedges[5,6], Timothy D. Morton[7], Allyson Bieryla[8], David R. Ciardi[1], William D. Cochran[9], Courtney D. Dressing[10], Mark E. Everett[11], Howard Isaacson[12,13], John H. Livingston[14], Carl Ziegler[15], Perry Berlind[16], Michael L. Calkins[16], Gilbert A. Esquerdo[16], David W. Latham[16], Michael Endl[17], Phillip J. MacQueen[17], Benjamin J. Fulton[18], Lea A. Hirsch[19], Andrew W. Howard[2], Lauren M. Weiss[20], Bridgette E. Allen[1,21], Arthur Berberyann[1,22], Krys N. Ciardi[1,23], Ava Dunlavy[1,24], Sofia H. Glassford[1,25], Fei Dai[26], Teruyuki Hirano[27,28,29], Motohide Tamura[14,30,31], Charles Beichman[18], Erica J. Gonzales[24,32], Joshua E. Schlieder[33], Thomas Barclay[34,35], Ian J. M. Crossfield[36], Emily A. Gilbert[37,38,39,40], Elisabeth C. Matthews[41], Steven Giacalone[42], and Erik A. Petigura[43]

[1] Caltech/IPAC-NASA Exoplanet Science Institute, Pasadena, CA 91125, USA; christia@ipac.caltech.edu
[2] Department of Astronomy, California Institute of Technology, Pasadena, CA 91125, USA
[3] Department of Astronomy, The University of Arizona, Tucson, AZ 85721, USA
[4] Sol Price School of Public Policy, University of Southern California, Los Angeles, CA 90089, USA
[5] Bay Area Environmental Research Institute, P.O. Box 25, Moffett Field, CA 94035, USA
[6] NASA Ames Research Center, Moffett Field, CA 94035, USA
[7] Department of Physics and Astronomy, University of Southern California, Los Angeles, CA 90089, USA
[8] Center for Astrophysics | Harvard & Smithsonian, 60 Garden Street, Cambridge, MA 02138, USA
[9] McDonald Observatory, The University of Texas, Austin, TX 78712, USA
[10] Department of Astronomy, University of California, Berkeley, CA 94720, USA
[11] NSF's Optical Infrared Astronomy Research Laboratory, 950 North Cherry Avenue Tucson, AZ 85719, USA
[12] Department of Astronomy, University of California Berkeley, Berkeley CA 94720, USA
[13] Centre for Astrophysics, University of Southern Queensland, Toowoomba, QLD, Australia
[14] Department of Astronomy, University of Tokyo, 7-3-1 Hongo, Bunkyo-ku, Tokyo 113-0033, Japan
[15] Department of Physics, Engineering and Astronomy, Stephen F. Austin State University, 1936 North Street, Nacogdoches, TX 75962, USA
[16] Center for Astrophysics | Harvard & Smithsonian, 60 Garden Street, Cambridge, MA 02138, USA
[17] McDonald Observatory, The University of Texas, Austin, TX 78712, USA
[18] Caltech/IPAC-NASA Exoplanet Science Institute, Pasadena, CA 91125, USA
[19] Kavli Center for Particle Astrophysics and Cosmology, Stanford University, Stanford, CA 94305, USA
[20] Department of Physics, University of Notre Dame, Notre Dame, IN 46556, USA
[21] University of Wisconsin-Stout, Menomonie, WI 54751, USA
[22] College of the Canyons, Santa Clarita, CA 91355, USA
[23] Rhode Island College, Providence, RI 02908, USA
[24] University of California, Santa Cruz, Santa Cruz CA 95065, USA
[25] University of California, Davis, Davis, CA 95616, USA
[26] Division of Geological and Planetary Sciences, 1200 E. California Boulevard, Pasadena, CA 91125, USA
[27] Astrobiology Center, 2-21-1 Osawa, Mitaka, Tokyo 181-8588, Japan
[28] National Astronomical Observatory of Japan, NINS, 2-21-1 Osawa, Mitaka, Tokyo 181-8588, Japan
[29] Department of Astronomical Science, School of Physical Sciences, The Graduate University for Advanced Studies (SOKENDAI), 2-21-1, Osawa, Mitaka, Tokyo, 181-8588, Japan
[30] Astrobiology Center, 2-21-1 Osawa, Mitaka-shi, Tokyo 181-8588, Japan
[31] National Astronomical Observatory, 2-21-1 Osawa, Mitaka-shi, Tokyo 181-8588, Japan
[32] Department of Physics, University of Notre Dame, 225 Nieuwland Science Hall, Notre Dame, IN 46556, USA
[33] Exoplanets and Stellar Astrophysics Laboratory, Code 667, NASA Goddard Space Flight Center, Greenbelt, MD 20771, USA
[34] University of Maryland, Baltimore County, 1000 Hilltop Circle, Baltimore, MD 21250, USA
[35] NASA Goddard Space Flight Center, 8800 Greenbelt Road, Greenbelt, MD 20771, USA
[36] Department of Physics and Astronomy, University of Kansas, Lawrence, KS 66045, USA
[37] Department of Astronomy and Astrophysics, University of Chicago, 5640 S. Ellis Avenue, Chicago, IL 60637, USA
[38] University of Maryland, Baltimore County, 1000 Hilltop Circle, Baltimore, MD 21250, USA
[39] The Adler Planetarium, 1300 South Lakeshore Drive, Chicago, IL 60605, USA
[40] NASA Goddard Space Flight Center, 8800 Greenbelt Road, Greenbelt, MD 20771, USA
[41] Observatoire de l'Université de Genève, Chemin des Maillettes 51, 1290 Versoix, Switzerland
[42] Department of Astronomy, University of California, Berkeley, CA 94720, USA
[43] Department of Physics and Astronomy, University of California, Los Angeles, CA 90095, USA

Abstract

The NASA K2 mission, salvaged from the hardware failures of the Kepler telescope, has continued Kepler's planet-hunting success. It has revealed nearly 500 transiting planets around the ecliptic plane, many of which are

---

[44] NASA Hubble Fellow.

the subject of further study, and over 1000 additional candidates. Here we present the results of an ongoing project to follow-up and statistically validate new K2 planets, in particular to identify promising new targets for further characterization. By analyzing the reconnaissance spectra, high-resolution imaging, centroid variations, and statistical likelihood of the signals of 91 candidates, we validate 60 new planets in 46 systems. These include a number of planets amenable to transmission spectroscopy (K2-384 f, K2-387 b, K2-390 b, K2-403 b, and K2-398 c), emission spectroscopy (K2-371 b, K2-370 b, and K2-399 b), and both (K2-405 b and K2-406 b); several systems with planets in or close to mean motion resonances (K2-381 and K2-398) including a compact, TRAPPIST-1-like system of five small planets orbiting a mid-M dwarf (K2-384); an ultra-short-period sub-Saturn in the hot Saturn desert (K2-399 b); and a super-Earth orbiting a moderately bright ($V = 11.93$), metal-poor ([Fe/H] $= -0.579 \pm 0.080$) host star (K2-408 b). In total we validate planets around four F stars, 26 G stars, 13 K stars, and three M dwarfs. In addition, we provide a list of 37 vetted planet candidates that should be prioritized for future follow-up observation in order to be confirmed or validated.

Unified Astronomy Thesaurus concepts: Exoplanet catalogs (488); Exoplanet systems (484)

1. Introduction

The NASA K2 mission operated from 2014 to 2018, observing 18 full campaigns along the ecliptic plane (Howell et al. 2014). During each campaign, of 51–89 days, the 1 m telescope acquired images every 30 minutes on between 10,000 and 30,000 stars brighter than $V \sim 16$. From these observations, nearly 500 transiting planets have been either confirmed or statistically validated, and an additional ~1000 candidates await confirmation.[45] While the NASA Kepler mission, which stared at one carefully chosen field of view for four years, produced a largely homogeneous data set designed for occurrence-rate studies, the K2 fields and targets were much more heterogeneous. The K2 campaigns spanned a range of Galactic latitudes ($-65°$ to $+65°$) and longitudes ($0°$ to $360°$), wildly varying the likelihood for contamination of the target star flux by background stars in a given pixel. The properties of the target stars themselves were not well constrained, being based in large part on photometric colors (Huber et al. 2016); some populations, such as cool stars, were subsequently characterized at higher fidelity (Dressing et al. 2017, 2019). In addition, the final target lists for each campaign were compiled from lists provided by guest observers, with stellar populations that varied systematically from campaign to campaign as projects with different scientific aims were developed or completed. Finally, unlike Kepler, there was no single, standard data-processing pipeline that was producing time series and signal detections that could be characterized for statistical studies.

The Scaling K2 project has had as its primary goal the production of a catalog of K2 planet candidates that were uniformly detected and characterized, with stellar and planet parameters that were calculated to reduce the impacts of systematic biases in the data, and using a pipeline for which we could measure the detection efficiency (completeness) and reliability. In Paper I (Hardegree-Ullman et al. 2020), we published our uniformly derived catalog of stellar parameters for the K2 targets, using the subset of targets with both photometric colors and spectroscopic parameters as a training set for a machine-learning algorithm to classify the much larger number of targets with only photometric colors. In Paper II (Zink et al. 2020a), we presented a pilot study of K2 Campaign 5, where we described our fully automated pipeline and released the first publicly available K2 transit candidate vetting code, EDI-Vetter. In Paper III (Zink et al. 2020b), we found

comparable occurrence rates from K2 Campaign 5 and Kepler in the same parameter space, validating the pipeline and vetting algorithms. Finally, in Paper IV (Zink et al. 2021), we presented our full, uniform K2 planet candidate catalog from Campaigns 1–8 and 10–18 (Campaign 9 being a specialized microlensing campaign that was unsuitable for our transit search). Here, we validate a significant number of planet candidates from those works and other previously published K2 planet candidate catalogs. In Section 2 we describe the validation process, including the follow-up observations that were acquired, and the vespa and centroid analyses. In Section 3 we discuss the newly validated planets, and highlight some of the more interesting new planetary systems. Finally, in Section 4 we briefly discuss the candidates that did not pass our validation thresholds, and highlight additional candidates that passed visual inspection but require additional follow-up observations to validate.

2. Candidate Validation

The planet candidate catalog presented in Paper IV contained 747 transit signals that were classified by the EDI-Vetter vetting algorithm as planet candidates, 366 of which were newly reported. In this work, we acquire and analyze additional observations and attempt to statistically validate as bona fide planets those planet candidates that had passed our EDI-Vetter vetting thresholds. Removing the 273 known planets, we visually inspected the phase-folded, detrended light curves produced in Paper IV for each of the 474 candidates to identify the most promising candidates for additional follow-up. Light curves that showed signals which appeared by eye to be caused by stellar variability, eclipsing binaries, or instrumental systematics, as compared to planet candidates, were discarded (and are noted as "FP" in that catalog). For each of the 329 remaining candidates, we retrieved the following information: (i) the renormalized unit weight error (RUWE) score from Gaia EDR3, to flag potential binary stars (Gaia Collaboration et al. 2021); (ii) the status on the NASA Exoplanet Archive, to determine whether it was a new candidate, whether it had been previously deemed a false positive by another publication, or whether there were additional published candidates in the same system that our pipeline had missed; and (iii) the follow-up observations and observing notes that had been uploaded to ExoFOP,[46] if any, to determine whether it had already been deemed a false positive, and, if not, to assess whether any additional follow-up data were needed. In a number of cases we

---

obtained additional follow-up observations to complement the data that had already been archived.

In order to consider whether a given candidate was ready to be validated, we required a single-lined reconnaissance spectrum, to mitigate the presence of spectroscopic binaries, and no evidence of additional stars in the high-resolution image, to constrain the presence of bound companions or chance alignments of the target star with more distant background stars. We note that while in many cases the indication of additional stars in the spectroscopy, high-resolution imaging, or RUWE value may not actually disprove the existence of a planet, disentangling the true source of the transiting signal in these cases and deriving accurate stellar and planet parameters is beyond the scope of this work. We leave these as planet candidates for now, noting the presence of companions where observed, and highlighting them as interesting future cases to solve. We gathered the required observations to test validation of 91 planet candidates around 78 stars; we list these stars and their properties in Table 1. The stellar parameters are drawn from Paper I, to provide a uniform source of stellar (and planetary) parameters in this work; however we note that the planet candidate catalog presented in Paper IV is designed to be agnostic to the stellar parameters, and to allow users to update the parameters to their desired values at will. The planet parameters are fit as in Paper IV, using the `batman` and `emcee` Python packages (Goodman & Weare 2010; Foreman-Mackey et al. 2013; Kreidberg 2015) and assuming circular orbits to measure the posterior distributions of the orbital period, transit midpoint, the planet-to-star radius ratio, the transit impact parameter, and the semimajor axis to stellar radius ratio. As described in Paper IV, quadratic limb-darkening parameters are fixed to values derived using the ATLAS model coefficients for the Kepler bandpasses (Claret & Bloemen 2011), in concert with the Paper I stellar parameters.

2.1. Follow-up Observations

2.1.1. Hale/PHARO and Keck/NIRC2

High-resolution adaptive optics (AO) imaging were obtained with the PHARO instrument (Hayward et al. 2001) on the Palomar 200 inch Hale telescope, and the NIRC2 instrument on the Keck II telescope. The PHARO observations were obtained using the P3K natural guide star AO system (Dekany et al. 2013) in standard five-point quincunx dither patterns. The dither positions were each observed three times and offset in position from each other by $0\rlap{.}{''}500$ for a total of 15 frames. The NIRC2 observations were obtained using the natural guide star AO system (Wizinowich et al. 2000) in the standard three-point dither pattern that is used to avoid the noisier left lower quadrant of the detector. The dither pattern was repeated twice, with each dither offset from the previous dither by $0\rlap{.}{''}500$. Schlieder et al. (2021) presents additional details on the NIRC2 follow-up observing program. Both the PHARO and NIRC2 observations were typically obtained in the narrowband $Br - \gamma$ filter ($\lambda_o = 2.1686$; $\Delta\lambda = 0.0326 \,\mu$m).

The PHARO and NIRC2 data were processed and analyzed with a custom set of IDL tools. Flat fields were produced using a median average of dark subtracted sky frames. Sky frames were generated from the median average of the dithered science frames; each science image was then sky-subtracted and flat-fielded. The reduced science frames were combined into a single combined image using an intrapixel interpolation that conserves flux, shifts the individual dithered frames by the appropriate fractional pixels, and median-coadds the frames.

2.1.2. Gemini/DSSI and WIYN/NESSI

Speckle imaging observations were obtained using the instruments DSSI (Horch et al. 2012) at the Gemini South 8 m telescope on Cerro Pachon and NESSI (Scott et al. 2018) at the WIYN 3.5 m telescope on Kitt Peak. Both instruments collimate the incoming beam from the telescope, split it into red and blue channels with a dichroic beamsplitter and pass the beams through a relatively narrowband filter before focusing each on a separate Andor Ixon EMCCD camera. Data were taken in time series composed of 1000 frames apiece with individual exposure times of 40 ms for WIYN/NESSI and 60 ms for Gemini/DSSI. The images themselves were subarray readouts of 256×256 pixels, corresponding to a $4\rlap{.}{''}6 \times 4\rlap{.}{''}6$ field of view ($0\rlap{.}{''}018$/pixel) for NESSI and a $2\rlap{.}{''}8 \times 2\rlap{.}{''}8$ field of view ($0\rlap{.}{''}011$/pixel) for DSSI. The number of 1000 frame image sets taken per star depended on target brightness and observing conditions, but 3–10 image sets were typically obtained for our science targets. The observing strategy was very similar with both instruments. Science targets were observed close in time, with nearby bright stars selected to represent point sources. The data were reduced following the procedures described in Howell et al. (2011).

2.1.3. Southern Astrophysical Research

We searched for close stellar companions to EPIC 211830293 with speckle imaging on the 4.1 m Southern Astrophysical Research (SOAR) telescope (Tokovinin 2018) on 2019 March 18 UT, observing in the visible Cousins *I* band. The observations were each sensitive to an approximately 5 mag fainter star at an angular distance of $1''$ from the targets, and the target was cleared of bright companions at angular separations within $\sim 3''$.

2.1.4. Keck/HIRES

We collected high-resolution spectra with Keck/HIRES on Maunakea from 2014 December to 2017 September. Those spectra collected for reconnaissance purposes have a resolution of 60,000, a typical signal-to-noise ratio (S/N) of 40/pixel at 550 nm, and a median seeing on Keck/HIRES of $1\rlap{.}{''}0$. Those stars fainter than $V \sim 10$ were observed with the C2 decker ($0\rlap{.}{''}87 \times 14\rlap{.}{''}0$), allowing for efficient removal of night-sky emission lines. The spectra were reduced with the standard pipeline of the California Planet Search (Howard et al. 2010).

2.1.5. Fred Lawrence Whipple Observatory/Tillinghast Reflector Echelle Spectrograph

The Tillinghast Reflector Echelle Spectrograph (TRES) is mounted on the 1.5 m telescope at the Fred Lawrence Whipple Observatory (FLWO) in Arizona, USA. TRES is a fiber-fed, optical spectrograph with a $R \sim 44,000$. The TRES spectra were extracted as described in Buchhave et al. (2010) and were visually inspected to determine that the spectra are single-lined.

2.1.6. McDonald/TS23

The McDonald Observatory reconnaissance spectra were obtained with the Tull Coude Spectrometer (Tull et al. 1995) of the McDonald Observatory 2.7 m Harlan J. Smith Telescope.

Table 1
Stellar Parameters of the Candidate Systems as Derived in Paper I

EPIC ID	$T_{\rm eff}$ (K)	R_s ($R_\odot$)	M_s ($M_\odot$)	log g (dex)	[Fe/H] (dex)	V (mag)	K (mag)	RUWE	Spectrum	Imaging
204750116	5561 ± 138	$1.051^{+0.065}_{-0.061}$	$0.823^{+0.369}_{-0.25}$	4.313 ± 0.15	-0.021 ± 0.235	11.37	9.62	1.10	TRES	NIRC2
205029914	5755 ± 138	$1.126^{+0.071}_{-0.065}$	$0.835^{+0.376}_{-0.253}$	4.257 ± 0.151	-0.312 ± 0.198	12.29	9.71	1.07	TRES[b]	NIRC2[a]
205111664	5601 ± 138	$0.94^{+0.065}_{-0.058}$	$0.825^{+0.366}_{-0.255}$	4.406 ± 0.15	-0.216 ± 0.235	12.49	9.88	1.10	TRES	NIRC2
205944181	5266 ± 138	$0.852^{+0.057}_{-0.052}$	$0.985^{+0.436}_{-0.306}$	4.568 ± 0.15	0.119 ± 0.235	12.60	10.65	0.94	TRES, HIRES	NIRC2, NESSI
205957328	5300 ± 138	$0.797^{+0.051}_{-0.05}$	$0.981^{+0.438}_{-0.299}$	4.63 ± 0.15	0.053 ± 0.235	12.65	10.64	0.92	TRES	NIRC2
205999468	5016 ± 138	$0.754^{+0.052}_{-0.047}$	$0.93^{+0.415}_{-0.29}$	4.65 ± 0.15	-0.046 ± 0.235	12.93	11.01	1.05	TRES, HIRES	PHARO
206055981	4348 ± 128	$0.625^{+0.041}_{-0.046}$	$0.756^{+0.231}_{-0.347}$	4.726 ± 0.150	-0.351 ± 0.235	13.80	10.96	0.97	HIRES, SpeX	NESSI
206135682	4663 ± 138	$0.663^{+0.047}_{-0.045}$	$0.746^{+0.334}_{-0.232}$	4.667 ± 0.15	-0.25 ± 0.235	13.54	11.04	1.01	TSpec	PHARO
206146957	5682 ± 138	$0.881^{+0.054}_{-0.049}$	$0.735^{+0.334}_{-0.224}$	4.418 ± 0.15	-0.234 ± 0.235	11.79	9.93	0.90	TRES	PHARO
206192335	5433 ± 138	$0.787^{+0.051}_{-0.046}$	$0.794^{+0.346}_{-0.248}$	4.542 ± 0.15	-0.201 ± 0.235	12.31	10.25	0.80	TRES, HIRES	NIRC2[a], NIRI[a], PHARO[a]
206317286	4752 ± 138	$0.758^{+0.052}_{-0.057}$	$0.832^{+0.253}_{-0.367}$	4.596 ± 0.15	0.019 ± 0.235	14.05	11.63	0.97	SpeX	NIRC2
211399359	4925 ± 138	$0.736^{+0.052}_{-0.049}$	$0.958^{+0.44}_{-0.298}$	4.683 ± 0.15	-0.107 ± 0.235	14.64	12.39	1.03	HIRES	NIRI, NIRC2
211428897	3780 ± 93	$0.408^{+0.012}_{-0.012}$	$0.405^{+0.009}_{-0.009}$	4.824 ± 0.027	-0.088 ± 0.170	14.09	9.62	1.07	SpeX, TSpec, TS23	NESSI, NIRC2, DSSI
211490999	5479 ± 27	$0.922^{+0.018}_{-0.018}$	$0.847^{+0.101}_{-0.088}$	4.437 ± 0.045	-0.064 ± 0.025	13.60	11.87	1.06	HIRES, TS23	NESSI, NIRI
211539054	6138 ± 138	$1.486^{+0.083}_{-0.079}$	$1.158^{+0.499}_{-0.349}$	4.156 ± 0.15	0.049 ± 0.235	10.47	9.16	0.90	TRES	PHARO
211711685	5509 ± 21	$0.919^{+0.016}_{-0.015}$	$0.802^{+0.073}_{-0.068}$	4.414 ± 0.035	0.044 ± 0.02	12.55	10.84	0.94	TRES	NIRC2
211965883	4128 ± 138	$0.646^{+0.05}_{-0.043}$	$0.725^{+0.326}_{-0.224}$	4.678 ± 0.15	-0.229 ± 0.235	14.63	11.36	1.08	TSpec	NESSI
212006318	5822 ± 138	$1.543^{+0.104}_{-0.095}$	$1.119^{+0.492}_{-0.344}$	4.107 ± 0.15	-0.091 ± 0.235	13.04	11.56	1.04	TRES	PHARO, NESSI
212351868	6051 ± 138	$2.481^{+0.145}_{-0.135}$	$1.936^{+0.856}_{-0.596}$	3.934 ± 0.15	-0.038 ± 0.235	9.99	8.72	0.96	HIRES[c]	NIRC2, NESSI
212530118	4200 ± 138	$0.691^{+0.053}_{-0.049}$	$0.821^{+0.371}_{-0.258}$	4.673 ± 0.15	-0.008 ± 0.235	14.05	10.99	0.98	SpeX	NESSI
212575828	4823 ± 138	$0.732^{+0.058}_{-0.052}$	$0.923^{+0.425}_{-0.291}$	4.674 ± 0.15	-0.206 ± 0.235	15.79	13.39	1.05	TSpec	DSSI
212585579	5896 ± 138	$1.086^{+0.065}_{-0.063}$	$0.811^{+0.356}_{-0.252}$	4.276 ± 0.15	-0.163 ± 0.235	12.81	11.29	1.15	TRES	NESSI, DSSI
212730483	4409 ± 138	$0.71^{+0.053}_{-0.048}$	$0.807^{+0.366}_{-0.256}$	4.642 ± 0.15	-0.088 ± 0.235	13.45	10.71	0.92	SpeX	NESSI
212797028	5980 ± 138	$1.869^{+0.115}_{-0.107}$	$1.209^{+0.537}_{-0.373}$	3.978 ± 0.15	0.009 ± 0.235	13.28	11.54	0.87	HIRES	NIRC2, DSSI, NESSI
213817056	5051 ± 138	$0.831^{+0.058}_{-0.054}$	$0.991^{+0.457}_{-0.309}$	4.595 ± 0.151	-0.324 ± 0.198	13.17	10.46	1.20	TRES	NIRC2
214173069	4603 ± 138	$0.751^{+0.056}_{-0.052}$	$0.856^{+0.375}_{-0.265}$	4.615 ± 0.15	-0.045 ± 0.235	13.21	10.51	0.81	TRES	DSSI
214419545	5911 ± 138	$1.32^{+0.078}_{-0.072}$	$0.993^{+0.416}_{-0.302}$	4.194 ± 0.15	-0.049 ± 0.235	11.65	9.68	0.72	TRES	NIRC2
216892056	3705 ± 138	$0.471^{+0.014}_{-0.014}$	$0.472^{+0.011}_{-0.011}$	4.767 ± 0.027	0.016 ± 0.235	13.50	9.13	1.20	TRES	NIRI, DSSI
217192839	4473 ± 138	$0.675^{+0.052}_{-0.047}$	$0.754^{+0.337}_{-0.239}$	4.653 ± 0.15	-0.244 ± 0.235	13.01	10.30	1.02	TRES, HIRES	NIRI, DSSI
217977895	5452 ± 138	$0.811^{+0.053}_{-0.047}$	$0.922^{+0.401}_{-0.284}$	4.585 ± 0.15	-0.027 ± 0.235	12.98	11.05	0.95	TRES	DSSI
218668602	5129 ± 138	$0.804^{+0.055}_{-0.051}$	$1.061^{+0.459}_{-0.327}$	4.655 ± 0.15	0.187 ± 0.235	12.68	10.46	0.93	TRES	NIRC2
220221272	3623 ± 138	$0.348^{+0.011}_{-0.01}$	$0.33^{+0.009}_{-0.009}$	4.874 ± 0.028	0.068 ± 0.198	14.26[a]	11.29	1.31	SpeX	NESSI
220294712	6145 ± 43	$1.206^{+0.034}_{-0.033}$	$1.024^{+0.194}_{-0.163}$	4.286 ± 0.07	-0.116 ± 0.04	12.34	10.97	1.00	HIRES, TS23, TRES	NIRC2, PHARO[a], DSSI, NESSI
220400100	4648 ± 138	$0.728^{+0.055}_{-0.048}$	$0.832^{+0.374}_{-0.258}$	4.632 ± 0.15	-0.014 ± 0.235	13.60	11.25	1.00	TS23	NESSI
220459477	4844 ± 138	$0.761^{+0.057}_{-0.052}$	$0.927^{+0.412}_{-0.286}$	4.64 ± 0.15	-0.224 ± 0.235	14.65	12.24	0.96	TSpec	NESSI
220510874	5749 ± 22	$0.97^{+0.023}_{-0.022}$	$0.911^{+0.088}_{-0.083}$	4.424 ± 0.036	0.074 ± 0.02	13.17	11.53	0.90	TS23	NESSI
220571481	6017 ± 138	$1.139^{+0.068}_{-0.063}$	$0.888^{+0.382}_{-0.271}$	4.272 ± 0.15	-0.077 ± 0.235	13.24	11.66	0.95	TS23	NESSI
220696233	3572 ± 138	$0.585^{+0.018}_{-0.018}$	$0.57^{+0.051}_{-0.048}$	4.66 ± 0.046	0.126 ± 0.235	16.22	12.29	1.08	SpeX	PHARO, NESSI
226042826	5140 ± 138	$0.976^{+0.067}_{-0.062}$	$1.478^{+0.655}_{-0.462}$	4.625 ± 0.151	0.035 ± 0.198	11.79	9.75	0.98	TRES	DSSI
245943455	5367 ± 138	$0.897^{+0.058}_{-0.053}$	$0.842^{+0.376}_{-0.259}$	4.456 ± 0.15	0.124 ± 0.235	12.82	10.93	1.09	HIRES, TRES	NIRI, PHARO, NESSI
245955351	5436 ± 138	$0.812^{+0.051}_{-0.049}$	$0.918^{+0.406}_{-0.275}$	4.585 ± 0.15	-0.061 ± 0.235	13.19	11.34	0.97	HIRES, TRES	NIRI[a], PHARO[a], NESSI
245991048	5782 ± 138	$1.084^{+0.067}_{-0.061}$	$0.802^{+0.357}_{-0.246}$	4.273 ± 0.15	-0.034 ± 0.235	12.30	10.18	1.06	HIRES, TRES	NESSI, PHARO, NIRI
245995977	5558 ± 138	$0.966^{+0.059}_{-0.056}$	$0.789^{+0.351}_{-0.239}$	4.368 ± 0.15	-0.116 ± 0.235	13.57	11.72	0.95	HIRES	NIRI, PHARO
246074314	5543 ± 138	$0.566^{+0.112}_{-0.076}$	$0.757^{+0.341}_{-0.24}$	4.973 ± 0.15	-0.543 ± 0.278	12.36[a]	10.71	0.97	TRES	NESSI
246084398	5726 ± 138	$1.058^{+0.07}_{-0.065}$	$0.841^{+0.37}_{-0.258}$	4.314 ± 0.15	-0.238 ± 0.235	12.82	11.24	1.19	TRES	NESSI
246429049	5678 ± 138	$1.071^{+0.065}_{-0.06}$	$0.881^{+0.381}_{-0.269}$	4.321 ± 0.15	0.076 ± 0.235	11.84	10.28	1.04	TRES	NESSI

Table 1
(Continued)

EPIC ID	$T_{\rm eff}$ (K)	R_s ($R_\odot$)	M_s ($M_\odot$)	log$g$ (dex)	[Fe/H] (dex)	V (mag)	K (mag)	RUWE	Spectrum	Imaging
210797580	5377 ± 138	$0.971^{+0.065}_{-0.057}$	$0.984^{+0.428}_{-0.303}$	4.454 ± 0.15	0.018 ± 0.235	11.11	9.24	0.99	HIRES, TRES	NESSI, NIRC2
246876040	4938 ± 138	$0.631^{+0.044}_{-0.04}$	$0.478^{+0.214}_{-0.147}$	4.515 ± 0.15	-0.388 ± 0.235	12.72	9.57	1.11	TRES	NESSI
246891819	5007 ± 138	$0.783^{+0.054}_{-0.051}$	$0.952^{+0.421}_{-0.293}$	4.628 ± 0.15	-0.033 ± 0.235	14.66	11.37	1.07	TSpec, HIRES	NIRC2
246947582	4692 ± 138	$1.14^{+0.086}_{-0.079}$	$1.232^{+0.548}_{-0.386}$	4.413 ± 0.15	0.037 ± 0.235	15.79	11.22	1.08	TSpec	NIRC2[a]
246953392	5236 ± 138	$0.92^{+0.062}_{-0.057}$	$0.954^{+0.429}_{-0.293}$	4.488 ± 0.15	0.237 ± 0.235	13.24	10.81	0.91	TRES	NESSI
247164043	6265 ± 138	$1.272^{+0.067}_{-0.066}$	$0.988^{+0.419}_{-0.293}$	4.223 ± 0.15	-0.088 ± 0.235	9.48	8.23	1.06	TRES	NIRC2
247383003	5387 ± 138	$0.966^{+0.06}_{-0.057}$	$0.937^{+0.406}_{-0.285}$	4.435 ± 0.15	0.11 ± 0.235	11.83	9.95	1.29	TRES	NIRC2, NESSI
247698108	4993 ± 138	$4.259^{+0.338}_{-0.314}$	$1.249^{+0.585}_{-0.385}$	3.279 ± 0.15	-0.325 ± 0.235	14.68	10.78	0.97	HIRES	NIRC2
247724061	5496 ± 154	$1.289^{+0.093}_{-0.085}$	$1.041^{+0.468}_{-0.322}$	4.235 ± 0.151	-0.1 ± 0.275	12.03	10.45	1.21	TRES	NESSI
248222323	5895 ± 138	$1.427^{+0.085}_{-0.079}$	$1.128^{+0.5}_{-0.347}$	4.184 ± 0.15	0.085 ± 0.235	12.41	9.47	1.19	TRES	NIRC2
248463350	5946 ± 20	$1.239^{+0.032}_{-0.03}$	$0.945^{+0.09}_{-0.083}$	4.227 ± 0.034	-0.257 ± 0.019	13.15	11.72	1.19	HIRES, TRES	NIRC2, NESSI
248472140	5690 ± 38	$1.541^{+0.048}_{-0.047}$	$0.783^{+0.131}_{-0.114}$	3.956 ± 0.063	0.252 ± 0.036	13.03	11.38	5.89	TRES, HIRES	NIRC2, NESSI
248518307	3578 ± 138	$0.382^{+0.012}_{-0.012}$	$0.374^{+0.009}_{-0.009}$	4.847 ± 0.028	-0.051 ± 0.235	15.12	10.41	1.05	TSpec	NESSI
248527514	4213 ± 138	$0.675^{+0.051}_{-0.046}$	$0.87^{+0.395}_{-0.269}$	4.719 ± 0.15	-0.098 ± 0.235	14.20	11.11	1.09	TSpec	NESSI
248621597	5716 ± 138	$1.28^{+0.089}_{-0.082}$	$0.944^{+0.419}_{-0.29}$	4.197 ± 0.15	-0.378 ± 0.235	13.03	11.38	0.96	TRES	NESSI
248639411	4626 ± 49	$0.799^{+0.024}_{-0.023}$	$0.87^{+0.186}_{-0.15}$	4.573 ± 0.08	0.072 ± 0.047	13.51	11.01	1.05	HIRES, TSpec	NIRC2, NESSI
248740016	5872 ± 138	$1.025^{+0.059}_{-0.058}$	$0.863^{+0.381}_{-0.258}$	4.352 ± 0.15	-0.074 ± 0.235	11.15	9.64	0.89	TRES	NESSI
248758353	5511 ± 138	$0.886^{+0.056}_{-0.052}$	$0.784^{+0.34}_{-0.241}$	4.439 ± 0.15	-0.162 ± 0.235	12.36	10.58	0.90	TRES	NESSI
248827616	6216 ± 138	$1.75^{+0.106}_{-0.1}$	$1.566^{+0.695}_{-0.474}$	4.147 ± 0.15	-0.184 ± 0.235	11.92	10.36	0.98	HIRES, TRES	NIRC2
248861279	3748 ± 138	$0.552^{+0.016}_{-0.016}$	$0.552^{+0.015}_{-0.015}$	4.695 ± 0.027	0.005 ± 0.235	14.56	10.75	1.05	TSpec	NIRC2, NESSI
248874928	4927 ± 138	$0.765^{+0.054}_{-0.05}$	$1.034^{+0.459}_{-0.314}$	4.685 ± 0.15	0.132 ± 0.235	12.86	10.55	1.05	TRES, HIRES	NIRC2, NESSI
249223471	5784 ± 138	$0.961^{+0.058}_{-0.054}$	$0.798^{+0.339}_{-0.245}$	4.374 ± 0.15	-0.038 ± 0.235	9.47	8.03	1.05	TRES, HIRES	DSSI
249403651	5563 ± 138	$0.927^{+0.058}_{-0.052}$	$0.881^{+0.39}_{-0.267}$	4.45 ± 0.15	0.014 ± 0.235	11.97	10.21	1.08	TRES	DSSI
249816490	5335 ± 138	$0.784^{+0.051}_{-0.047}$	$0.813^{+0.368}_{-0.249}$	4.559 ± 0.15	-0.171 ± 0.235	11.93	9.98	1.10	TRES	DSSI
249827330	5631 ± 138	$1.783^{+0.115}_{-0.109}$	$0.949^{+0.423}_{-0.289}$	3.916 ± 0.15	-0.201 ± 0.235	12.94	11.13	1.04	TRES	DSSI
249865296	6117 ± 138	$1.319^{+0.088}_{-0.08}$	$1.03^{+0.469}_{-0.314}$	4.212 ± 0.15	-0.197 ± 0.235	12.96	11.43	1.14	TRES	DSSI
249924395	5742 ± 138	$1.228^{+0.077}_{-0.072}$	$0.886^{+0.374}_{-0.271}$	4.204 ± 0.15	-0.036 ± 0.235	12.76	11.04	1.05	TRES	DSSI
211732116	5789 ± 21	$0.907^{+0.018}_{-0.017}$	$0.731^{+0.067}_{-0.061}$	4.386 ± 0.035	-0.292 ± 0.02	12.80	11.29	0.95	TRES	NIRC2
211830293	5278 ± 20	$1.851^{+0.045}_{-0.044}$	$0.811^{+0.077}_{-0.07}$	3.812 ± 0.033	0.168 ± 0.018	12.13	10.21	0.96	TRES[b]	HRCam
212222383	5937 ± 138	$1.149^{+0.067}_{-0.062}$	$0.908^{+0.394}_{-0.281}$	4.275 ± 0.15	-0.176 ± 0.235	10.42	9.01	0.86	TRES	PHARO
212705192	5778 ± 138	$2.155^{+0.135}_{-0.128}$	$1.54^{+0.679}_{-0.477}$	3.958 ± 0.15	-0.265 ± 0.235	12.20	10.28	1.11	TRES[d]	NESSI
211784767	6044 ± 138	$1.58^{+0.096}_{-0.088}$	$1.288^{+0.554}_{-0.39}$	4.149 ± 0.15	-0.075 ± 0.235	11.97	10.56	1.29	TRES	PHARO

Notes. The uncertainties on $T_{\rm eff}$, log$g$, and [Fe/H] are rms uncertainties from the machine-learning process. The instrument key is as follows: HIRES = Keck/HIRES; TRES = FLWO/TRES; TS23 = McDonald/TS23; TSpec = Hale/TripleSpec; SpeX = IRTF/Spex; PHARO = Hale/PHARO; NIRC2 = Keck/NIRC2, NIRI = Gemini/NIRI; DSSI = Gemini/DSSI; NESSI = WIYN/NESSI; HRCam = SOAR/HRCam.
[a] Contaminating star(s) detected in high-resolution imaging or spectroscopy.
[b] Radial velocities indicate stellar mass companion.
[c] Too high $v\sin i$ to detect possible stellar companions in spectrum.
[d] Double-lined spectroscopic binary.

This is a cross-dispersed echelle white-pupil spectrograph, which gives a spectral resolving power of 60,000 in its "TS23" setup, which was used for these observations. We used an exposure meter to achieve our target S/N of ~25/pixel. Data were reduced and the spectra were extracted using standard CCD techniques.

2.1.7. Infrared Telescope Facility/SpeX and Hale/TripleSpec

Medium-resolution reconnaissance spectra were obtained using SpeX on the NASA Infrared Telescope Facility (IRTF), and TripleSpec on the Palomar 200 inch Hale telescope. The SpeX observations were conducted in short-wavelength, cross-dispersed mode, using the $0''3 \times 15''$ slit to obtain $R \approx 2000$ spectra. The observations were taken after the SpeX upgrade in 2014 and cover 0.7–2.55 μm. The TripleSpec observations were obtained using the fixed $1'' \times 30''$ slit, with simultaneous coverage from 1.0 to 2.4 μm at a resolution $R = 2500$–2700. The SpeX spectra were reduced using the publicly available `Spextool` pipeline (Cushing et al. 2004), and the TripleSpec spectra using a specialized version of `Spextool` adapted for

use with TripleSpec data (available upon request from M. Cushing). The spectra were corrected for telluric contamination using the `xtellcor` package (Vacca et al. 2003), which is included in both versions of the `Spextool` pipeline. Additional details on the observing mode and data reduction can be found in Dressing et al. (2017, 2019).

2.2. Validation with vespa

The many thousands of Kepler candidates detected early in the mission quickly outpaced the capacity of the dedicated network of follow-up telescopes to confirm them. This bottleneck ushered in the era of statistical validation, where the likelihood that a given transit signal around a given target star is explained by a planet is compared to the likelihood that it is explained by a suite of astrophysical false positives. These could include, for instance, eclipsing binaries, background/blended eclipsing binaries, and hierarchical eclipsing stellar systems. A number of codes were developed to analyze Kepler candidates, including `BLENDER` (Torres et al. 2011), `PASTIS` (Díaz et al. 2014), and `vespa` (Morton et al. 2016). The latter of these is a publicly available Python package[47] that has been used to validate over a thousand Kepler planets (Morton et al. 2016), and has been used in the validation of the vast majority of K2 planets to date (Montet et al. 2015; Crossfield et al. 2016; Sinukoff et al. 2016; Dressing et al. 2017; Livingston et al. 2018; Mayo et al. 2018; Heller et al. 2019; Castro González et al. 2020).

In this analysis we use `vespa` version 0.6, and for each candidate calculate the false positive probability (FPP) that the candidate transit signal is due to a bona fide planet. These values are given in Table 2. We set a threshold of <1% to consider a planet validated. As inputs, `vespa` uses stellar parameters (position, parallax, photometry, T_{eff}, $\log g$, and [Fe/H]), transit signal parameters (period, Rp/Rs), the detrended light curve, and any available contrast curves from the high-resolution follow-up imaging. The latter are useful for constraining the potential parameter space within which nearby or blended eclipsing binaries could have remained undetected. In each case, we calculate the maximum radius for contaminating background sources from the size of the aperture used to generate the photometry, and the maximum allowed secondary eclipse depth using $0.1 \times (Rp/Rs)^2$. Since `vespa` treats each candidate in multiplanet systems independently, we separately calculate and apply a multiplicity boost for these candidates. This boost, first introduced in Lissauer et al. (2012) for Kepler and first adapted for K2 by Sinukoff et al. (2016), relies on the fact that the conceivable false positive scenarios become significantly less probable when there are multiple transit signals in the same light curve; the likelihood, for instance, that two eclipsing binary systems are coincident along the line of sight is much lower than the likelihood of a star hosting two transiting planets, given what we know about the occurrence rate of multiplanet systems. Following the method of Sinukoff et al. (2016), we calculated a multiplicity boost for each K2 campaign. The boost for Campaign c is given by $X_c = F_{multi,c}/F_{cand,c}$, where $F_{cand,c}$ is the fraction of targets in the campaign with planet candidates, and $F_{multi,c}$ is the fraction of planet candidate hosts in the campaign with more than one planet candidate. The calculated X_c values are given in Table 3; we did not calculate values for Campaigns 11 or 17 as there are no confirmed or candidate multiplanet systems in those campaigns. We calculated a different value for each campaign due to the varying Galactic latitudes and longitudes, which dramatically alter the stellar density in the field of view, and the likelihood of a given pixel containing a potentially contaminating eclipsing binary.

2.3. Centroid Testing

One area in which K2 observations were significantly degraded compared to Kepler observations was pointing stability. In order for K2 to point accurately, it relied on the two remaining functional reaction wheels balancing against the radiation pressure from the Sun. This created an unstable equilibrium, where the spacecraft was continuously rolling slightly out of position and then being adjusted back to its original pointing. Unlike Kepler, which achieved subpixel pointing precision (Haas et al. 2010), K2 was hampered by drift on the order of ~1 pixel over several hours (see Saunders et al. 2019). The subsequent increased sampling of the intrapixel and interpixel sensitivity variations, and time-dependent flux loss in the optimal aperture, significantly increased the correlated noise in the K2 light curves, on a timescale unfortunately comparable to typical transit durations. The motion in the light curves was substantially corrected by several teams (e.g., Vanderburg & Johnson 2014; Aigrain et al. 2016; Luger et al. 2016).

For the exquisitely precise Kepler pointing, measuring the change in position of the center of light from a target star (the centroid) during transit was a powerful tool for discriminating between true planet candidates and background or nearby eclipsing binaries (Bryson et al. 2013). For K2, however, the significantly worse pointing stability has thus far largely precluded the centroid test from being implemented (see Kostov et al. 2019, for some success). The lack of a centroid test has led to the retraction of a number of previously validated K2 planets which were found to be eclipsing binaries within the same pixel (Cabrera et al. 2017). Here we use the new implementation of a centroid test for unstable/moving data from the `vetting`[48] Python package (Hedges 2021), which accounts for the motion of the spacecraft.

In brief, the approach of this centroid test is to (i) find the weighted average position of the source inside the pipeline aperture in the x- and y-dimensions; (ii) correct these centroids for motion by detrending against the `POS_CORR` arguments from the pipeline-processed target pixel file (which estimate the position of the source on the detector) using the same self flat-fielding approach used by Vanderburg & Johnson (2014) for K2 data; (iii) remove a Gaussian-smoothed, long-term trend with a width of 21 cadences to remove long-term drifts due to velocity aberration; and (iv) employ a Student's t-test to assess the likelihood of the distribution of centroids during transit being drawn from the distribution of centroids out of transit. This likelihood can then be used to discount false positives. Here, we used a threshold of $p = 0.05$ to define a significant difference in the two distributions; candidates with $p < 0.05$ were deemed to have a significant offset between their in- and out-of-transit centroids and were not considered validated. The threshold was chosen after performing the centroid test on known confirmed planets and false positives.

---

[47] https://github.com/timothydmorton/VESPA

[48] https://github.com/ssdatalab/vetting

7

Table 2
Validation Parameters of the Candidate Systems

Candidate ID	Period (days)	HEBs	HEBs ($2 \times P$)	EBs	EBs ($2 \times P$)	BEBs	BEBs ($2 \times P$)	Planets	FPP	Centroid p-value
Validated										
204750116.01	23.4481724	2.54×10^{-12}	1.31×10^{-08}	3.02×10^{-04}	7.05×10^{-04}	5.73×10^{-04}	2.48×10^{-05}	0.998	1.60×10^{-03}	0.5219
205111664.01	15.937039	3.72×10^{-06}	3.10×10^{-06}	4.23×10^{-05}	8.59×10^{-05}	1.64×10^{-06}	3.81×10^{-06}	1.000	1.40×10^{-04} [a]	0.4962
206055981.01	20.6450985	1.13×10^{-05}	2.00×10^{-07}	6.47×10^{-04}	1.87×10^{-05}	4.34×10^{-05}	7.21×10^{-38}	0.999	7.21×10^{-04} [a]	0.5842
206135682.01	5.02559754	1.77×10^{-05}	1.85×10^{-04}	3.69×10^{-05}	5.19×10^{-05}	7.43×10^{-05}	1.83×10^{-04}	0.999	1.90×10^{-05} [*]	0.2070
206135682.02	20.2010847	1.26×10^{-08}	3.36×10^{-08}	7.63×10^{-06}	1.23×10^{-05}	1.73×10^{-04}	1.10×10^{-04}	1.000	3.44×10^{-05} [*]	0.3671
206135682.03	9.66018618	1.42×10^{-04}	3.94×10^{-07}	9.19×10^{-06}	2.28×10^{-07}	2.38×10^{-04}	2.06×10^{-06}	1.000	2.46×10^{-05}[*]	0.1385
206146957.01	5.76161216	2.5×10^{-06}	1.44×10^{-05}	9.31×10^{-07}	1.24×10^{-05}	$0.0 \times 10^{+00}$	$0.0 \times 10^{+00}$	1.000	3.02×10^{-05} [*]	0.4584
206317286.01	17.5154723	7.57×10^{-66}	1.44×10^{-51}	3.25×10^{-05}	1.11×10^{-03}	7.81×10^{-05}	8.07×10^{-05}	0.999	8.16×10^{-05} [*]	0.1811
211399359.01	3.11490475	8.14×10^{-65}	9.25×10^{-30}	8.13×10^{-173}	1.58×10^{-104}	1.89×10^{-13}	2.09×10^{-82}	1.000	1.89×10^{-13}	0.1241
211490999.01	9.84407732	5.48×10^{-14}	5.9×10^{-18}	3.23×10^{-03}	1.57×10^{-04}	$0.00 \times 10^{+00}$	$0.00 \times 10^{+00}$	0.997	3.39×10^{-03} [a]	0.4752
211539054.01	11.0206598	3.81×10^{-07}	3.16×10^{-08}	1.76×10^{-03}	3.73×10^{-04}	$0.00 \times 10^{+00}$	$0.00 \times 10^{+00}$	0.998	2.13×10^{-03} [a]	0.3779
212006318.01	14.453895	2.43×10^{-05}	1.39×10^{-05}	9.96×10^{-05}	3.97×10^{-03}	$0.00 \times 10^{+00}$	1.55×10^{-07}	0.996	4.11×10^{-03} [a]	0.1458
212530118.01	12.8322355	6.79×10^{-05}	2.48×10^{-14}	9.12×10^{-04}	2.01×10^{-05}	1.37×10^{-04}	2.16×10^{-07}	0.999	1.14×10^{-03} [a]	0.5774
212575828.01	2.06043843	5.11×10^{-05}	2.31×10^{-05}	6.49×10^{-04}	2.23×10^{-05}	1.67×10^{-04}	$0.00 \times 10^{+00}$	0.999	9.12×10^{-04} [a]	0.4968
214173069.01	8.7779358	1.54×10^{-05}	1.19×10^{-06}	1.20×10^{-03}	1.12×10^{-03}	1.41×10^{-03}	1.63×10^{-03}	0.995	5.38×10^{-03} [a]	0.8487
214419545.01	9.4013125	2.21×10^{-05}	2.24×10^{-07}	5.19×10^{-05}	1.94×10^{-06}	8.61×10^{-03}	1.42×10^{-04}	0.991	8.82×10^{-03}	0.6540
217192839.01	16.0346559	7.26×10^{-06}	7.51×10^{-08}	6.96×10^{-05}	4.15×10^{-06}	2.41×10^{-45}	3.69×10^{-62}	1.000	1.46×10^{-05} [a,c]	0.3334
217192839.02	7.938933355	3.01×10^{-03}	5.22×10^{-05}	3.93×10^{-02}	1.55×10^{-03}	2.08×10^{-19}	3.32×10^{-42}	0.956	8.22×10^{-03} [a,c]	0.2215
217192839.03	26.803023	3.52×10^{-04}	1.43×10^{-05}	5.92×10^{-03}	1.16×10^{-04}	$0.00 \times 10^{+00}$	$0.00 \times 10^{+00}$	0.994	1.16×10^{-03} [a,c]	0.2891
217977895.01	21.7001564	4.33×10^{-10}	4.05×10^{-20}	4.6×10^{-04}	3.18×10^{-07}	2.16×10^{-03}	9.68×10^{-42}	0.997	2.62×10^{-03} [a]	0.3721
218668602.01	1.86596186	6.93×10^{-05}	2.16×10^{-06}	4.41×10^{-04}	1.53×10^{-06}	1.53×10^{-03}	7.84×10^{-05}	0.998	2.12×10^{-03}	0.1391
220221272.01	13.6274904	2.03×10^{-04}	6.59×10^{-05}	4.25×10^{-04}	8.15×10^{-04}	1.37×10^{-05}	7.62×10^{-07}	0.998	1.12×10^{-04} [a,c]	0.5460
220221272.02	6.679581962	3.59×10^{-04}	3.79×10^{-04}	6.58×10^{-04}	2.84×10^{-03}	7.76×10^{-07}	1.76×10^{-05}	0.996	3.14×10^{-04} [a,c]	0.5203
220221272.03	4.194766393	1.6×10^{-03}	4.52×10^{-04}	4.10×10^{-03}	2.69×10^{-03}	8.53×10^{-06}	8.68×10^{-07}	0.991	6.57×10^{-04} [a,c]	0.1135
220221272.04	9.715042543	2.66×10^{-03}	5.22×10^{-03}	1.14×10^{-02}	3.06×10^{-02}	2.25×10^{-05}	1.16×10^{-05}	0.950	3.85×10^{-03} [a,c]	0.4207
220221272.05	2.231527238	8.26×10^{-04}	8.01×10^{-04}	9.14×10^{-03}	1.13×10^{-02}	1.25×10^{-07}	5.02×10^{-06}	0.978	7.20×10^{-03} [a,c]	0.6315
220459477.01	2.3808672	6.28×10^{-08}	1.26×10^{-19}	2.83×10^{-13}	5.47×10^{-20}	1.08×10^{-05}	4.86×10^{-12}	1.000	1.09×10^{-05} [a]	0.1107
220510874.01	7.4732234	3.07×10^{-205}	1.99×10^{-98}	1.09×10^{-13}	3.34×10^{-05}	1.01×10^{-23}	2.61×10^{-14}	1.000	3.34×10^{-05} [a]	0.6971
220696233.01	28.7353275	1.50×10^{-257}	2.87×10^{-122}	3.25×10^{-10}	7.11×10^{-15}	8.07×10^{-12}	2.98×10^{-62}	1.000	3.33×10^{-10} [a]	0.3918
245943455.01	6.33906865	8.97×10^{-51}	3.45×10^{-65}	8.02×10^{-08}	1.07×10^{-12}	$0.00 \times 10^{+00}$	$0.00 \times 10^{+00}$	1.000	8.02×10^{-08} [a]	0.0938
245991048.01	8.5835664	1.14×10^{-04}	3.95×10^{-05}	2.03×10^{-03}	2.31×10^{-03}	$0.00 \times 10^{+00}$	$0.00 \times 10^{+00}$	0.996	6.41×10^{-05} [a,c]	0.2457
245991048.02	20.8513367	9.04×10^{-05}	5.44×10^{-07}	3.86×10^{-03}	8.12×10^{-05}	2.02×10^{-225}	$0.00 \times 10^{+00}$	0.996	5.75×10^{-05} [a,c]	0.2053
245995977.01	3.31279234	5.36×10^{-08}	3.58×10^{-12}	2.22×10^{-08}	1.10×10^{-08}	$0.00 \times 10^{+00}$	$0.00 \times 10^{+00}$	1.000	8.68×10^{-08} [a]	0.6208
246074314.01	4.62265408	5.42×10^{-05}	1.08×10^{-07}	2.12×10^{-05}	3.21×10^{-07}	2.28×10^{-05}	1.78×10^{-245}	1.000	9.87×10^{-05} [a]	0.3581
246084398.01	15.3987228	8.04×10^{-06}	3.99×10^{-08}	2.07×10^{-03}	3.04×10^{-06}	3.38×10^{-05}	6.88×10^{-09}	0.998	2.12×10^{-03} [a]	0.5614
246429049.01	10.4131807	1.30×10^{-04}	5.69×10^{-05}	6.61×10^{-03}	2.03×10^{-03}	8.16×10^{-05}	9.30×10^{-05}	0.991	9.00×10^{-03} [a]	0.3512
210797580.01	2.1408398	2.10×10^{-04}	4.68×10^{-07}	1.90×10^{-03}	8.92×10^{-08}	1.24×10^{-03}	1.99×10^{-24}	9.97×10^{-01}	1.77×10^{-03} [a]	0.4204
246876040.01	5.09571665	2.12×10^{-08}	1.82×10^{-08}	8.35×10^{-22}	9.61×10^{-14}	4.38×10^{-04}	2.50×10^{-203}	1.000	4.38×10^{-04}[a]	0.2143
246891819.01	4.80335174	1.21×10^{-14}	7.23×10^{-12}	2.15×10^{-13}	1.34×10^{-08}	$0.00 \times 10^{+00}$	$0.00 \times 10^{+00}$	1.000	6.35×10^{-10} [a,c]	0.4413
246891819.02	8.49128189	1.42×10^{-05}	6.90×10^{-06}	1.12×10^{-04}	2.34×10^{-04}	$0.00 \times 10^{+00}$	$0.00 \times 10^{+00}$	1.000	1.74×10^{-05} [a,c]	0.4640
246953392.01	0.67386241	5.32×10^{-04}	4.92×10^{-04}	3.04×10^{-03}	4.24×10^{-03}	2.34×10^{-04}	1.83×10^{-04}	0.991	4.16×10^{-04} [a,c]	0.4124
246953392.02	25.7605085	2.83×10^{-10}	1.48×10^{-11}	1.40×10^{-10}	4.29×10^{-15}	8.03×10^{-05}	2.00×10^{-76}	1.000	1.07×10^{-05} [a]	0.3421
247383003.01	3.57232573	1.03×10^{-04}	1.07×10^{-05}	6.81×10^{-03}	1.06×10^{-03}	$0.00 \times 10^{+00}$	$0.00 \times 10^{+00}$	0.992	7.99×10^{-03} [a]	0.5226
248463350.01	6.39302548	1.08×10^{-03}	9.01×10^{-04}	6.17×10^{-03}	2.33×10^{-02}	$0.00 \times 10^{+00}$	$0.00 \times 10^{+00}$	0.969	4.80×10^{-04} [a,c]	0.3000
248463350.02	18.787839	5.67×10^{-05}	4.65×10^{-04}	3.32×10^{-05}	1.56×10^{-02}	$0.00 \times 10^{+00}$	$0.00 \times 10^{+00}$	0.984	2.43×10^{-04} [a,c]	0.3974
248472140.01	0.75997781	1.54×10^{-04}	1.24×10^{-07}	2.66×10^{-04}	3.6×10^{-04}	$0.00 \times 10^{+00}$	$0.00 \times 10^{+00}$	0.999	7.80×10^{-04} [a]	0.1608
248518307.01	3.86505292	8.36×10^{-05}	1.22×10^{-04}	5.2×10^{-04}	4.29×10^{-04}	6.66×10^{-05}	1.28×10^{-04}	0.999	1.35×10^{-03} [a]	0.5332
248527514.01	6.29309867	9.99×10^{-04}	3.01×10^{-05}	2.45×10^{-03}	2.17×10^{-04}	7.93×10^{-05}	9.35×10^{-07}	0.996	3.78×10^{-03} [a]	0.3051
248621597.01	17.2747396	5.62×10^{-06}	1.77×10^{-06}	4.11×10^{-09}	1.94×10^{-04}	2.09×10^{-06}	3.45×10^{-06}	1.000	2.07×10^{-04} [a]	0.4934
248758353.01	33.5899786	4.19×10^{-11}	2.49×10^{-09}	1.03×10^{-14}	1.05×10^{-05}	2.13×10^{-11}	$0.00 \times 10^{+00}$	1.000	1.05×10^{-05} [a]	0.6589

Table 2
(Continued)

Candidate ID	Period (days)	HEBs	HEBs ($2 \times P$)	EBs	EBs ($2 \times P$)	BEBs	BEBs ($2 \times P$)	Planets	FPP	Centroid p-value
248861279.01	13.1153647	3.91×10^{-05}	2.88×10^{-63}	5.71×10^{-04}	2.52×10^{-04}	$0.00 \times 10^{+00}$	$0.00 \times 10^{+00}$	0.999	8.62×10^{-04} [a]	0.4292
248874928.01	3.43545277	1.06×10^{-07}	4.42×10^{-06}	1.47×10^{-14}	1.24×10^{-10}	$0.00 \times 10^{+00}$	$0.00 \times 10^{+00}$	1.000	4.53×10^{-06} [a]	0.5057
249223471.01	22.5494062	1.01×10^{-06}	8.33×10^{-07}	1.53×10^{-04}	1.14×10^{-03}	6.18×10^{-08}	3.69×10^{-06}	0.999	1.30×10^{-03} [a]	0.6741
249403651.01	4.94190653	2.91×10^{-04}	6.29×10^{-06}	6.75×10^{-04}	3.79×10^{-05}	4.11×10^{-04}	2.08×10^{-08}	0.999	3.23×10^{-05} [a,c]	0.0826
249403651.02	9.22452977	1.52×10^{-04}	1.01×10^{-05}	2.35×10^{-03}	1.20×10^{-03}	3.99×10^{-04}	3.90×10^{-04}	0.995	1.03×10^{-04} [a,c]	0.0372
249816490.01	20.9789593	1.79×10^{-10}	3.29×10^{-14}	3.89×10^{-04}	3.04×10^{-07}	1.30×10^{-04}	6.63×10^{-45}	0.999	5.19×10^{-04} [a]	0.6675
249924395.01	1.90808365	1.47×10^{-05}	3.56×10^{-08}	1.77×10^{-05}	1.89×10^{-13}	6.74×10^{-06}	$0.00 \times 10^{+00}$	1.000	3.92×10^{-05} [a]	0.4360
211732116.01	4.52195338	6.31×10^{-29}	5.21×10^{-09}	9.19×10^{-04}	2.49×10^{-05}	$0.00 \times 10^{+00}$	2.03×10^{-87}	0.999	6.80×10^{-05} [a,c]	0.5403
211732116.02	16.4344499	7.11×10^{-06}	1.1×10^{-05}	1.52×10^{-02}	1.74×10^{-02}	1.04×10^{-07}	3.68×10^{-07}	0.967	2.42×10^{-03} [a,c]	0.5749
212222383.01	5.77647524	7.28×10^{-05}	7.41×10^{-08}	1.55×10^{-03}	7.53×10^{-05}	9.60×10^{-29}	2.30×10^{-20}	0.998	1.70×10^{-03} [a]	0.6183
Not yet validated										
205944181.01	2.47558277	1.47×10^{-04}	4.03×10^{-04}	2.63×10^{-01}	4.13×10^{-02}	$0.00 \times 10^{+00}$	$0.00 \times 10^{+00}$	0.695	3.05×10^{-01} [a]	0.3263
205957328.01	14.3523671	2.83×10^{-04}	1.3×10^{-04}	1.13×10^{-02}	7.23×10^{-03}	9.53×10^{-04}	2.02×10^{-03}	0.978	2.2×10^{-02}	0.6039
205999468.01	12.2634336	2.58×10^{-03}	1.6×10^{-03}	3.67×10^{-02}	3.79×10^{-02}	4.25×10^{-08}	2.05×10^{-05}	0.921	7.9×10^{-02} [a]	0.6805
211428897.01	1.61088909	$0.0 \times 10^{+00}$	2.55×10^{-04}	9.24×10^{-03}	1.87×10^{-02}	$0.00 \times 10^{+00}$	$0.00 \times 10^{+00}$	0.972	2.8×10^{-02}	0.5961
211428897.02	2.17805786	-	-	-	-	-	-	-	error	0.3319
211428897.03	4.96824247	$0.0 \times 10^{+00}$	1.14×10^{-89}	2.27×10^{-03}	3.54×10^{-02}	$0.00 \times 10^{+00}$	$0.00 \times 10^{+00}$	0.962	3.8×10^{-02}	0.2088
211428897.04	6.26462338	3.08×10^{-238}	6.04×10^{-03}	2.71×10^{-01}	1.52×10^{-01}	$0.00 \times 10^{+00}$	$0.00 \times 10^{+00}$	0.571	4.29×10^{-01}	0.3817
211711685.01	15.462807	1.13×10^{-16}	2.82×10^{-07}	8.47×10^{-06}	1.29×10^{-04}	2.89×10^{-28}	4.46×10^{-08}	1.000	1.38×10^{-04} [a]	0.0088
211965883.01	10.5551697	4.34×10^{-05}	1.02×10^{-03}	2.2×10^{-02}	1.26×10^{-02}	7.07×10^{-04}	4.98×10^{-06}	0.964	3.6×10^{-02} [a]	0.4895
212351868.01	2.50028488	6.01×10^{-02}	7.09×10^{-06}	7.90×10^{-01}	4.47×10^{-16}	1.45×10^{-31}	$0.00 \times 10^{+00}$	0.149	8.51×10^{-01}	0.3189
212585579.01	3.0219382	2.58×10^{-02}	4.17×10^{-03}	6.09×10^{-01}	6.51×10^{-02}	3.28×10^{-04}	8.33×10^{-08}	0.296	7.04×10^{-01} [a]	0.1374
212730483.01	3.49096697	1.05×10^{-27}	2.29×10^{-03}	4.31×10^{-02}	7.86×10^{-02}	7.36×10^{-04}	3.21×10^{-03}	0.872	1.28×10^{-01} [a]	0.6583
212797028.01	29.9835193	5.14×10^{-02}	4.03×10^{-02}	3.93×10^{-01}	4.06×10^{-01}	2.15×10^{-09}	7.17×10^{-13}	0.110	8.9×10^{-01}	0.4869
213817056.01	13.6118493	2.90×10^{-99}	5.38×10^{-39}	1.94×10^{-79}	2.80×10^{-44}	4.99×10^{-02}	4.13×10^{-06}	0.950	5.00×10^{-02}	0.8036
216892056.01	2.78585897	7.67×10^{-04}	6.54×10^{-03}	1.58×10^{-02}	6.22×10^{-02}	$0.00 \times 10^{+00}$	$0.00 \times 10^{+00}$	0.915	8.5×10^{-02} [a]	0.2193
217192839.04	40.9341414	4.2×10^{-03}	6.71×10^{-04}	1.08×10^{-01}	1.48×10^{-02}	3.49×10^{-162}	9.49×10^{-53}	0.872	2.6×10^{-02} [a,c]	0.6511
220294712.01	23.6110924	7.03×10^{-02}	2.03×10^{-04}	1.84×10^{-01}	3.93×10^{-02}	3.68×10^{-01}	3.38×10^{-01}	2.89×10^{-48}	1.00	0.7637
220400100.01	10.7947008	1.90×10^{-05}	1.46×10^{-08}	3.58×10^{-02}	5.17×10^{-04}	2.26×10^{-05}	6.96×10^{-109}	0.964	3.6×10^{-02} [a]	0.4229
220571481.01	8.78648628	1.06×10^{-02}	8.95×10^{-03}	2.53×10^{-01}	1.27×10^{-01}	5.67×10^{-04}	3.21×10^{-04}	0.599	4.01×10^{-01} [a]	0.4585
226042826.01	3.12897689	2.79×10^{-05}	9.32×10^{-05}	5.0×10^{-04}	8.90×10^{-04}	4.53×10^{-01}	5.46×10^{-01}	1.58×10^{-11}	1.00	$\ldots$ [d]
247164043.01	5.22835211	2.28×10^{-07}	1.61×10^{-08}	2.56×10^{-05}	5.56×10^{-12}	$0.00 \times 10^{+00}$	$0.00 \times 10^{+00}$	1.000	2.59×10^{-05} [a]	0.0452
247698108.01	20.3794342	3.98×10^{-03}	3.27×10^{-04}	2.93×10^{-02}	5.85×10^{-03}	4.57×10^{-01}	5.03×10^{-01}	3.12×10^{-04}	1.00	0.1459
247724001.01	1.248905	1.46×10^{-02}	1.90×10^{-02}	9.41×10^{-02}	3.22×10^{-01}	1.48×10^{-02}	7.94×10^{-03}	0.528	4.72×10^{-01} [a]	0.0795
248222323.01	9.42690097	3.88×10^{-02}	2.81×10^{-03}	2.38×10^{-01}	1.25×10^{-02}	6.71×10^{-02}	4.71×10^{-02}	0.594	4.06×10^{-01}	0.0134
248639411.01	3.57739438	1.05×10^{-04}	3.35×10^{-03}	4.64×10^{-08}	7.99×10^{-01}	$0.00 \times 10^{+00}$	$0.00 \times 10^{+00}$	0.198	8.02×10^{-01} [a]	0.2883
248740016.01	14.3907212	2.16×10^{-02}	1.10×10^{-02}	3.53×10^{-01}	2.53×10^{-01}	6.62×10^{-04}	3.28×10^{-04}	0.360	6.40×10^{-01} [a]	0.0892
248827616.01	2.57126699	2.03×10^{-03}	2.08×10^{-03}	4.78×10^{-02}	9.36×10^{-02}	$0.00 \times 10^{+00}$	$0.00 \times 10^{+00}$	0.855	1.45×10^{-01} [a]	0.4882
249827330.01	31.3960013	1.03×10^{-02}	5.39×10^{-05}	1.10×10^{-01}	2.89×10^{-04}	4.37×10^{-03}	4.35×10^{-103}	0.875	1.25×10^{-01} [a]	0.1697
249865296.01	28.8885889	9.35×10^{-09}	1.39×10^{-11}	1.52×10^{-22}	2.80×10^{-18}	3.15×10^{-84}	5.95×10^{-230}	1.00	9.37×10^{-09}	0.0418
212705192.01	2.26837914	1.43×10^{-03}	2.5×10^{-04}	9.52×10^{-02}	1.85×10^{-02}	2.83×10^{-04}	$0.00 \times 10^{+00}$	0.884	1.16×10^{-01}	0.3976
211784767.01	3.58048139	1.21×10^{-01}	8.3×10^{-03}	5.31×10^{-01}	6.08×10^{-02}	4.99×10^{-02}	2.21×10^{-01}	0.00895	9.91×10^{-01}	0.4486

Note. HEBs: the calculated probability that the signal is caused by a hierarchical eclipsing binary; HEBs ($2 \times P$): the same for a binary with twice the measured orbital period. EBs: the calculated probability that the signal is caused by an eclipsing binary; EBs ($2 \times P$): the same for an eclipsing binary with twice the period. BEBs: the calculated probability that the signal is caused by a background eclipsing binary; BEBs: ($2 \times P$) the same for a background eclipsing binary with twice the period. Planets: the calculated probability that the signal is caused by a bona fide planet. FPP: the final `vespa` false positive probability.
[a] Contrast curve(s) used.
[b] Multiplicity boost used.
[c] Too crowded for valid `centroid` test.

8

Table 3
Campaign-specific Multiplicity Boost Values

Campaign	$X2$
1	25.9251
2	8.1286
3	15.9445
4	13.1029
5	9.0566
6	11.8727
7	5.5419
8	13.6017
10	35.6843
11	…
12	70.3960
13	21.1136
14	67.4368
15	44.0871
16	13.9069
17	…
18	50.3128

Note. Campaigns 11 and 17 have no multiplanet systems, either in Paper IV or previously published planets and candidate lists, with which to calculate a multiplicity boost.

3. Validated Planets

We consider planet candidates with reconnaissance spectra and high-resolution imaging that show no evidence of stellar companions, a vespa FPP of <1%, and a centroid value of >0.05 to be statistically validated. In total, examining 91 candidates in 78 systems, we validate 60 planets in 46 systems. The properties of the new host stars are shown in the top panel of Figure 1, and the properties of the new planets are shown in the bottom panel. The parameters of the new planets are provided in Table 4. In total we validate 60 new planets in 46 systems, ranging in period from the ultra-short-period (USP) K2-396 b (0.673 day) and K2-399 b (0.760 day) to K2-403 b (33.590 days), and in size from the Earth-sized K2-381 c (1.075 $R_\oplus$) and K2-384 b (1.191 $R_\oplus$) to the hot-Jupiter-sized K2-371 b (13.024 $R_\oplus$). We validate 36 new single-planet systems, six new two-planet systems, two new three-planet systems, one new five-planet system, and one new planet in a system with a previously validated planet. The phase-folded light curves with the best-fitting transit models are shown in Figures 3–6, and the centroid plots are shown in Figures 7–9.

In this section we discuss some of the most interesting new systems; Appendix appendix describes the remaining validated planets in detail. For each planet, we estimate the planet mass using the Chen & Kipping (2017) mass–radius relationship. Although this is an empirical relationship which is uncorrected for observational biases, it has the advantage of covering the entire radius range of the planets validated here; our mass estimates and metrics subsequently derived from those mass estimates are provided as guideposts toward interesting systems, and should not be considered a robust characterization of the planets' properties. From the mass estimate, we calculate the maximum semiamplitude of the radial velocity (RV) variations that the planet would induce on the host star. In addition, we estimate the transmission and emission spectroscopy metrics (TSM and ESM; Kempton et al. 2018). Estimated values and metrics for the newly validated planets are provided in Table 5. These metrics were designed to rank planets by their
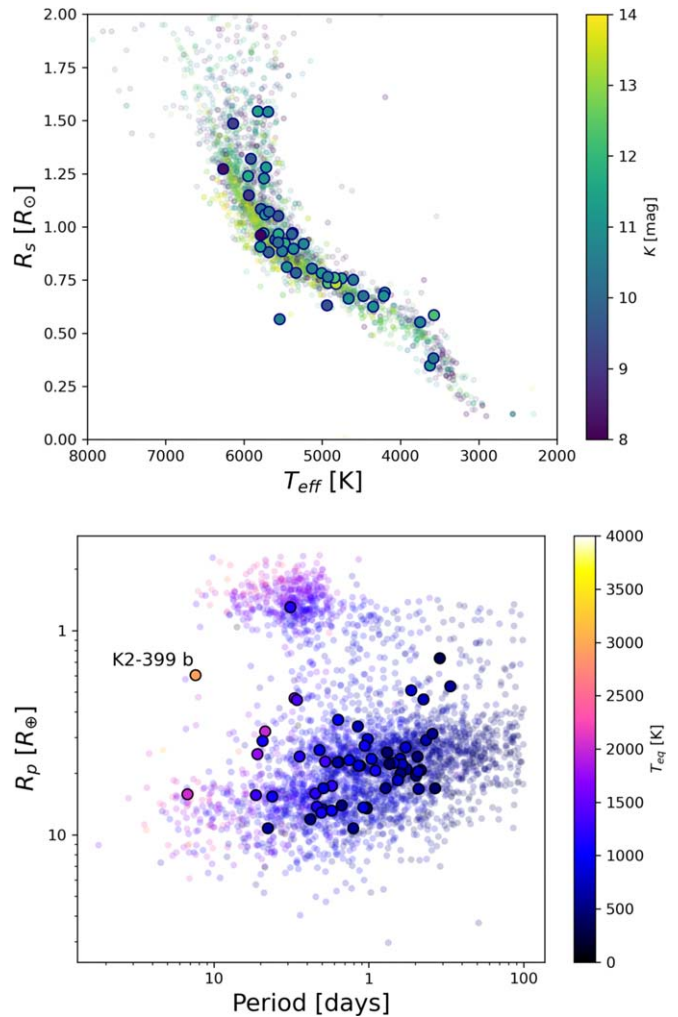
Figure 1. Some properties of the systems containing newly validated planets. Top: the new host stars (large circles with black edges) compared to the host stars of known planets at the NASA Exoplanet Archive. Bottom: the new planets (large circles with black edges) compared to the planets with measured radii and orbital periods shorter than 100 days at the NASA Exoplanet Archive. K2-399 b is highlighted, which is an ultra-hot, Saturn-sized planet in a relatively unpopulated region of parameter space.

putative NASA James Webb Space Telescope (JWST) transmission and emission spectroscopy S/N, respectively, taking into account the brightness of the target star and either the cloud-free scale height of the atmosphere (TSM) or the brightness temperature of the planet (ESM). This allows us to comment on the respective favorability of our newly validated planets as JWST targets compared to the thresholds set out in Kempton et al. (2018). Figure 2 shows the distribution of the TSM and ESM values of our newly validated planets compared with the JWST Cycle 1 exoplanet target list; there are a number of new planets, particularly larger than 3 $R_\oplus$, that may be interesting targets for future atmospheric follow-up. Where there are multiple planets in a system, we check for low-order mean motion resonances and, where found, estimate transit timing variations. Table 6 shows which of the newly validated planets were also observed by the NASA Transiting Exoplanet Survey Satellite (TESS) mission, and in which sector, determined using the Web TESS Viewing Tool.[49] Although

---

Table 4
Derived Planet Parameters of the Newly Validated Planetary Systems

Planet	Candidate ID	Camp	Period (days)	R_p/R_s	R_p ($R_\oplus$)	T_{mid} (2454833-JD)	b	a/R_s
K2-365 b	204750116.01	2	$23.448172^{+0.000766}_{-0.000996}$	$0.0253^{+0.001}_{-0.0}$	$2.906^{+0.195}_{-0.176}$	$2065.8326^{+0.0019}_{-0.0013}$	$0.328^{+0.197}_{-0.215}$	$30.65^{+1.48}_{-2.96}$
K2-366 b	205111664.01	2	$15.937039^{+0.000796}_{-0.001144}$	$0.0228^{+0.001}_{-0.001}$	$2.359^{+0.187}_{-0.167}$	$2073.4351^{+0.0028}_{-0.0032}$	$0.718^{+0.073}_{-0.093}$	$27.63^{+3.08}_{-3.23}$
K2-367 b	206055981.01	3	$20.645099^{+0.000995}_{-0.001375}$	$0.0353^{+0.002}_{-0.002}$	$2.413^{+0.225}_{-0.196}$	$2164.3941^{+0.0020}_{-0.0014}$	$0.83^{+0.052}_{-0.063}$	$45.05^{+6.05}_{-6.59}$
K2-368 b	206135682.01	3	$5.025598^{+0.000287}_{-0.000342}$	$0.0184^{+0.001}_{-0.001}$	$1.332^{+0.107}_{-0.1}$	$2145.7672^{+0.0025}_{-0.0027}$	$0.272^{+0.209}_{-0.188}$	$16.2^{+0.88}_{-1.3}$
K2-368 c	206135682.02	3	$9.660186^{+0.001164}_{-0.001169}$	$0.0188^{+0.001}_{-0.001}$	$1.361^{+0.114}_{-0.106}$	$2144.8722^{+0.0037}_{-0.0052}$	$0.306^{+0.219}_{-0.207}$	$25.98^{+1.87}_{-2.35}$
K2-368 d	206135682.03	3	$20.201085^{+0.002354}_{-0.002736}$	$0.0269^{+0.001}_{-0.001}$	$1.948^{+0.152}_{-0.143}$	$2155.5374^{+0.0026}_{-0.0018}$	$0.287^{+0.2}_{-0.193}$	$42.92^{+1.77}_{-3.54}$
K2-369 b	206146957.01	3	$5.761612^{+0.000846}_{-0.000714}$	$0.0137^{+0.001}_{-0.001}$	$1.313^{+0.101}_{-0.095}$	$2146.8716^{+0.0052}_{-0.0053}$	$0.727^{+0.076}_{-0.102}$	$14.31^{+1.66}_{-1.62}$
EPIC 206317286 c	206317286.01	3	$17.515472^{+0.002288}_{-0.002965}$	$0.0253^{+0.001}_{-0.001}$	$2.094^{+0.176}_{-0.16}$	$2144.8215^{+0.0071}_{-0.0031}$	$0.268^{+0.205}_{-0.183}$	$34.54^{+1.69}_{-2.6}$
K2-370 b	210797580.01	13	$2.14084^{+3.6e-05}_{-3.8e-05}$	$0.0302^{+0.001}_{-0.005}$	$3.207^{+0.224}_{-0.548}$	$2989.1840^{+0.0008}_{-0.0008}$	$0.941^{+0.008}_{-0.216}$	$3.66^{+3.57}_{-0.23}$
K2-371 b	211399359.01	5,18	$3.114905^{+9e-06}_{-9e-06}$	$0.1619^{+0.0}_{-0.0}$	$13.024^{+0.921}_{-0.868}$	$2308.4176^{+0.0001}_{-0.0001}$	$0.666^{+0.006}_{-0.006}$	$8.64^{+0.06}_{-0.05}$
K2-372 b	211490999.01	5,16,18	$9.844077^{+0.000565}_{-0.000575}$	$0.0292^{+0.001}_{-0.0}$	$2.945^{+0.077}_{-0.075}$	$2313.3287^{+0.0019}_{-0.0015}$	$0.337^{+0.103}_{-0.152}$	$20.01^{+0.77}_{-0.82}$
K2-373 b	211539054.01	5	$11.02066^{+0.001431}_{-0.001368}$	$0.0127^{+0.001}_{-0.001}$	$2.061^{+0.147}_{-0.14}$	$2317.2894^{+0.0042}_{-0.0043}$	$0.666^{+0.086}_{-0.123}$	$15.29^{+1.8}_{-1.69}$
K2-374 b	211732116.01	16	$4.521953^{+0.00032}_{-0.000409}$	$0.0161^{+0.001}_{-0.001}$	$1.593^{+0.061}_{-0.058}$	$3266.6869^{+0.0040}_{-0.0032}$	$0.235^{+0.139}_{-0.153}$	$11.44^{+0.33}_{-0.33}$
K2-374 c	211732116.02	16	$16.43445^{+0.002378}_{-0.002702}$	$0.0223^{+0.001}_{-0.001}$	$2.213^{+0.091}_{-0.086}$	$3276.2376^{+0.0065}_{-0.0056}$	$0.649^{+0.05}_{-0.054}$	$27.11^{+0.88}_{-0.86}$
K2-375 b	212006318.01	5	$14.453895^{+0.004773}_{-0.004175}$	$0.0133^{+0.001}_{-0.001}$	$2.243^{+0.186}_{-0.174}$	$2314.3436^{+0.0105}_{-0.0111}$	$0.284^{+0.214}_{-0.19}$	$16.9^{+1.07}_{-1.37}$
K2-376 b	212222383.01	16	$5.776475^{+0.000261}_{-0.000237}$	$0.0138^{+0.001}_{-0.001}$	$1.736^{+0.125}_{-0.119}$	$3263.7426^{+0.0025}_{-0.0022}$	$0.854^{+0.039}_{-0.048}$	$11.58^{+1.48}_{-1.39}$
K2-377 b	212530118.01	6	$12.832235^{+0.001554}_{-0.001616}$	$0.0224^{+0.001}_{-0.001}$	$1.693^{+0.146}_{-0.132}$	$2397.1429^{+0.0052}_{-0.0050}$	$0.262^{+0.209}_{-0.181}$	$30.04^{+1.77}_{-2.32}$
K2-389 b	212575828.01	6	$2.060438^{+0.000118}_{-7.4e-05}$	$0.036^{+0.002}_{-0.001}$	$2.88^{+0.27}_{-0.23}$	$2384.8493^{+0.0018}_{-0.0034}$	$0.402^{+0.208}_{-0.247}$	$9.52^{+0.81}_{-1.17}$
K2-379 b	214173069.01	7	$8.777247^{+0.000625}_{-0.000611}$	$0.0266^{+0.004}_{-0.001}$	$2.181^{+0.363}_{-0.198}$	$2470.9091^{+0.0039}_{-0.0027}$	$0.481^{+0.334}_{-0.293}$	$34.56^{+2.71}_{-7.32}$
K2-380 b	214419545.01	7	$9.401312^{+0.000596}_{-0.000506}$	$0.0189^{+0.001}_{-0.001}$	$2.729^{+0.186}_{-0.176}$	$2469.9354^{+0.0020}_{-0.0017}$	$0.883^{+0.024}_{-0.03}$	$15.19^{+1.58}_{-1.47}$
K2-381 b	217192839.02	7	$7.9389334^{+0.000596}_{-0.000592}$	$0.0146^{+0.001}_{-0.002}$	$1.075^{+0.142}_{-0.104}$	$2471.8440^{+0.0033}_{-0.0063}$	$0.505^{+0.311}_{-0.301}$	$31.05^{+4.25}_{-7.49}$
K2-381 c	217192839.01	7	$16.034656^{+0.001844}_{-0.001572}$	$0.0271^{+0.001}_{-0.001}$	$2.0^{+0.184}_{-0.148}$	$2471.2916^{+0.0030}_{-0.0027}$	$0.338^{+0.249}_{-0.221}$	$39.39^{+2.21}_{-5.33}$
K2-381 d	217192839.03	7	$26.803023^{+0.002775}_{-0.003048}$	$0.0229^{+0.002}_{-0.001}$	$1.689^{+0.18}_{-0.139}$	$2474.9152^{+0.0038}_{-0.0043}$	$0.497^{+0.225}_{-0.286}$	$59.43^{+7.25}_{-11.72}$
K2-382 b	217977895.01	7	$21.700156^{+0.002021}_{-0.001915}$	$0.0234^{+0.001}_{-0.001}$	$2.072^{+0.152}_{-0.133}$	$2481.3647^{+0.0045}_{-0.0036}$	$0.346^{+0.197}_{-0.213}$	$40.81^{+2.57}_{-4.03}$
K2-383 b	218668602.01	7	$1.865962^{+8.5e-05}_{-6.8e-05}$	$0.0178^{+0.001}_{-0.0}$	$1.564^{+0.118}_{-0.106}$	$2469.0928^{+0.0016}_{-0.0023}$	$0.268^{+0.211}_{-0.183}$	$7.77^{+0.35}_{-0.64}$
K2-384 b	220221272.05	8	$2.231527^{+0.000194}_{-0.000325}$	$0.0284^{+0.003}_{-0.012}$	$1.076^{+0.232}_{-0.06}$	$2560.7157^{+0.0045}_{-0.0075}$	$0.517^{+0.296}_{-0.295}$	$16.59^{+33.69}_{-3.33}$
K2-384 c	220221272.03	8	$4.194766^{+0.000309}_{-0.000189}$	$0.0314^{+0.003}_{-0.002}$	$1.191^{+0.053}_{-0.075}$	$2561.4158^{+0.0023}_{-0.0035}$	$0.446^{+0.345}_{-0.273}$	$24.63^{+3.74}_{-5.04}$
K2-384 d	220221272.02	8	$6.679582^{+0.000719}_{-0.000498}$	$0.0367^{+0.003}_{-0.002}$	$1.392^{+0.118}_{-0.075}$	$2559.4243^{+0.0042}_{-0.0039}$	$0.367^{+0.385}_{-0.265}$	$27.93^{+2.83}_{-5.65}$
K2-384 e	220221272.04	8	$9.715043^{+0.001003}_{-0.000739}$	$0.0354^{+0.004}_{-0.002}$	$1.345^{+0.139}_{-0.082}$	$2565.9666^{+0.0026}_{-0.0049}$	$0.471^{+0.33}_{-0.325}$	$38.39^{+5.44}_{-11.22}$
K2-384 f	220221272.01	8	$13.62749^{+0.000342}_{-0.000574}$	$0.0585^{+0.002}_{-0.001}$	$2.222^{+0.091}_{-0.082}$	$2559.6002^{+0.0009}_{-0.0012}$	$0.467^{+0.079}_{-0.072}$	$47.7^{+1.46}_{-1.42}$
K2-385 b	220459477.01	8	$2.380867^{+0.000161}_{-0.000216}$	$0.0185^{+0.001}_{-0.001}$	$1.539^{+0.145}_{-0.126}$	$2560.4544^{+0.0049}_{-0.0038}$	$0.361^{+0.213}_{-0.236}$	$10.07^{+0.72}_{-1.05}$
K2-386 b	220510874.01	8	$7.473223^{+0.000374}_{-0.000312}$	$0.0219^{+0.0}_{-0.0}$	$2.32^{+0.071}_{-0.067}$	$2562.9056^{+0.0024}_{-0.0025}$	$0.246^{+0.124}_{-0.154}$	$16.23^{+0.46}_{-0.58}$
K2-387 b	220696233.01	8	$28.735327^{+0.000992}_{-0.000994}$	$0.1146^{+0.002}_{-0.002}$	$7.322^{+0.268}_{-0.264}$	$2568.9787^{+0.0011}_{-0.0011}$	$0.711^{+0.03}_{-0.034}$	$55.42^{+2.09}_{-2.1}$
K2-388 b	245943455.01	12	$6.339069^{+0.000225}_{-0.000186}$	$0.0374^{+0.002}_{-0.001}$	$3.66^{+0.33}_{-0.229}$	$2908.7944^{+0.0017}_{-0.0017}$	$0.388^{+0.301}_{-0.248}$	$14.71^{+1.04}_{-3.11}$
K2-389 b	245991048.01	12	$8.584043^{+0.000888}_{-0.002026}$	$0.0185^{+0.001}_{-0.0}$	$2.184^{+0.118}_{-0.114}$	$2909.7820^{+0.0007}_{-0.0004}$	$0.32^{+0.25}_{-0.204}$	$20.68^{+1.38}_{-2.14}$
K2-389 c	245991048.02	12	$20.851337^{+0.002804}_{-0.002981}$	$0.0172^{+0.001}_{-0.001}$	$2.04^{+0.151}_{-0.138}$	$2914.1012^{+0.0050}_{-0.0055}$	$0.399^{+0.178}_{-0.243}$	$28.9^{+2.04}_{-3.02}$
K2-390 b	245995977.01	12	$3.312792^{+0.0001}_{-0.000104}$	$0.0442^{+0.002}_{-0.002}$	$4.662^{+0.313}_{-0.343}$	$2906.9029^{+0.0013}_{-0.0012}$	$0.893^{+0.018}_{-0.045}$	$5.51^{+0.93}_{-0.44}$
K2-391 b	246074314.01	12	$4.622654^{+0.000223}_{-0.000252}$	$0.0222^{+0.001}_{-0.001}$	$1.371^{+0.284}_{-0.188}$	$2908.5165^{+0.0017}_{-0.0017}$	$0.434^{+0.285}_{-0.297}$	$11.92^{+1.2}_{-2.64}$
K2-392 b	246084398.01	12	$15.398723^{+0.002422}_{-0.00193}$	$0.016^{+0.001}_{-0.001}$	$1.85^{+0.161}_{-0.154}$	$2906.6737^{+0.0037}_{-0.0091}$	$0.711^{+0.078}_{-0.116}$	$24.32^{+2.8}_{-2.86}$
K2-393 b	246429049.01	12	$10.413181^{+0.000932}_{-0.000697}$	$0.0201^{+0.001}_{-0.001}$	$2.352^{+0.175}_{-0.167}$	$2906.3926^{+0.0037}_{-0.0053}$	$0.803^{+0.045}_{-0.061}$	$18.38^{+2.1}_{-1.98}$
K2-394 b	246876040.01	13	$5.095717^{+0.000115}_{-0.000115}$	$0.0245^{+0.001}_{-0.001}$	$1.692^{+0.136}_{-0.126}$	$2992.2859^{+0.0010}_{-0.0012}$	$0.636^{+0.107}_{-0.171}$	$15.96^{+2.29}_{-2.08}$
K2-395 b	246891819.01	13	$4.803352^{+0.000335}_{-0.000466}$	$0.0304^{+0.001}_{-0.001}$	$2.597^{+0.192}_{-0.178}$	$2992.0089^{+0.0042}_{-0.0030}$	$0.25^{+0.206}_{-0.176}$	$14.44^{+0.51}_{-1.08}$
K2-395 c	246891819.02	13	$8.491282^{+0.000335}_{-0.000304}$	$0.0397^{+0.002}_{-0.002}$	$3.395^{+0.28}_{-0.257}$	$2990.5786^{+0.0016}_{-0.0016}$	$0.677^{+0.095}_{-0.119}$	$22.43^{+2.81}_{-3.05}$
K2-396 b	246953392.01	13	$0.673862^{+1.6e-05}_{-1.9e-05}$	$0.0157^{+0.0}_{-0.0}$	$1.579^{+0.114}_{-0.103}$	$2987.9636^{+0.0016}_{-0.0014}$	$0.266^{+0.206}_{-0.177}$	$3.29^{+0.14}_{-0.24}$
K2-396 c	246953392.02	13	$25.76051^{+0.001999}_{-0.001887}$	$0.0311^{+0.003}_{-0.001}$	$3.124^{+0.178}_{-0.112}$	$2996.4180^{+0.0018}_{-0.0018}$	$0.475^{+0.32}_{-0.301}$	$39.31^{+4.12}_{-12.04}$
K2-397 b	247383003.01	13	$3.572326^{+0.00018}_{-0.000155}$	$0.0229^{+0.001}_{-0.001}$	$2.417^{+0.187}_{-0.183}$	$2990.5751^{+0.0020}_{-0.0022}$	$0.892^{+0.029}_{-0.036}$	$10.11^{+1.3}_{-1.24}$
K2-398 b	248463350.01	14	$6.393025^{+0.001139}_{-0.00075}$	$0.0168^{+0.001}_{-0.001}$	$2.274^{+0.113}_{-0.111}$	$3076.0449^{+0.0042}_{-0.0048}$	$0.523^{+0.073}_{-0.086}$	$11.59^{+0.43}_{-0.46}$
K2-398 c	248463350.02	14	$18.787839^{+0.000877}_{-0.000993}$	$0.0377^{+0.001}_{-0.001}$	$5.098^{+0.154}_{-0.146}$	$3078.6845^{+0.0015}_{-0.0015}$	$0.701^{+0.028}_{-0.031}$	$23.55^{+0.92}_{-0.89}$
K2-399 b	248472140.01	14	$0.759978^{+1e-05}_{-1e-05}$	$0.0359^{+0.006}_{-0.003}$	$6.049^{+1.047}_{-0.481}$	$3073.2191^{+0.0006}_{-0.0006}$	$0.974^{+0.012}_{-0.008}$	$1.89^{+0.09}_{-0.09}$
K2-400 b	248518307.01	14	$3.865053^{+0.000186}_{-0.000182}$	$0.0279^{+0.001}_{-0.001}$	$1.163^{+0.051}_{-0.049}$	$3075.6234^{+0.0025}_{-0.0026}$	$0.208^{+0.165}_{-0.14}$	$19.12^{+0.79}_{-0.85}$
K2-401 b	248527514.01	14	$6.293099^{+0.000571}_{-0.000707}$	$0.0306^{+0.002}_{-0.002}$	$2.262^{+0.209}_{-0.192}$	$3073.9531^{+0.0067}_{-0.0048}$	$0.621^{+0.115}_{-0.223}$	$20.97^{+3.0}_{-2.66}$
K2-402 b	248621597.01	14	$17.27474^{+0.002593}_{-0.003175}$	$0.0192^{+0.001}_{-0.001}$	$2.678^{+0.213}_{-0.195}$	$3087.4286^{+0.0036}_{-0.0044}$	$0.468^{+0.165}_{-0.249}$	$23.11^{+2.15}_{-2.66}$
K2-403 b	248758353.01	14	$33.589979^{+0.000768}_{-0.000768}$	$0.0551^{+0.001}_{-0.002}$	$5.333^{+0.357}_{-0.387}$	$3075.9613^{+0.0014}_{-0.0011}$	$0.723^{+0.05}_{-0.147}$	$39.87^{+7.11}_{-3.12}$
K2-404 b	248861279.01	14	$13.115365^{+0.000443}_{-0.000609}$	$0.042^{+0.001}_{-0.001}$	$2.53^{+0.084}_{-0.083}$	$3084.8369^{+0.0010}_{-0.0008}$	$0.481^{+0.05}_{-0.06}$	$34.74^{+1.15}_{-1.08}$
K2-405 b	248874928.01	14	$3.435471^{+3.6e-05}_{-3.1e-05}$	$0.0548^{+0.001}_{-0.004}$	$4.569^{+0.085}_{-0.123}$	$3075.9959^{+0.0004}_{-0.0004}$	$0.871^{+0.02}_{-0.097}$	$6.33^{+4.28}_{-0.57}$
K2-406 b	249223471.01	15	$22.549406^{+0.001377}_{-0.001433}$	$0.0439^{+0.001}_{-0.001}$	$4.602^{+0.311}_{-0.292}$	$3177.3895^{+0.0025}_{-0.0023}$	$0.544^{+0.121}_{-0.255}$	$32.15^{+4.42}_{-3.45}$
K2-407 b	249403651.01	15	$4.941907^{+0.000661}_{-0.000696}$	$0.0127^{+0.001}_{-0.001}$	$1.283^{+0.097}_{-0.089}$	$3160.5101^{+0.0075}_{-0.0071}$	$0.309^{+0.209}_{-0.207}$	$12.77^{+0.86}_{-1.1}$

Table 4
(Continued)

Planet	Candidate ID	Camp	Period (days)	R_p/R_s	R_p ($R_\oplus$)	T_{mid} (2454833-JD)	b	a/R_s
K2-407 c	249403651.02	15	$9.22453^{+0.001322}_{-0.000911}$	$0.0134^{+0.0}_{-0.0}$	$1.36^{+0.096}_{-0.088}$	$3164.6545^{+0.0040}_{-0.0043}$	$0.259^{+0.207}_{-0.17}$	$18.76^{+1.03}_{-1.44}$
K2-408 b	249816490.01	15	$20.978959^{+0.001305}_{-0.001247}$	$0.0196^{+0.001}_{-0.0}$	$1.677^{+0.118}_{-0.109}$	$3158.5363^{+0.0039}_{-0.0042}$	$0.213^{+0.206}_{-0.154}$	$36.24^{+1.02}_{-2.4}$
K2-409 b	249924395.01	15	$1.908084^{+4.7e-05}_{-5.8e-05}$	$0.0185^{+0.001}_{-0.0}$	$2.482^{+0.174}_{-0.158}$	$3157.2841^{+0.0011}_{-0.0013}$	$0.418^{+0.167}_{-0.236}$	$5.32^{+0.41}_{-0.55}$

Note. Camp: the K2 campaign(s) in which our pipeline detected the signal.

TESS has smaller-aperture telescopes (10 cm) than K2 (1 m), and each TESS sector covers a shorter duration (27 days) than a K2 campaign (50–90 days), the additional data may be useful to, for instance, increase the observing baseline for potential transit timing variations.

3.1. EPIC 211399359

K2-371 b is a gas giant ($13.02^{+0.921}_{-0.868}$ $R_\oplus$) planet orbiting a moderately faint ($V = 14.65$ mag, $K_s = 12.39$ mag) K0V star (0.74 $R_\odot$, 0.96 $M_\odot$). This target was observed in Campaigns 5 and 18, and a short-period candidate, EPIC 211399359.01, was identified by Pope et al. (2016) and Barros et al. (2016) that we validate here. Planet b orbits at a distance of 0.041 au, with a period of 3.114905 days and an equilibrium temperature of ~1000 K. The host star has a clean, single-lined Keck/HIRES spectrum, and Keck/NIRC2 and Gemini/NIRI AO imaging which show no contaminating stellar companions. The vespa FPP value is 1.89×10^{-13}, without requiring use of the available contrast curves. The centroid p-value is 0.1241, which is consistent with the source of the transiting signal being on the target star. This planet falls into the range of Chen & Kipping (2017) with a degenerate mass–radius relation; taking a representative mass of ~1500 $M_\oplus$, we find a TSM of 8.0. This lies below the fourth quintile threshold of 96 for giant planets suggested by Kempton et al. (2018); however, the ESM value is ~38, well above the 7.5 threshold suggested in that paper (the predicted value of a single secondary eclipse of GJ 1132 b in the JWST MIRI LRS bandpass), indicating that it is potentially a good target for emission spectroscopy measurements.

3.2. EPIC 206135682

K2-368 is a moderately faint ($V = 13.54$ mag, $K_s = 11.04$ mag) K5V star (0.66 $R_\odot$, 0.75 $M_\odot$) orbited by a compact system of three super-Earth planets that was observed in Campaign 3. K2-368 b is a 1.332 $R_\oplus$ planet, orbiting at a distance of 0.052 au, with a period of 5.025598 days and an equilibrium temperature of ~800 K; it was first noted as EPIC 206135682.01 by Vanderburg et al. (2016) and Kruse et al. (2019). It has a vespa FPP value of 1.90×10^{-05} and a centroid p-value of 0.2070. Using the Chen & Kipping (2017) mass–radius relation predicts a mass of ~2.3 $M_\oplus$. K2-368 c is a 1.361 $R_\oplus$ planet, orbiting at a distance of 0.081 au, with a period of 9.660186 days and an equilibrium temperature of ~650 K; it was first noted as EPIC 206135682.03 by Kruse et al. (2019). It has a vespa FPP value of 2.46×10^{05} and a centroid p-value of 0.1385. Using the Chen & Kipping (2017) mass–radius relation predicts a mass of ~2.5 $M_\oplus$. K2-368 d is a 1.948 $R_\oplus$ planet, orbiting at a distance of 0.132 au, with a period of 20.201018 days and an equilibrium

temperature of ~500 K; it was first noted as EPIC 206135682.02 by Kruse et al. (2019). It has a vespa FPP value of 3.44×10^{05} and a centroid p-value of 0.3671. Using the Chen & Kipping (2017) mass–radius relation predicts a mass of ~4.6 $M_\oplus$. These mass estimates for the three planets result in challenging estimated RV semiamplitudes ($K = 1.1$ m s^{-1}, 0.91 m s^{-1} and 1.3 m s^{-1} for planets b, c, and d, respectively), and TSM (~1.7, ~1.4, ~11) and ESM (~0.6, ~0.3, ~0.3) values indicating they would be challenging atmospheric targets. We note that Kruse et al. (2019) also detected a longer-period candidate at 37.8 days that was not recovered by our pipeline.

Planets b and d lie close to the 4:1 mean motion resonance, having a period ratio of 4.0196. Planet c, in between, lies interior to the 2:1 resonance with b, and exterior to the 2:1 resonance with d. The TTVFaster code of Agol & Deck (2016) predicts transit timing variation (TTV) amplitudes for planets b, c, and d of 31 s, 89 s, and 18 s respectively, assuming circular orbits. This precision is well below the timing precision of individual K2 transits, given the 30 minutes observing cadence, however may be accessible with higher-cadence follow-up observations. If the orbits are noncircular, the amplitudes of these TTVs will increase; the amplitudes listed above should be considered lower limits.

3.3. EPIC 210797580

K2-370 b is a sub-Neptune (3.207 $R_\oplus$) planet orbiting a bright ($V = 11.11$ mag, $K_s = 9.24$ mag) G8V star (0.97 $R_\odot$, 0.98 $M_\odot$), observed in Campaign 13. It was first noted in Paper IV as EPIC 210797580.01; it orbits the star at a distance of 0.032 au, with a period of 2.140840 days and an equilibrium temperature of ~1420 K. This makes it the second hottest, second brightest known planet in the 3–4 $R_\oplus$ size range after K2-100 b. The host star has a clean, single-lined FLWO/TRES spectrum, and Keck/NIRC2 and WIYN/NESSI imaging which show no contaminating stellar companions. The vespa FPP value is 1.77×10^{-03}, using the three available contrast curves. The centroid p-value is 0.4204, which is consistent with the source of the transiting signal being on the target star. Using the Chen & Kipping (2017) mass–radius relation predicts a mass of ~10.4 $M_\oplus$. This would result in a measurable RV semiamplitude ($K \sim 5.2$ m s^{-1}), but predicts a TSM (~71) that is below the recommended level of interest for atmospheric follow-up recommended by Kempton et al. (2018). However, due to the planet's high temperature, the ESM is predicted to be ~10, above 7.5 (the predicted value of a single secondary eclipse of GJ 1132 b in the JWST MIRI LRS bandpass), indicating that it is potentially a good target for emission spectroscopy measurements.

Table 5
Estimated Values and Metrics for the Newly Validated Planets

Planet	Candidate ID	T_{eq} (K)	M_p ($M_\oplus$)	K (m s^{-1})	TSM	ESM
K2-365 b	204750116.01	~710	8.65 ± 5.47	2.20 ± 1.50	22.2	1.26
K2-366 b	205111664.01	~770	6.34 ± 3.66	1.83 ± 1.15	18.2	1.14
K2-367 b	206055981.01	~450	6.47 ± 4.02	1.82 ± 1.22	14.6	0.41
K2-368 b	206135682.01	~800	2.34 ± 1.34	1.06 ± 0.66	1.7	0.58
K2-368 c	206135682.02	~650	2.49 ± 1.31	0.91 ± 0.53	1.4	0.35
K2-368 d	206135682.03	~500	4.64 ± 2.73	1.32 ± 0.85	10.9	0.31
K2-369 b	206146957.01	~1080	2.2 ± 1.3	0.96 ± 0.62	2.3	0.82
EPIC 206317286 c	206317286.01	~570	5.37 ± 3.13	1.49 ± 0.95	7.6	0.32
K2-370 b	210797580.01	~1420	10.42 ± 6.6	5.22 ± 3.55	71.1	9.92
K2-371 b	211399359.01	~1000	~1500	~700	8.0	37.84
K2-372 b	211490999.01	~870	9.2 ± 5.37	3.07 ± 1.80	12.6	1.01
K2-373 b	211539054.01	~1130	5.15 ± 2.85	1.34 ± 0.81	13.9	1.02
K2-374 b	211732116.01	~1210	3.62 ± 1.87	1.72 ± 0.90	9.7	0.75
K2-374 c	211732116.02	~790	5.71 ± 3.48	1.77 ± 1.08	10.8	0.58
K2-375 b	212006318.01	~1000	5.83 ± 3.37	1.42 ± 0.89	4.3	0.31
K2-376 b	212222383.01	~1240	4.1 ± 2.36	1.56 ± 0.98	20.6	1.61
K2-377 b	212530118.01	~530	3.93 ± 2.34	1.22 ± 0.79	7.7	0.31
K2-389 b	212575828.01	~1130	9.02 ± 5.52	4.78 ± 3.18	11.6	1.55
K2-379 b	214173069.01	~680	5.59 ± 3.33	1.92 ± 1.24	16.6	1.03
K2-380 b	214419545.01	~1110	7.96 ± 4.6	2.42 ± 1.52	19.4	1.79
K2-381 b	217192839.02	~670	1.28 ± 0.83	0.39 ± 0.27	1.7	0.34
K2-381 c	217192839.01	~530	5.04 ± 3.01	1.95 ± 1.27	14.9	0.57
K2-381 d	217192839.03	~440	3.85 ± 2.25	0.99 ± 0.63	9.7	0.20
K2-382 b	217977895.01	~610	5.15 ± 3.23	1.25 ± 0.84	10.2	0.37
K2-383 b	218668602.01	~1270	3.26 ± 1.66	1.63 ± 0.92	18.4	1.70
K2-384 b	220221272.05	~600	1.28 ± 0.83	0.72 ± 0.47	6.3	1.44
K2-384 c	220221272.03	~480	1.72 ± 0.86	1.22 ± 0.61	5.1	0.83
K2-384 d	220221272.02	~410	2.71 ± 1.4	2.25 ± 1.16	4.4	0.60
K2-384 e	220221272.04	~370	2.39 ± 1.36	1.50 ± 0.85	4.1	0.35
K2-384 f	220221272.01	~330	5.71 ± 3.33	5.85 ± 3.41	45.6	0.54
K2-385 b	220459477.01	~1100	3.2 ± 1.79	1.61 ± 0.99	7.5	0.66
K2-386 b	220510874.01	~1010	6.21 ± 3.66	2.16 ± 1.28	11.5	0.87
K2-387 b	220696233.01	~340	45.46 ± 31.68	13.80 ± 9.65	23.1	0.83
K2-388 b	245943455.01	~970	13.1 ± 8.36	5.08 ± 3.48	30.3	3.33
K2-389 b	245991048.01	~1050	5.65 ± 3.3	2.04 ± 1.30	16.4	1.24
K2-389 c	245991048.02	~780	5.26 ± 2.73	1.42 ± 0.82	10.7	0.55
K2-390 b	245995977.01	~1310	20.24 ± 12.4	10.17 ± 6.73	30.3	5.63
K2-391 b	246074314.01	~900	2.49 ± 1.71	1.15 ± 0.84	3.3	1.06
K2-392 b	246084398.01	~840	4.45 ± 2.52	1.28 ± 0.79	6.4	0.36
K2-393 b	246429049.01	~950	6.34 ± 4.06	2.02 ± 1.39	15.6	1.16
K2-394 b	246876040.01	~890	3.93 ± 2.03	2.39 ± 1.37	29.6	2.46
K2-395 b	246891819.01	~910	7.64 ± 4.5	2.99 ± 1.91	16.4	1.70
K2-395 c	246891819.02	~750	11.81 ± 7.02	3.82 ± 2.47	19.8	1.83
K2-396 b	246953392.01	~1990	3.4 ± 1.94	2.56 ± 1.60	18.4	2.31
K2-396 c	246953392.02	~590	10.0 ± 6.01	2.23 ± 1.46	14.6	0.69
K2-397 b	247383003.01	~1210	6.74 ± 4.06	2.94 ± 1.92	28.4	3.06
K2-398 b	248463350.01	~1240	6.08 ± 3.59	2.17 ± 1.29	7.7	0.68
K2-398 b	248463350.02	~870	23.41 ± 13.1	5.85 ± 3.29	14.5	1.64
K2-399 b	248472140.01	~2780	32.28 ± 22.16	26.62 ± 18.49	51.7	16.63
K2-400 b	248518307.01	~570	1.65 ± 0.8	1.29 ± 0.63	4.0	0.97
K2-401 b	248527514.01	~660	5.83 ± 3.73	2.22 ± 1.53	15.3	1.07
K2-402 b	248621597.01	~870	7.8 ± 4.74	2.00 ± 1.32	7.4	0.52
K2-403 b	248758353.01	~580	24.91 ± 16.38	5.81 ± 4.08	33.0	2.16
K2-404 b	248861279.01	~450	7.33 ± 4.06	2.95 ± 1.64	19.9	0.76
K2-405 b	248874928.01	~980	18.63 ± 10.87	7.72 ± 4.90	59.5	9.65
K2-406 b	249223471.01	~720	20.04 ± 12.4	5.27 ± 3.51	89.8	7.82
K2-407 b	249403651.01	~1110	2.11 ± 1.14	0.86 ± 0.51	1.8	0.68
K2-407 c	249403651.02	~900	2.49 ± 1.4	0.83 ± 0.51	1.5	0.49
K2-408 b	249816490.01	~610	3.89 ± 1.99	1.04 ± 0.59	12.4	0.44
K2-409 b	249924395.01	~1800	6.74 ± 4.06	3.77 ± 2.45	17.7	2.21

Planet	TESS Sector(s)	Planet	TESS Sector(s)
K2-367/EPIC 206055981	S42	K2-390/EPIC 245995977	S2, S29, S42
K2-368/EPIC 206135682	S42	K2-391/EPIC 246074314	S42
K2-369/EPIC 206146957	S42	K2-392/EPIC 246084398	S42
EPIC 206317286	S42	K2-393/EPIC 246429049	S42, S43, S44
K2-370/EPIC 210797580	S43, S44	K2-395/EPIC 246891819	S43, S44
K2-371/EPIC 211399359	S7, S34, S44–S46	K2-396/EPIC 246953392	S43, S44
K2-372/EPIC 211490999	S44–S46	K2-397/EPIC 247383003	S43, S44, S45
K2-373/EPIC 211539054	S7, S34, S44–S46	K2-398/EPIC 248463350	S45, S46
K2-374/EPIC 211732116	S44–S46	K2-399/EPIC 248472140	S35, S45, S46
K2-375/EPIC 212006318	S44–S46	K2-400/EPIC 248518307	S8, S35, S45, S46
K2-376/EPIC 212222383	S21, S44–S46	K2-401/EPIC 248527514	S8, S35, S45, S46
K2-384/EPIC 220221272	S3, S30, S42, S43	K2-402/EPIC 248621597	S45, S46
K2-385/EPIC 220459477	S42	K2-403/EPIC 248758353	S45, S46
K2-386/EPIC 220510874	S42, S43	K2-404/EPIC 248861279	S45, S46
K2-387/EPIC 220696233	S42, S45	K2-405/EPIC 248874928	S45, S46
K2-388/EPIC 245943455	S2, S29, S42	K2-406/EPIC 249223471	S11, S38
K2-389/EPIC 245991048	S2, S29, S42		
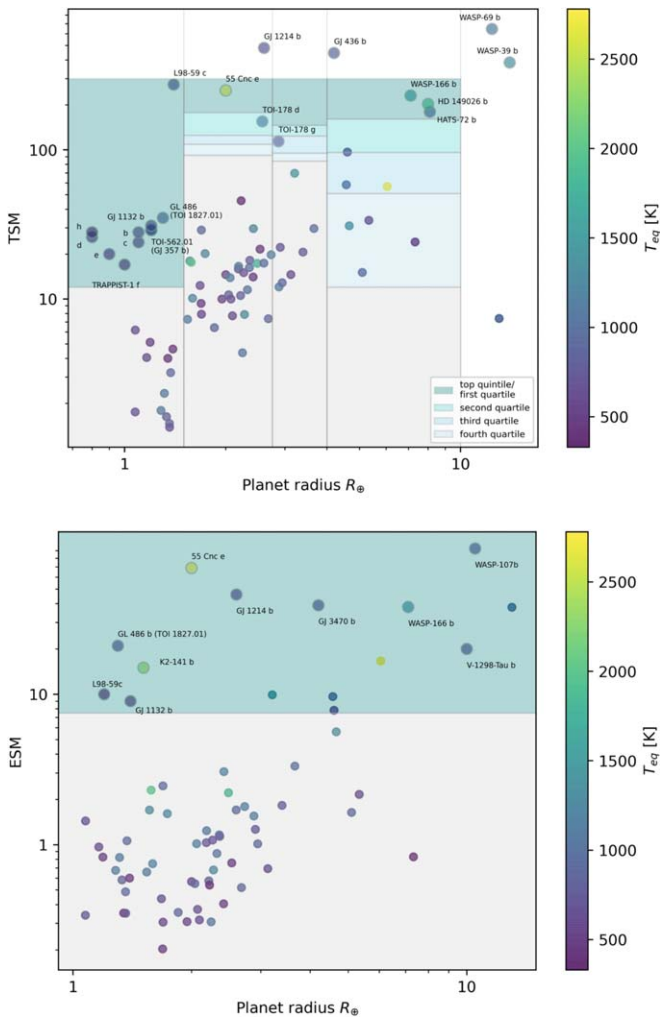
Figure 2. Transmission spectroscopy values (top) and emission spectroscopy values (bottom) for the newly validated planets (small points) and planets slated for observation in JWST Cycle 1 (large points), color-coded by their equilibrium temperature. In each case the shaded regions indicate areas of interest as identified by Kempton et al. (2018).

3.4. EPIC 217192839

K2-381 is a multiplanet system consisting of an Earth-sized planet (b; $1.075\,R_\oplus$), a sub-Neptune (c; $2.000\,R_\oplus$), a super-Earth (d; $1.689\,R_\oplus$), and a sub-Earth-sized candidate (.04; $0.758\,R_\oplus$). The host star is a moderately faint ($V = 13.01$ mag, $K_s = 10.30$ mag) K5V star ($0.68\,R_\odot$, $0.75\,M_\odot$), which was observed in Campaign 7. Planet b, noted as candidate EPIC 217192839.02 in Mayo et al. (2018) and Kruse et al. (2019), orbits the star at a distance of 0.071 au, with a period of 7.938933355 days and an equilibrium temperature of ∼670 K; at $1.075\,R_\oplus$, it is the smallest planet validated in this paper. Planet c, noted as candidate EPIC 217192839.01 in Mayo et al. (2018), Petigura et al. (2018), Kruse et al. (2019), and Zink et al. (2019), orbits the star at a distance of 0.113 au, with a period of 16.034656 days and an equilibrium temperature of ∼530 K. Planet d, noted as candidate EPIC 217192839.03 in Mayo et al. (2018) and Kruse et al. (2019), orbits the star at a distance of 0.160 au, with a period of 26.803023 days and an equilibrium temperature of ∼440 K. In addition, our pipeline identified a tentative fourth candidate, EPIC 217192839.04, with a period of 40.934141 days and a radius of $0.758\,R_\oplus$. Using the Chen & Kipping (2017) mass–radius relation results in masses of ∼$1.3\,M_\oplus$, ∼$5.0\,M_\oplus$, and ∼$3.9\,M_\oplus$ for planets b, c, and d respectively, with challenging RV semiamplitudes and low prospects for atmospheric follow-up.

K2-381 has a clean, single-lined FLWO/TRES spectrum, and both Gemini/NIRI AO and Gemini/DSSI speckle imaging which show no contaminating stellar companions. The vespa FPP values for planets b, c, and d are 8.22×10^{-03}, 1.46×10^{-05}, and 1.16×10^{-03}, respectively, using the available contrast curves. The centroid p-values are 0.2215, 0.3334, and 0.2891, which are consistent with the source of the transiting signal being on the target star. The tentative fourth candidate at ∼41 days does not meet our validation criteria (having an FPP of 2.56%), likely due to its low S/N.

Planets c and d lie within 0.3% of the 5:3 mean motion resonance. Figure 10 shows the location and analytically estimated widths of the 5:3 and 7:4 mean motion resonances
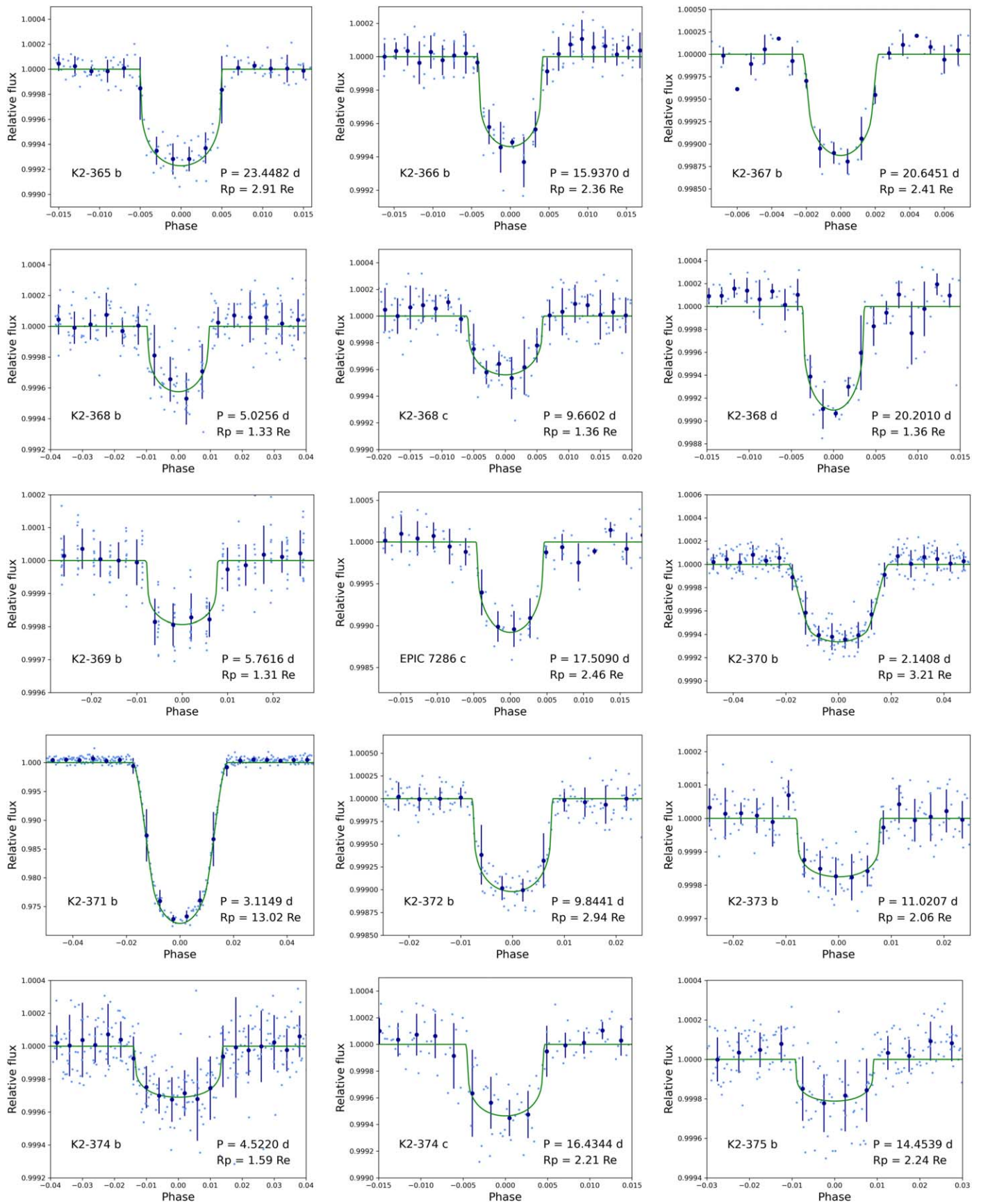
Figure 3. Validated planet folded light curves. The solid green line is the best-fit transit model; the large blue points are binned observations.
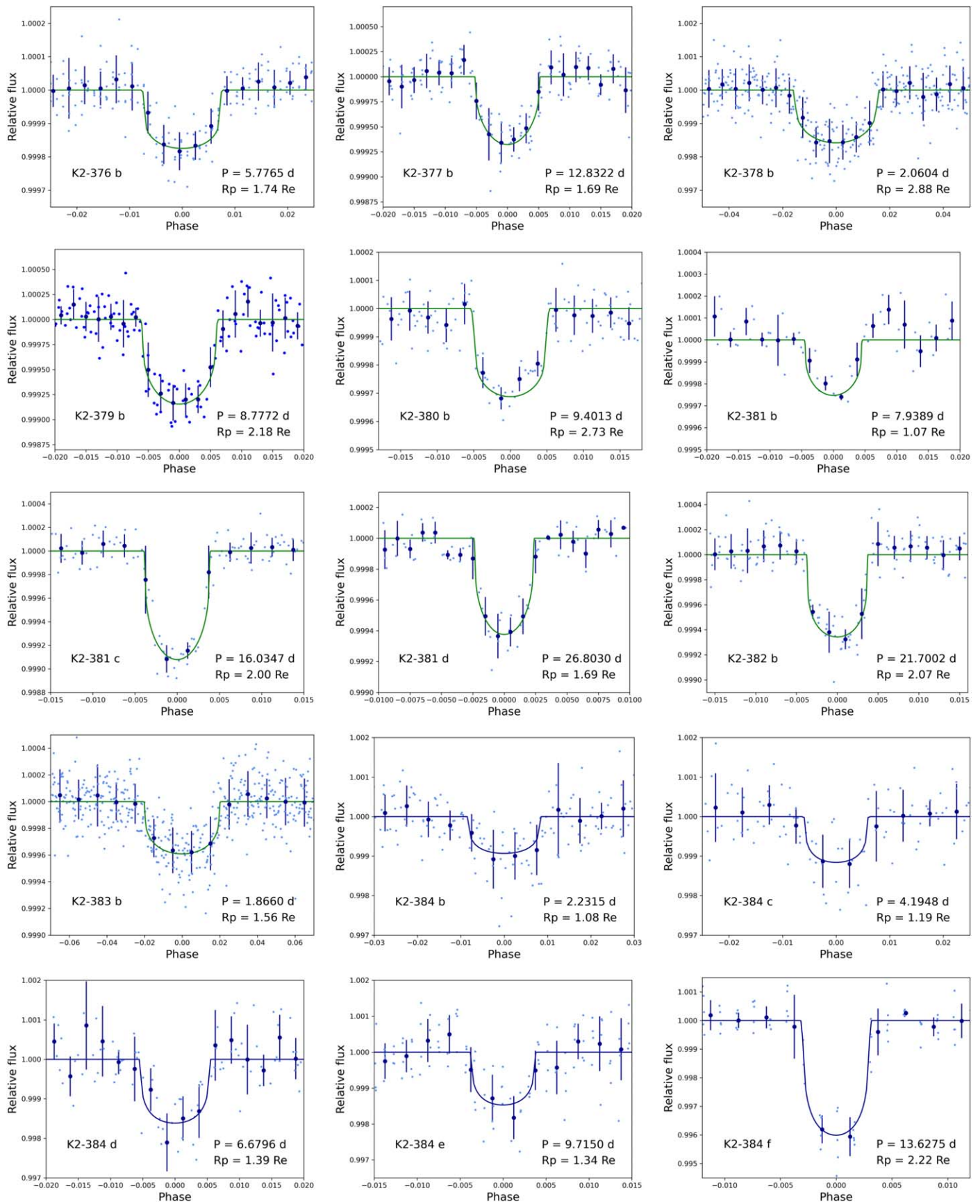
Figure 4. Validated planet folded light curves. Description as for Figure 3.
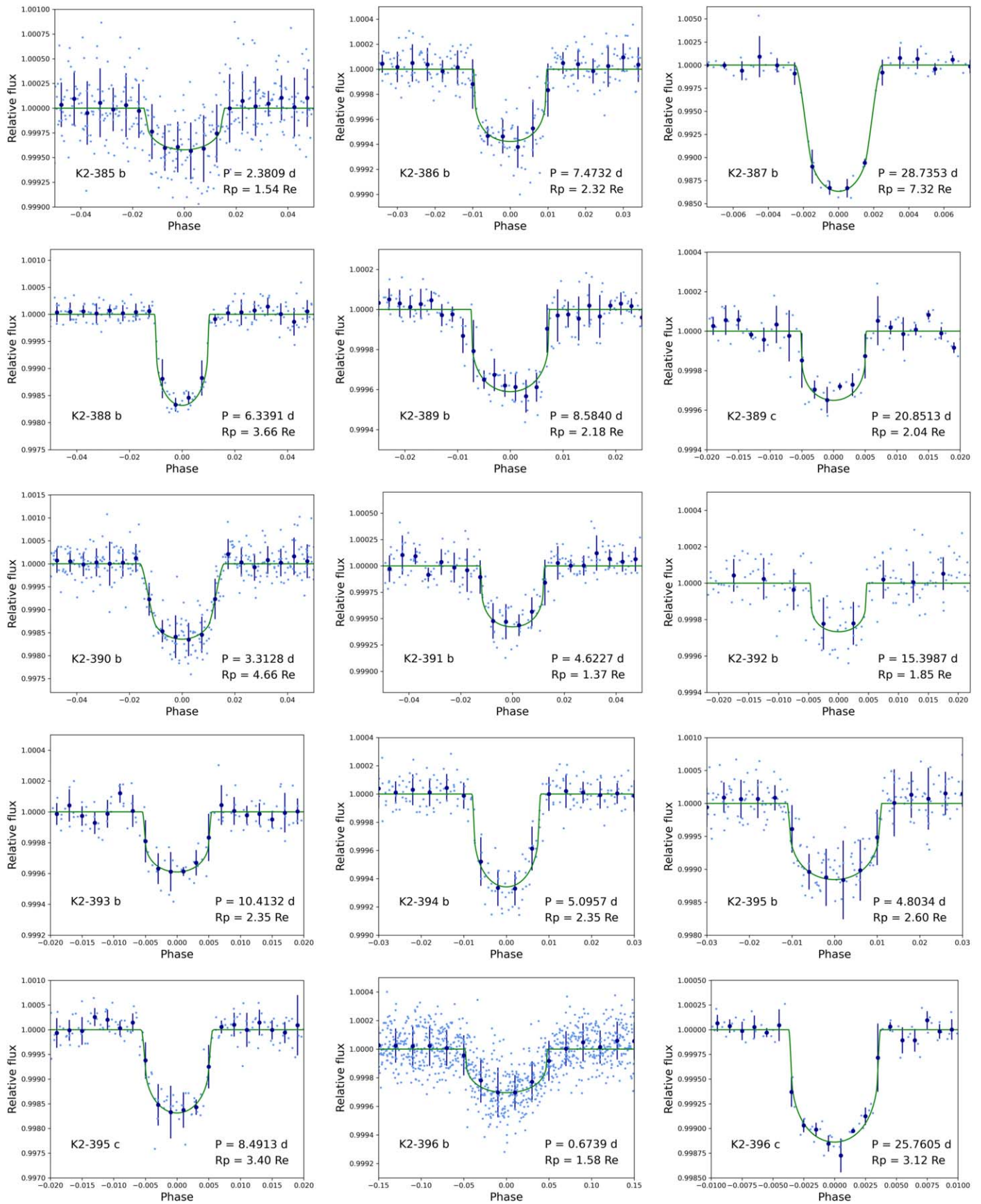
Figure 5. Validated planet folded light curves. Description as for Figure 3.
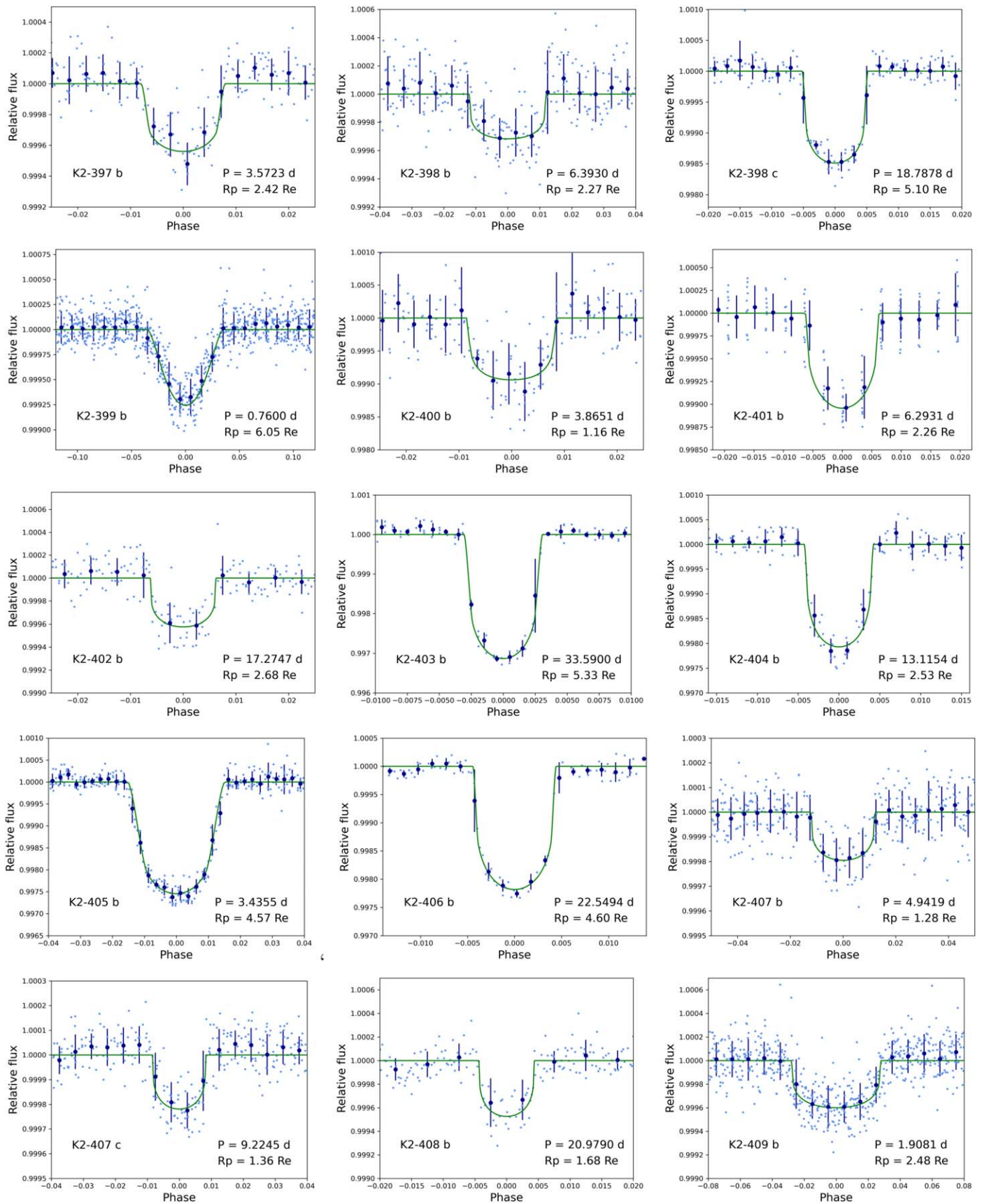
Figure 6. Validated planet folded light curves. Description as for Figure 3.
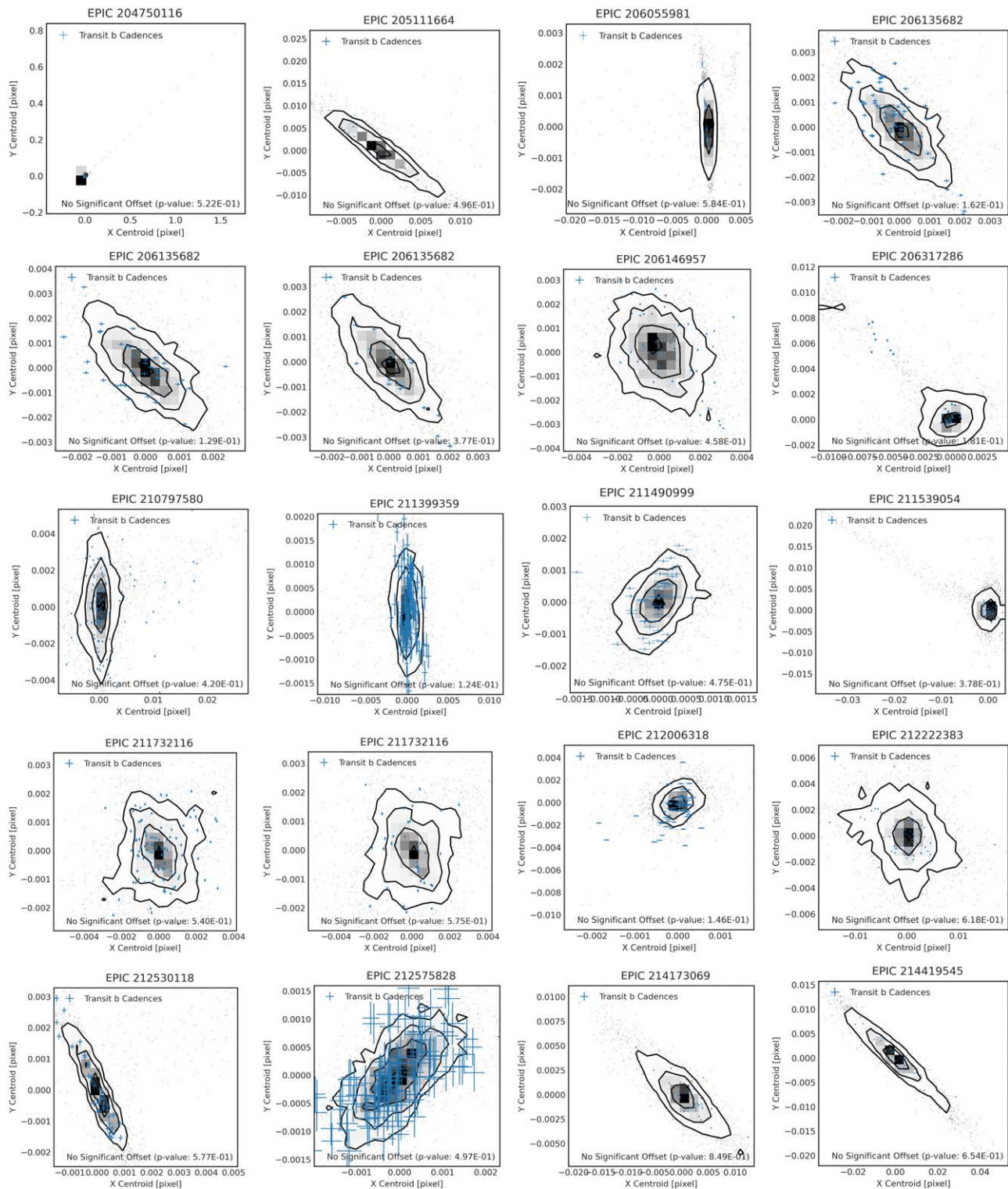
Figure 7. Validated planet centroid plots. The contours show the 1σ, 2σ, and 3σ contours for the centroid locations for out-of-transit cadences; the gray points show the remaining out-of-transit centroid locations that fall outside those contours. The blue points are the centroid locations of the in-transit cadences.

for K2-381 c and d, using the program from Volk & Malhotra (2020),[50] as in Hardegree-Ullman et al. (2021). For any modestly nonzero eccentricity, the planets are in resonance; having no constraints on the eccentricity from the light curve itself, we content ourselves with claiming they are near-resonant. Assuming circular orbits, the TTVFaster package (Agol & Deck 2016) predicts transit timing variations with amplitudes of 1.4 minutes for planet c and 1.8 minutes for planet d; increasing the eccentricity to 0.2 increases these to 24 and 54 minutes. Planets c and d are also both in the radius valley (Fulton et al. 2017), making an attempt to constrain their bulk density with masses derived by transit timing variations a potentially valuable prospect.

---

[50] https://github.com/katvolk/analytical-resonance-widths
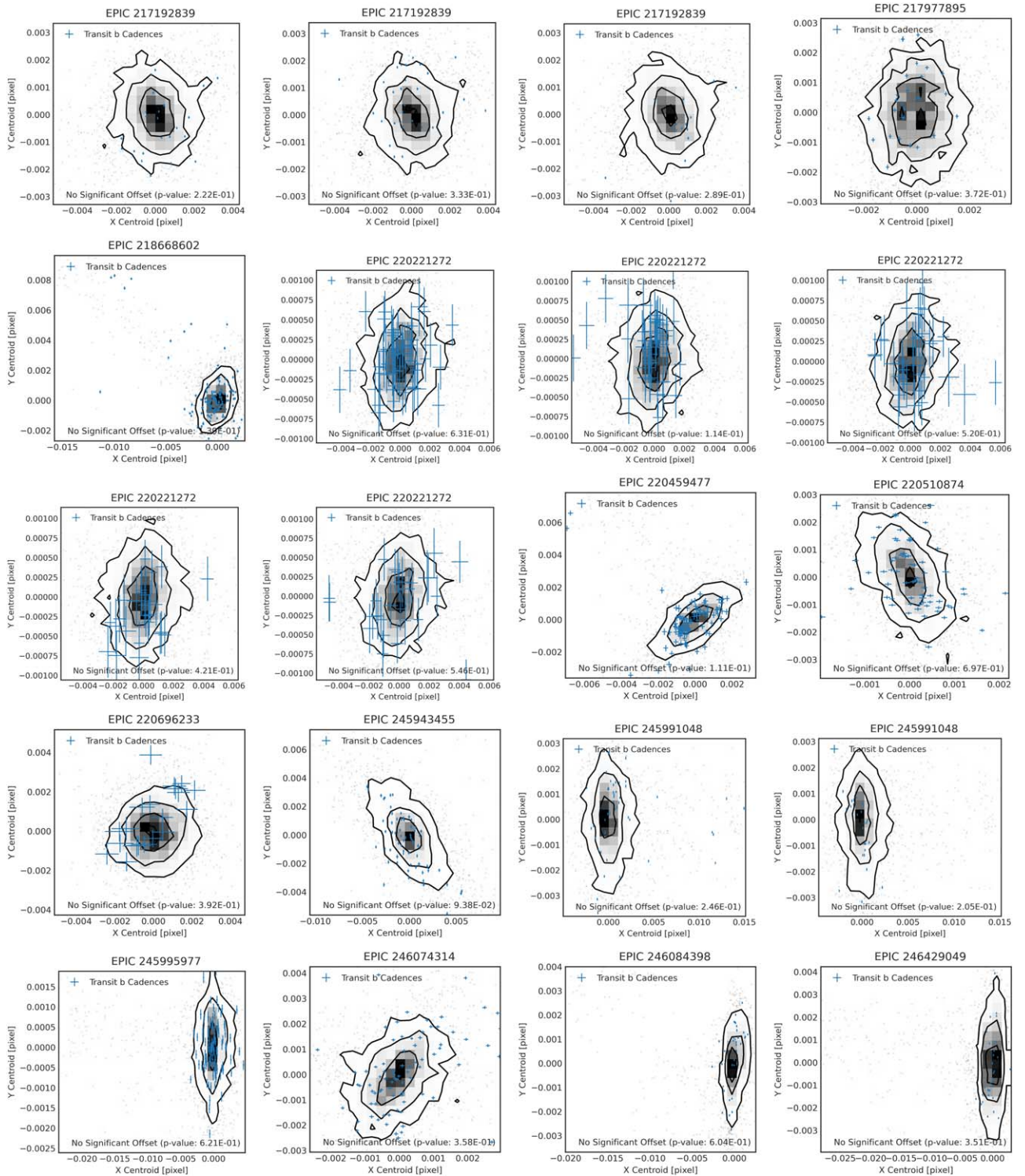
Figure 8. Validated planet centroid plots. Description as for Figure 7.

3.5. EPIC 220221272

K2-384 is a moderately faint (Kepmag = 14.26 mag, K_s = 11.29 mag) M4V star (0.348 $R_\odot$, 0.330 $M_\odot$) that was observed in Campaign 8. It hosts a compact system of five planets, ranging from Earth- to sub-Neptune-sized, including multiple pairs close to or in mean motion resonances. Planet b has a period of 2.231527 days and a radius of 1.076 $R_\oplus$; planet c has a period of 4.194766 days and a radius of 1.191 $R_\oplus$;

planet d has a period of 6.679581 days and a radius of 1.392 $R_\oplus$; planet e has a period of 9.715043 days and a radius of 1.345 $R_\oplus$; and planet f has a period of 13.627490 days and a radius of 2.222 $R_\oplus$. The planets range in equilibrium temperature from 330–600 K, and, using the Chen & Kipping (2017) mass–radius relation, in mass from ∼1.3–5.7 $M_\oplus$. The host star has a clean, single-lined IRTF/SpeX spectrum, and WIYN/ NESSI speckle imaging at both 562 nm and 832 nm that show no contaminating stellar companions. The vespa FPP values
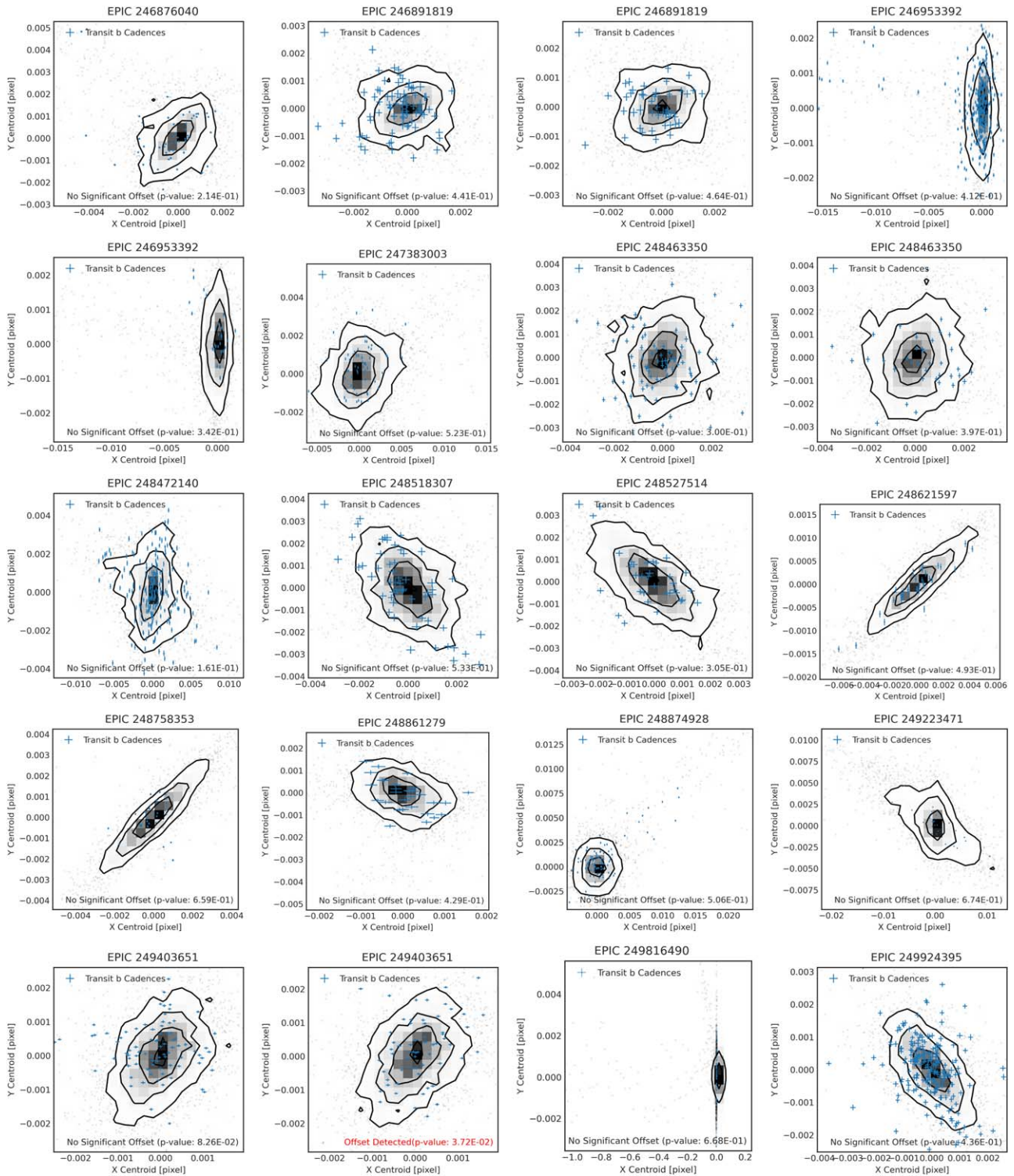
Figure 9. Validated planet centroid plots. Description as for Figure 7.

are 7.20×10^{-3}, 6.57×10^{-4}, 3.14×10^{-4}, 3.85×10^{-3}, and 1.12×10^{-4} for planets b–f, respectively, using the available contrast curves and the Campaign 8 multiplicity boost. The centroid *p*-values are 0.6315, 0.1135, 0.5203, 0.4207, and 0.5460, respectively.

Figure 11 shows the proximity of the observed period ratios to the location and analytically estimated widths of the resonances in the system; planets b and c are close to the 3:1 resonance, planets c and d are close to the 8:5 resonance, and

planets e and f are in the 7:5 resonance. This is reminiscent of other compact systems with chains of resonances and near-resonances, such as TRAPPIST-1 (Gillon et al. 2017) and K2-138 (Christiansen et al. 2018). Assuming circular orbits, the TTVFaster package (Agol & Deck 2016) predicts transit timing variations with amplitudes of 0.28, 0.83, 3.33, 12.26, and 3.97 minutes for planets b–f, respectively. Planet e, being somewhat smaller than planet f in the 7:5 resonance, is predicted to exhibit the largest transit timing variations, which
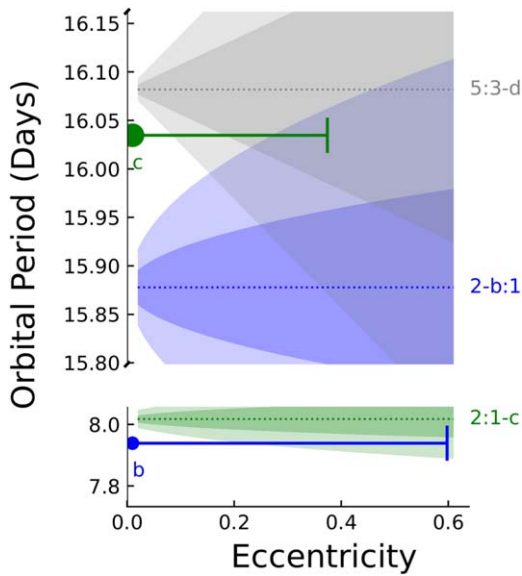
Figure 10. Resonance locations in the K2-381 system. The orbital period is shown on the y-axis and eccentricity is on the x-axis; note that the y-axes of the two subplots are discontinuous and not to scale. The locations of planets b and c are shown with green and blue circles, respectively, and the solid horizontal lines extend to the eccentricity at which each planet would cross the next planet's orbit. The shaded regions show, as a function of eccentricity, the location and analytically estimated widths of the 2:1 mean motion resonance for planets b and c, and the 5:3 mean motion resonance for planets c and d; the label "5:3-d" indicates, for instance, that a test particle at that location would complete three orbits in the same amount of time that planet c takes to complete five orbits. The shaded regions surrounding each resonance line are the resonance widths corresponding to the lower (dark shading) and upper (light shading) planet mass limits, as propagated from the uncertainty on the planets' radii.

would be detectable for a number of facilities (e.g., Palomar/ WIRC; Vissapragada et al. 2020), but difficult to discern in the 30 minutes cadence K2 data. Given the magnitude of the target and the small nature of the planets, these would be challenging RV measurements, with predicted amplitudes ranging from 0.7–5.9 m s^{-1}, but potentially a worthwhile investment. Although this is a slightly fainter target than TRAPPIST-1 ($K_s = 11.29$ mag compared to $K_s = 10.30$), and a larger host star, the transmission spectroscopy metric for planet f ($\sim$46) is higher than the values for the most promising TRAPPIST-1 planets (20–26 for planets c, d, and e). Indeed, the K2-384 system is one of the closest analogs to the TRAPPIST-1 system that has been found, as the only other M dwarfs hosting five or more transiting planets—Kepler-186 (Quintana et al. 2014) and Kepler-296 (Barclay et al. 2015)—are early M dwarfs (0.472 $R_\odot$ and 0.480 $R_\odot$, respectively), where K2-384 is a mid-M dwarf (0.348 $R_\odot$) and TRAPPIST-1 is a late-M dwarf (0.119 $R_\odot$).

3.6. EPIC 220696233

K2-387 b is a sub-Saturn (7.322 $R_\oplus$) planet orbiting a faint ($V = 16.22$ mag, $K_s = 12.29$ mag) M1V star that was observed in Campaign 8. It orbits the star at a distance of 0.152 au, with a period of 28.735327 days. With an equilibrium temperature of $\sim$340 K, it is the coolest planet validated in this work. It was previously noted as EPIC 220696233.01 by Petigura et al. (2018) and Kruse et al. (2019). The host star has a clean, single-lined IRTF/SpeX spectrum, and both Palomar AO
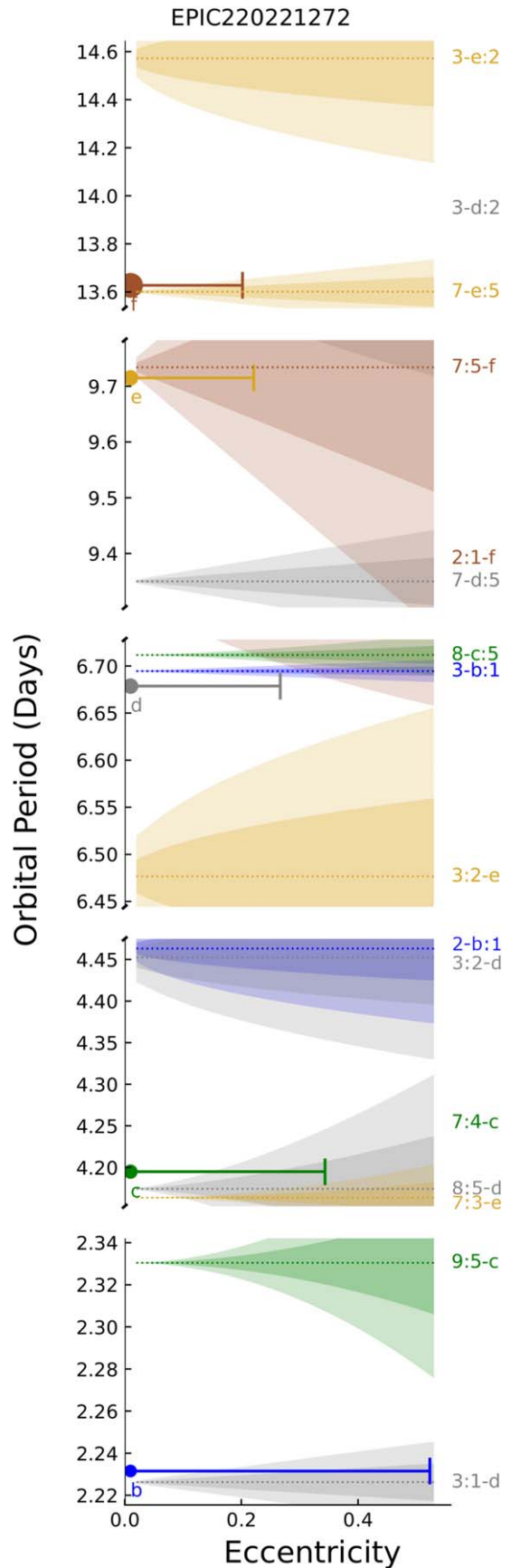
Figure 11. The location and analytically estimated widths of the low-order mean motion resonances in the K2-384 system. See Figure 10 for a description.

imaging and WIYN/NESSI speckle imaging that show no contaminating stellar companions. The vespa FPP value is 3.33×10^{-10} using the available contrast curves. The centroid p-value is 0.3918, which is consistent with the source of the transiting signal being on the target star. Using the Chen & Kipping (2017) mass–radius relation predicts a mass of $\sim 45\,M_\oplus$. This would result in a measurable RV semiamplitude ($K \sim 14$ m s^{-1}), although the star is very faint. The estimated planet mass produces a predicted TSM value (~ 23) in the fourth quartile of interest for atmospheric follow-up as defined by Kempton et al. (2018), and an ESM value (~ 0.8) that is below the recommended threshold. However, we note that K2-387 b occupies a relatively unpopulated region of period–radius parameter space (see Figure 1). There are few cool (<500 K) gas giant planets known, and even fewer orbiting cool host stars. The TSM value is one of the most favorable for known planets in this size and temperature regime.

3.7. EPIC 245995977

K2-390 is a moderately faint ($V = 13.57$ mag, $K_s = 11.72$ mag) G4V star ($0.97\,R_\odot$, $0.79\,M_\odot$) that was observed in Campaign 12. It is orbited by a Neptune-sized planet on the edge of the hot Neptune desert that was first noted in Paper IV. K2-390 b is a $4.662\,R_\oplus$ planet, orbiting at a distance of 0.040 au, with a period of 3.312792 days and an equilibrium temperature of ~ 1310 K. The host star has a clean, single-lined Keck/HIRES spectrum, and Gemini/NIRI and Palomar/PHARO AO imaging that show no contaminating stellar companions. The vespa FPP value is 8.68×10^{-8}, using the available contrast curves. The centroid p-value is 0.6208, which is consistent with the source of the transiting signal being on the target star. Using the Chen & Kipping (2017) mass–radius relation predicts a mass of $\sim 20\,M_\oplus$. This would result in a readily measurable RV semiamplitude ($K \sim 10.2$ m s^{-1}), and predicts a TSM value (~ 30) that puts K2-390 b in the fourth quartile for atmospheric follow-up priority according to the thresholds in Kempton et al. (2018). The ESM value (~ 5.7) is comparable to but below the 7.5 threshold for atmospheric follow-up recommended by Kempton et al. (2018).

3.8. EPIC 246876040

K2-394 is a moderately bright ($V = 12.72$ mag, $K_s = 9.57$ mag) G8V star ($0.63\,R_\odot$, $0.48\,M_\odot$) that was observed in Campaign 13. It is orbited by a super-Earth-sized planet, K2-394 b, which was previously noted as EPIC 246876040.01 by Zink et al. (2019). It is a $1.692\,R_\oplus$ planet, orbiting at a distance of 0.045 au, with a period of 5.095717 days and an equilibrium temperature of ~ 890 K. The host star has a clean, single-lined FLWO/TRES spectrum, and WIYN/NESSI speckle imaging at 562 nm and 832 nm that show no contaminating stellar companions. The vespa FPP value is 4.38×10^{-4}, using the available contrast curves. The centroid p-value is 0.2143, which is consistent with the source of the transiting signal being on the target star. Using the Chen & Kipping (2017) mass–radius relation predicts a mass of $\sim 3.9\,M_\oplus$. This would result in a measurable RV semiamplitude ($K \sim 2.4$ m s^{-1}), but predicts TSM (~ 30) and ESM (~ 2.4) values that indicate atmospheric follow-up would be challenging, compared to the thresholds recommended by Kempton et al. (2018). Given its

relatively small size and relatively small host star, the TSM value does make it somewhat comparable to other close-in super-Earth planets, such as LTT 1445 A b (TSM ~ 40; Winters et al. 2019) and L 98–59 c (TSM ~ 34; Demangeon et al. 2021).

3.9. EPIC 248463350

K2-398 is a moderately faint ($V = 13.15$ mag, $K_s = 11.72$ mag) G2V star ($1.24\,R_\odot$, $0.95\,M_\odot$) that was observed in Campaign 14. It is orbited by two rather disparately sized planets that were first noted in Paper IV. K2-398 b is a $2.274\,R_\oplus$ sub-Neptune-sized planet, orbiting at a distance of 0.066 au, with a period of 6.393025 days and an equilibrium temperature of ~ 1240 K. K2-398 c is a $5.098\,R_\oplus$ Neptune-sized planet, orbiting at a distance of 0.136 au, with a period of 18.787839 days and an equilibrium temperature of ~ 870 K. The host star has clean, single-lined Keck/HIRES and FLWO/TRES spectra, and Keck/NIRC2 AO imaging and WIYN/NESSI speckle imaging at 562 nm and 832 nm that show no contaminating stellar companions. Planets b and c have vespa FPP values of 4.80×10^{-4} and 2.43×10^{-4}, respectively, using the available contrast curves and the C14 multiplicity boost. The centroid p-values are 0.3000 and 0.3974, respectively, which is consistent with the source of the transiting signals being on the target star. For K2-398 b the Chen & Kipping (2017) mass–radius relation predicts a mass of $\sim 6.1\,M_\oplus$. This would result in a measurable RV semiamplitude ($K \sim 2.2$ m s^{-1}), but predicts TSM (~ 7.7) and ESM (~ 0.7) values that indicate atmospheric follow-up would be challenging, compared to the thresholds recommended by Kempton et al. (2018). For K2-398 c the Chen & Kipping (2017) mass–radius relation predicts a mass of $\sim 23\,M_\oplus$. This would result in a measurable RV semiamplitude ($K \sim 5.9$ m s^{-1}), and predicts a TSM value (~ 15) that puts K2-398 c in the fourth quartile of atmospheric follow-up priority according to the thresholds in Kempton et al. (2018). The ESM value (~ 1.6) indicates that atmospheric follow-up would be challenging. Given the proximity of the planets to the 3:1 mean motion resonance we investigated further with the analytic code of Volk & Malhotra (2020), but do not find the planets to plausibly be in resonance.

3.10. EPIC 248472140

K2-399 b is an USP sub-Saturn ($6.049\,R_\oplus$) planet orbiting a moderately bright ($V = 12.48$ mag, $K_s = 10.93$ mag) F9V star ($1.54\,R_\odot$, $0.78\,M_\odot$), observed in Campaign 14. It was first noted in Paper IV; it orbits the star at a very close distance of 0.015 au, less than twice the stellar radius above the stellar surface, with a period of 0.759989 day. With a correspondingly very high equilibrium temperature of ~ 2780 K, it is the hottest validated planet in this analysis, and the hottest planet between the size of Neptune and Jupiter discovered to date. It's uniqueness is illustrated in the right panel of Figure 1; the single nearby planet in the figure is Kepler 1520 b, which is 500 K cooler and 3.5 mag fainter. This means that K2-399 b may be an excellent probe of the ways in which atmospheres of planets in this size range respond to incredibly high insolation fluxes. Dai et al. (2021) note that USP Neptunes are more similar to USP Jupiters, in having "lonely" system configurations than smaller USP planets; there is no evidence for

additional transiting planets in the light curve of K2-399. Dai et al. (2021) also note that USP Neptunes are more likely to orbit metal-rich stars than their smaller USP counterparts; K2-399 has a significantly supersolar metallicity of [Fe/H] = 0.252 ± 0.036 dex.

K2-399 has a clean, single-lined FLWO/TRES spectrum, and Keck/NIRC2 AO imaging that shows no contaminating stellar companions. The Gaia RUWE value is 5.89, which is higher than expected for a single star, but that is not corroborated by the follow-up observations. The vespa FPP value is 7.80×10^{-4} using the available contrast curve. The centroid p-value is 0.1608, which is consistent with the source of the transiting signal being on the target star. Using the Chen & Kipping (2017) mass–radius relation predicts a mass of $\sim 32\,M_\oplus$, resulting in a readily measurable RV semiamplitude ($K \sim 27\,\mathrm{m\,s}^{-1}$). Although the predicted TSM (~ 52) falls below the recommended threshold in Kempton et al. (2018), the predicted ESM (~ 16.6) is well above the threshold of 7 due to the high equilibrium temperature of the planet. We encourage additional characterization of this unique USP sub-Saturn.

3.11. EPIC 248758353

K2-403 is a moderately bright ($V = 12.36$ mag, $K_s = 10.58$ mag) G4V star ($0.89\,R_\odot$, $0.78\,M_\odot$) that was observed in Campaign 14. It is orbited by a warm sub-Saturn-sized planet that was first noted in Paper IV. K2-403 b is a $5.333\,R_\oplus$ planet, orbiting at a distance of 0.188 au, with a period of 33.589979 days and an equilibrium temperature of ~ 575 K. The host star has a clean, single-lined FLWO/TRES spectrum, and WIYN/NESSI speckle imaging at 562 nm and 832 nm that show no contaminating stellar companions. The vespa FPP value is 1.05×10^{-5}, using the available contrast curves. The centroid p-value is 0.6589, which is consistent with the source of the transiting signal being on the target star. Using the Chen & Kipping (2017) mass–radius relation predicts a mass of $\sim 25\,M_\oplus$. This would result in a measurable RV semiamplitude ($K \sim 5.8\,\mathrm{m\,s}^{-1}$). A predicted TSM of ~ 33 places K2-403 b in the fourth quartile of large ($> 4\,R_\oplus$) planets as defined by Kempton et al. (2018). The ESM (~ 2.1) value indicates emission spectroscopy would be challenging, compared to the threshold of 7.5 recommended by Kempton et al. (2018).

3.12. EPIC 248874928

K2-405 b is a Neptune-sized ($4.569\,R_\oplus$) planet orbiting a moderately bright ($V = 12.86$ mag, $K_s = 10.55$ mag) K0V star ($0.77\,R_\odot$, $1.03\,M_\odot$) observed in Campaign 14. It was first noted in Paper IV; it orbits the star at a distance of 0.045 au, with a period of 3.435471 days and an equilibrium temperature of ~ 980 K. The host star has a clean, single-lined FLWO/TRES spectrum, and both Keck/NIRC2 AO imaging and WIYN speckle imaging that show no contaminating stellar companions. The vespa FPP value is 7.80×10^{-4} using the available contrast curves. The centroid p-value is 0.5057, which is consistent with the source of the transiting signal being on the target star. Using the Chen & Kipping (2017) mass–radius relation predicts a mass of $\sim 19\,M_\oplus$. This would result in a measurable RV semiamplitude ($K \sim 7.7\,\mathrm{m\,s}^{-1}$), and predicts a TSM ($\sim 60$) value that puts K2-405 b in the third quartile (> 51) for atmospheric follow-up recommended by Kempton et al. (2018). The ESM value (~ 9.6) is comparable to

the GJ 1132 b value of 7.5, indicating that K2-405 b may also be a favorable planet for further emission spectroscopy characterization.

3.13. EPIC 249223471

K2-406 is a bright ($V = 9.47$ mag, $K_s = 8.03$ mag) G4V star ($0.96\,R_\odot$, $0.80\,M_\odot$) that was observed in Campaign 15. It is orbited by a Neptune-sized planet that was first noted in Paper IV. K2-406 b is a $4.602\,R_\oplus$ planet, orbiting at a distance of 0.145 au, with a period of 22.549406 days and an equilibrium temperature of ~ 720 K. The host star has clean, single-lined Keck/HIRES and FLWO/TRES spectra, and Keck/NIRC2 AO imaging and Gemini/DSSI speckle imaging at 692 nm and 880 nm that shows no contaminating stellar companions. The vespa FPP value is 1.30×10^{-3}, using the available contrast curves. The centroid p-value is 0.6741, which is consistent with the source of the transiting signal being on the target star. Using the Chen & Kipping (2017) mass–radius relation predicts a mass of $\sim 20\,M_\oplus$. This would result in a measurable RV semiamplitude ($K \sim 5.3\,\mathrm{m\,s}^{-1}$). A predicted TSM of ~ 90 places K2-403 b near the top of the third quartile of large ($> 4\,R_\oplus$) planets as defined by Kempton et al. (2018). The predicted ESM (~ 7.7) value is comparable to the benchmark GJ 1132 b value of 7.5; K2-403 b may therefore be a high-quality target for future atmospheric observations.

3.14. EPIC 249816490

K2-408 b is a super-Earth-sized ($1.677\,R_\oplus$) planet orbiting a bright ($V = 11.93$ mag, $K_s = 9.98$ mag) G7V star ($0.78\,R_\odot$, $0.81\,M_\odot$), observed in Campaign 15. It was first noted in Paper IV; it orbits the star at a distance of 0.14 au, with a period of 20.978959 days and an equilibrium temperature of ~ 610 K. The host star has a clean, single-lined FLWO/TRES spectrum, and Gemini/DSSI imaging which shows no contaminating stellar companions. The vespa FPP value is 5.19×10^{-4} using the available contrast curve. The centroid p-value is 0.6675, which is consistent with the source of the transiting signal being on the target star. Using the Chen & Kipping (2017) mass–radius relation predicts a mass of $\sim 3.9\,M_\oplus$. This would result in a challenging RV semiamplitude ($K \sim 1.0\,\mathrm{m\,s}^{-1}$), and predicts TSM ($\sim 12$) and ESM ($\sim 0.4$) values that indicate atmospheric follow-up would be challenging, compared to the thresholds recommended by Kempton et al. (2018). However, the FLWO/TRES spectrum points to the stellar host having a significantly substellar metallicity ([Fe/H] = -0.579 ± 0.080 dex), which makes this one of the most metal-poor stars known to host a super-Earth (see Figure 12). Understanding the lowest-metallicity protoplanetary disks that can give rise to planet formation is a critical input into planet formation theories (e.g., Dawson et al. 2015; Lee & Chiang 2015). K2-408 b represents a unique opportunity for the next generation of extreme-precision RV instruments to measure the density of a super-Earth orbiting a metal-poor star. The only planets smaller than $2\,R_\oplus$ orbiting stars at such low spectroscopically confirmed metallicity with measured radii and masses are the three planets in the comparably bright L 98-59 system ([Fe/H] = -0.46 ± 0.26 dex, $V = 11.69$ mag, $K_s = 7.10$), and two K2 planets around fainter targets (K2-344 b: [Fe/H] = -0.95 ± 0.02 dex, $V = 13.44$ mag, $K_s = 9.66$ mag, and K2-349 b: [Fe/H] = -0.66 ± 0.04 dex, $V = 14.40$
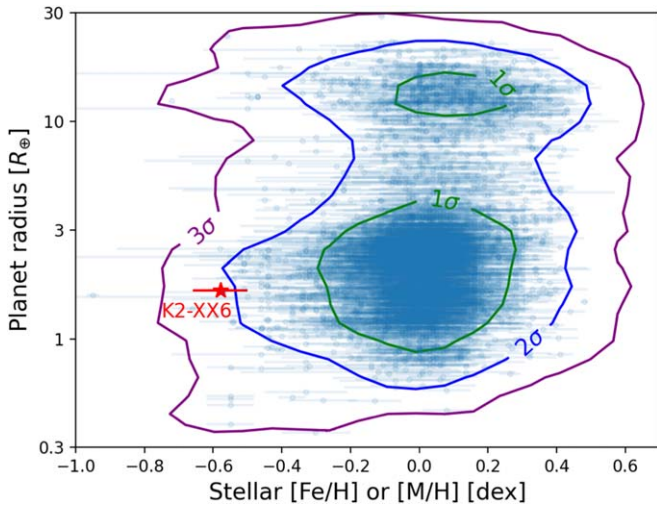
Figure 12. The metallicity distribution of the host stars of planets with measured radii (3411 planets at the NASA Exoplanet Archive). The green, blue, and purple contours enclose 68%, 95%, and 99.7% of the data, respectively. K2-408 b has one of the lowest well-constrained metallicities measured to date for an exoplanet host star.

mag, $K_s = 12.20$ mag; de Leon et al. 2021). We encourage further follow-up of this system.

4. Planet Candidates that Did not Pass our Validation Tests

Table 2 also lists the planet candidates that did not pass our set of validation tests. These include the following:

1. Stars that were revealed with high-resolution imaging to have nearby companions:
   (a) EPIC 205029914
   (b) EPIC 206192335
   (c) EPIC 246947582
   (d) EPIC 220294712
   (e) EPIC 245955351
   (f) EPIC 211428897
2. Stars that were revealed with reconnaissance spectra to be double-lined spectroscopic binaries or to have velocities inconsistent with planetary companions:
   (a) EPIC 211830293
   (b) EPIC 212705192
   (c) EPIC 219388192 (Nowak et al. 2017)
   (d) EPIC 211830293
3. Candidate signals that failed our `vespa` FPP threshold, likely due to being v-shaped:
   (a) EPIC 205944181.01
   (b) EPIC 211784767.01
   (c) EPIC 212585579.01
   (d) EPIC 216892056.01
   (e) EPIC 220571481.01
   (f) EPIC 247724061.01
   (g) EPIC 248222323.01
   (h) EPIC 248827616.01
   (i) EPIC 211800191.01
   (j) EPIC 212797028.01
   (k) EPIC 216334329.01
4. Candidate signals that failed our `vespa` FPP threshold, likely due to distortion by incompletely removed stellar rotation and pulsation signals:

(a) EPIC 211965883.01
(b) EPIC 249827330.01
(c) EPIC 248639411.01
(d) EPIC 248740016.01
5. Candidate signals that failed our `vespa` FPP threshold, likely due to having too low S/N:
   (a) EPIC 212730483.01
   (b) EPIC 226042826.01
6. Candidate signals that failed our `vespa` FPP threshold, likely due to a potential secondary eclipse:
   (a) EPIC 247698108.01
   (b) EPIC 212351868.01
7. Candidate signals that marginally failed our FPP threshold (having FPP values 0.01–0.10) but otherwise looked promising:
   (a) EPIC 205999468.01
   (b) EPIC 213817056.01
   (c) EPIC 220400100.01
   (d) EPIC 205957328.01
8. Candidate signals that passed our other tests but failed the `centroid` test ($p < 0.05$) as not conclusively being on the target star:
   (a) EPIC 249865296.01
   (b) EPIC 247164043.01
   (c) EPIC 211711685.01

We discuss several of these in more detail below.

EPIC 205957328.01 has a 14.35 days period sub-Neptune candidate, noted by Vanderburg et al. (2016), Mayo et al. (2018), and Kruse et al. (2019), with a radius of $\sim 1.9\,R_\oplus$. It does not pass our validation threshold, with an FPP of 0.022 (possibly due to one transit which has an inconsistent depth with the remaining transits), but we note that the light curve also shows a potential single transit, at BJD = 2457043.5, of a much longer period candidate, EPIC 205957328.02, shown in Figure 13. The duration of the putative event is ~ 46.3 hr, implying an orbital period of >80 yr. The depth of the event is consistent with a sub-Neptune planet with a radius of $\sim 2.3\,R_\oplus$. This putative candidate would be challenging to confirm, given the timescale to observe a second transit or obtain sufficient orbital coverage with RV observations.

The light curve of EPIC 211428897 shows five candidate signals, with periods ranging from 1.61 to 6.27 days, reported by Pope et al. (2016; EPIC 211428897.01), Petigura et al. (2018; EPIC 211428897.01 and .02), Dressing et al. (2017; EPIC 211428897.01, .02, and .03), and Kruse et al. (2019; EPIC 211428897.01, .02, .03, .04, and .05). High-resolution imaging of EPIC 211428897, which is relatively red ($V = 14.1$, $K_s = 9.6$) and was originally classified as an M2 dwarf (Rodríguez Martínez et al. 2019), shows two nearly equal brightness stars separated by $\sim 1''$. Given that the transits are relatively shallow, ranging in depth from 500–700 ppm, they are likely still planetary in nature after accounting for the dilution regardless of which star they orbit. We note that the candidates may not all be orbiting one of the stars; the work of disentangling which signals are associated with which host star is left for a future analysis.

Similarly, EPIC 245955351 shows two candidate signals, first reported in Paper IV, with periods of 7.98 and 18.43 days. The target, originally classified as a G6V star (Hardegree-Ullman et al. 2021), has a much fainter companion $\sim 3''$ away
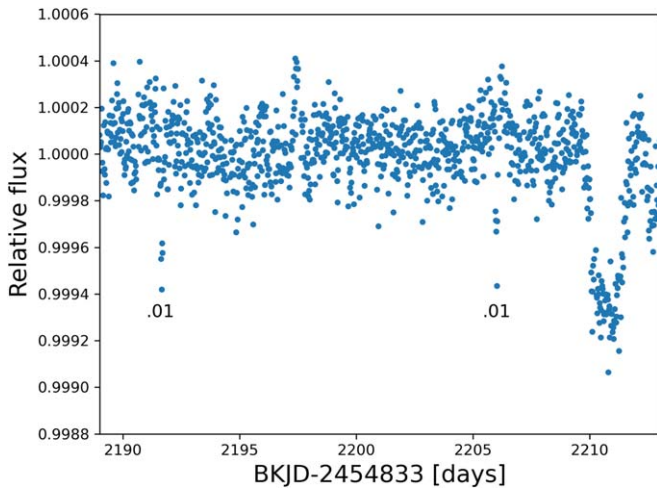
Figure 13. A portion of the light curve of EPIC 205957328, showing two transits of the short-period candidate EPIC 205957328.01, and a potential single transit of a longer-period candidate centered at ∼2211 days.

that is revealed by high-resolution AO imaging. If the signals are associated with the bright star, they likely remain planetary in nature, and indeed have low FPP values (4.72×10^{-3} and 8.34×10^{-5}, respectively). However, if either or both of them are orbiting the fainter companion, the dilution is such that the radius of the transiting object would become too large to be planetary. Given the relatively deep signals (∼1000 ppm and ∼3000 ppm), ground-based, seeing-limited photometry could be used to determine whether the signals were on the bright star.

EPIC 249559552 shows two candidate signals, first reported in Paper IV, with periods of 7.82 and 19.52 days, very close to the 5:2 resonance. The target, originally classified as a K3V star (Hardegree-Ullman et al. 2021), has a much fainter companion ∼0″4 away that is revealed by speckle imaging. As above, if the signals are associated with the bright star, they likely remain planetary in nature; however, either or both may be on the nearby faint companion, which would preclude their planetary nature. In this case, the two stars are close enough on the sky that ground-based photometry would likely be insufficient to disentangle them, and something like a high-precision spectrograph behind an AO system would be necessary (e.g., PARVI on the Palomar Hale Telescope, iLocator on the Large Binocular Telescope, or HISPEC on Keck).

Finally, three candidates passed all our validation tests except the centroid test. Their centroid plots are shown in Figure 14; faint gray points are the centroid positions for out-of-transit observations in the light curve, blue points with error bars are the centroid positions for the in-transit observations. EPIC 249865296.01 and EPIC 247164043.01 have marginally significant offsets ($p = 0.0418$ and 0.0452, respectively), and the distribution of their in-transit points do not clearly point in an obvious direction for a potential contaminating source; however, they fail to pass our threshold and so we do not

validate them. EPIC 211711685.01 has a very significant centroid offset ($p = 0.0089$). Interestingly, most of the in-transit centroid positions for this candidate are in-family with the out-of-transit centroid positions, but a small number of in-transit points lie significantly offset from the location of the target star. As a result, we do not validate that the transiting signal is a planet on EPIC 21171168. However, identifying the true source of the transiting signal is beyond the scope of this paper.

In addition to the above candidates, which had sufficient follow-up observations for us to attempt validation, we note a number of relatively bright (Kepmag < 13) candidates in Table 7 that remain in our program. They pass visual inspection as clean planet candidates but still require either reconnaissance spectra or high-resolution imaging to proceed. We did not attempt to validate them, but highlight them for observers hoping to prioritize candidates for further follow-up.

5. Conclusions

In total, we validate 60 new K2 planets in 46 systems, out of 91 total candidates. This is a validation rate of 66%, having already down-selected the full catalog in Paper IV to the most likely planetary signals by visual inspection. The most promising new planets for transmission spectroscopy are K2-384 f, K2-387 b, K2-390 b, K2-403 b, and K2-398 c, while the most promising new planets for emission spectroscopy are K2-371 b, K2-370 b, and K2-399 b. K2-406 b and K2-405 b show interesting TSM and ESM values, making them potentially valuable atmospheric characterization targets. In addition to these new planets, in Table 7 we highlight 37 planet candidates orbiting bright host stars that pass visual inspection and warrant further follow-up.

We note that many additional planets remain in the K2 data. Besides the planet candidates listed above, Paper IV also includes 109 planet candidates that pass visual inspection orbiting stars $13 < Kp < 15$, and 90 planet candidates that pass visual inspection orbiting stars $Kp > 15$ that require additional follow-up observations. There are also hundreds of additional K2 planet candidates at the NASA Exoplanet Archive; although Paper IV presented a large, uniform catalog of planet candidates, comparison with larger catalogs such as Kruse et al. (2019) show that our catalog was incomplete. Given the plethora of archival data from multiple missions now available, there remain strong reasons to pursue K2 planet confirmation. There are significant ongoing and upcoming opportunities to exploit and expand upon the K2 data, including (i) a reobservation of the ecliptic plane by the TESS mission (Ricker et al. 2015) during its first extended mission; (ii) opportunities for measuring transit timing variations or searching for additional transits with CHEOPS (Broeg et al. 2013); (iii) a new generation of extreme-precision RV instruments to map out the composition of different classes and subclasses of planets; and (iv) opportunities for characterizing exoplanet atmospheres to an unprecedented level of detail with JWST and high-resolution, ground-based spectroscopy for statistical samples of planets.
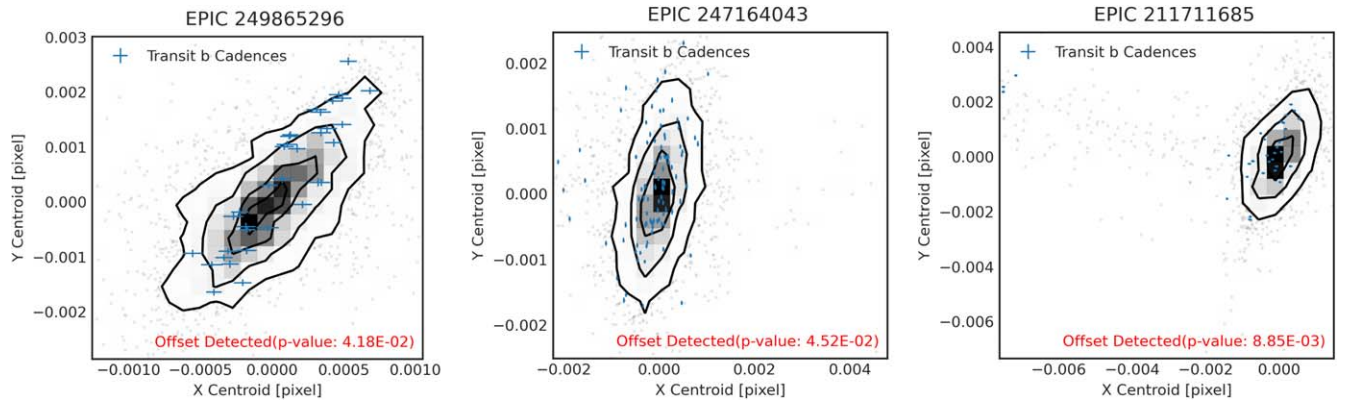
Figure 14. Centroid plots for candidates with significant (p-value < 0.05) centroid offsets during transit. The contours show the 1σ, 2σ, and 3σ contours for the centroid locations for out-of-transit cadences; the gray points show the remaining out-of-transit centroid locations that fall outside those contours. The blue points are the centroid locations of the in-transit cadences.

Table 7
Bright K2 Planet Candidates from Paper IV that Require Additional Follow-up Observations for Validation

Candidate ID	Camp	Period (days)	R_p ($R_\oplus$)	T_{mid} (2454833-JD)	R_p/R_s	Kepmag (mag)	RUWE	Spectrum	Imaging
201445732.01	1	5.60203111	1.916	1978.88960	0.0149	11.95	0.88	-	Y
204308061.01	2	22.6435563	1.297	2067.43865	0.0143	10.17	0.92	-	-
204888276.01	2	16.5604729	1.217	2067.53685	0.0299	12.54	-	Y	-
205483055.01	2	22.970936	2.394	2063.81798	0.0219	12.93	0.90	-	-
205489894.01	2	14.6573703	1.693	2074.07547	0.0313	12.34	1.14	Y	-
205943325.01	3	27.2701915	2.500	2151.27679	0.0142	11.28	0.99	Y	-
206133795.01	3	13.8506388	2.882	2147.80162	0.0152	11.63	1.04	-	Y
206329937.01	3	10.4990647	20.92	2151.04875	0.0338	11.79	1.23	-	-
210550063.01	4	2.16604744	2.611	2229.8188	0.0208	11.15	1.31	-	Y
210678858.02	4	14.8489834	2.466	2237.22147	0.0287	12.74	1.08	-	Y
210945680.01	4	20.6006563	2.166	2242.51612	0.0187	11.32	0.99	-	Y
211505089.01	5	24.443649	1.737	2313.9657	0.0222	12.94	1.48	Y	-
211897272.01	5	11.2356761	2.706	2310.56874	0.0266	12.57	1.16	-	-
212346723.01	6	15.9483772	2.345	2397.08637	0.0171	12.99	0.96	-	-
212652418.01	6	19.1374173	2.802	2401.96834	0.0191	12.27	1.11	-	Y
212691727.01	6	6.43038282	4.309	2386.5697	0.0374	12.66	0.92	-	Y
212833814.01	6	27.8083498	2.144	2403.11012	0.0130	10.72	0.97	-	Y
216363472.01	7	8.69447821	1.401	2468.88249	0.0129	11.87	1.01	-	Y
218332621.01	7	9.81158865	4.245	2469.06837	0.0207	12.75	0.87	-	Y
218701083.01	7	5.04906822	2.594	2471.91113	0.0161	12.49	0.93	-	Y
246067130.01	12	6.78653927	1.200	2906.07556	0.0113	11.74	0.87	-	Y
246777408.01	13	2.46563986	30.19	2988.02272	0.1107	11.21	1.21	-	-
248865761.01	14	13.0710405	2.285	3085.12075	0.0168	12.94	1.06	Y	-
248869142.01	14	28.8483394	3.657	3086.94431	0.0191	10.39	0.98	-	-
249373875.01	15	7.52210942	2.249	3159.14609	0.0149	12.34	1.23	-	-
249418609.01	15	15.3206064	1.770	3170.06807	0.0145	12.35	1.13	-	-
249476992.01	15	7.9436039	1.992	3161.75698	0.0210	12.79	1.21	-	Y
249703125.01	15	10.3073874	2.602	3157.55787	0.0272	12.88	1.26	-	Y
249731291.01	15	10.2053773	6.310	3160.91941	0.0245	12.92	0.97	-	Y
249731291.02	15	23.3367386	5.824	3179.76842	0.0226	12.92	0.97	-	Y
249822095.01	15	1.69671578	5.738	3157.01732	0.0264	12.80	1.13	-	Y
250106132.01	15	22.1223653	3.715	3157.32569	0.0351	11.19	0.90	Y	-
211396431.01	16	8.51418384	38.30	3266.73236	0.0418	11.77	1.18	-	Y
251304634.01	16	4.39250294	1.110	3264.36688	0.0152	12.25	1.02	Y	-
251399501.01	16	11.6349883	2.605	3272.15823	0.0218	12.10	1.25	Y	-
212479997.01	17	8.9317272	9.390	3348.03092	0.0478	10.80	1.07	-	-
211408558.01	18	9.96768882	2.005	3427.65262	0.0178	11.51	1.13	-	Y

Note. "Y" indicates that reconnaissance spectra or high-resolution imaging have already been obtained (many are available on ExoFOP); "-" indicates that they are still needed.

Software: EVEREST (Luger et al. 2016, 2018), TERRA (Petigura et al. 2013), EDI-Vetter (Zink et al. 2020a), K2SFF (Vanderburg & Johnson 2014), PyMC3 (Salvatier et al. 2015), Exoplanet (Foreman-Mackey et al. 2019), Robo-Vetter (Thompson et al. 2018), batman Kreidberg (2015), emcee (Foreman-Mackey et al. 2013).

Appendix A
Validated Planets

A.1. EPIC 204750116

K2-365 b is a sub-Neptune ($2.906\,R_\oplus$) planet orbiting a bright ($V = 11.37$ mag, $K_s = 9.62$ mag) G4V star ($1.05\,R_\odot$, $0.82\,M_\odot$) observed in Campaign 2. It was noted as EPIC 204750116.01 by Vanderburg et al. (2016), Rizzuto et al. (2018), Mayo et al. (2018), and Kruse et al. (2019), and it orbits the star at a distance of 0.150 au, with a period of 23.448172 days and an equilibrium temperature of 710 K. The host star has a clean, single-lined FLWO/TRES spectrum, and Keck/NIRC2 imaging which shows no contaminating stellar companions. The vespa FPP value is 0.0016, without requiring use of the available contrast curves. The centroid p-value is 0.5219, which is consistent with the source of the transiting signal being on the target star. Using the Chen & Kipping (2017) mass–radius relation predicts a mass of $\sim 8.7\,M_\oplus$. This would result in a measurable RV semiamplitude ($K \sim 2.2\,\mathrm{m\,s^{-1}}$), but predicts TSM ($\sim 22$) and ESM ($\sim 1.3$) values that indicate atmospheric follow-up would be challenging, compared to the thresholds recommended by Kempton et al. (2018). We note that our pipeline was able to marginally detect the shorter-period candidate, EPIC 204750116.02, reported by Kruse et al. (2019), but with insufficient S/N to attempt validation, and it remains a candidate.

A.2. EPIC 205111664

K2-366 is a moderately bright ($V = 12.49$ mag, $K_s = 9.88$ mag) G4V star ($0.94\,R_\odot$, $0.83\,M_\odot$) that was observed in Campaign 2. It is orbited by a sub-Neptune-sized planet that was previously noted as EPIC 205111664.01 by Vanderburg et al. (2016) and Kruse et al. (2019). K2-366 b is a $2.359\,R_\oplus$ planet, orbiting at a distance of 0.116 au, with a period of 15.937039 days and an equilibrium temperature of ~ 770 K. The host star has a clean, single-lined FLWO/TRES spectrum, and Keck/NIRC2 AO imaging that shows no contaminating stellar companions. The vespa FPP value is 1.40×10^{-4}, without requiring use of the contrast curve. The centroid p-value is 0.4962, which is consistent with the source of the transiting signal being on the target star. Using the Chen & Kipping (2017) mass–radius relation predicts a mass of $\sim 6.3\,M_\oplus$. This would result in a challenging RV semiamplitude ($K \sim 1.8\,\mathrm{m\,s^{-1}}$), and predicts TSM ($\sim 18$) and ESM ($\sim 1.1$) values that indicate atmospheric follow-up would be challenging, compared to the thresholds recommended by Kempton et al. (2018).

A.3. EPIC 206055981

K2-367 is a moderately faint ($V = 13.80$ mag, $K_s = 10.96$ mag) K5V star ($0.63\,R_\odot$, $0.76\,M_\odot$) that was observed in Campaign 3. It is orbited by a sub-Neptune-sized planet, K2-367 b, which was previously identified as EPIC 206055981.01 by Vanderburg et al. (2016) and Kruse et al. (2019). It is a

2.413 $R_\oplus$ planet, orbiting at a distance of 0.134 au, with a period of 20.645099 days and a relatively cool (for our sample) equilibrium temperature of ∼450 K. The host star has clean, single-lined Keck/HIRES and IRTF/SpeX spectra, and WIYN/NESSI speckle imaging at 562 nm and 832 nm that show no contaminating stellar companions. The vespa FPP value is 0.000721, using the available contrast curves. The centroid p-value is 0.5842, which is consistent with the source of the transiting signal being on the target star. Using the Chen & Kipping (2017) mass–radius relation predicts a mass of ∼6.5 $M_\oplus$. This would result in a challenging RV semiamplitude ($K \sim 1.8\,\mathrm{m\,s^{-1}}$), especially given the faint host star, and predicts TSM (∼15) and ESM (∼0.4) values that indicate atmospheric follow-up would be challenging, compared to the thresholds recommended by Kempton et al. (2018).

A.4. EPIC 206146957

K2-369 is a bright ($V = 11.79$ mag, $K_s = 9.93$ mag) G3V star (0.88 $R_\odot$, 0.74 $M_\odot$) that was observed in Campaign 3. It is orbited by a super-Earth-sized planet, K2-369 b, which was previously identified as EPIC 206146957.01 by Vanderburg et al. (2016), Mayo et al. (2018), and Kruse et al. (2019). It is a 1.313 $R_\oplus$ planet, orbiting at a distance of 0.057 au, with a period of 5.761612 days and an equilibrium temperature of ∼1080 K. The host star has a clean, single-lined FLWO/TRES spectra, and Palomar/PHARO AO imaging that shows no contaminating stellar companions. The vespa FPP value is 3.02×10^{-5}, using the available contrast curve. The centroid p-value is 0.4584, which is consistent with the source of the transiting signal being on the target star. Using the Chen & Kipping (2017) mass–radius relation predicts a mass of ∼2.2 $M_\oplus$. This would result in a challenging RV semiamplitude ($K \sim 1.0\,\mathrm{m\,s^{-1}}$), and predicts TSM (∼2.3) and ESM (∼0.8) values that indicate atmospheric follow-up would be challenging, compared to the thresholds recommended by Kempton et al. (2018).

A.5. EPIC 206317286

EPIC 206317286 (K2-303) is a moderately faint ($V = 14.05$ mag, $K_s = 11.64$ mag) K3V star (0.76 $R_\odot$, 0.83 $M_\odot$) that was observed in Campaign 3. It was previously found to host a short-period (1.58 days) Earth-sized (0.96 $R_\oplus$) planet, EPIC 206317286 b (EPIC 206317286.02; Heller et al. 2019). An additional longer-period candidate, EPIC 206317286.01, was noted by Vanderburg et al. (2016) and Kruse et al. (2019), and was recovered by our pipeline. EPIC 206317286 c is a 2.464 $R_\oplus$ sub-Neptune-sized planet, orbiting at a distance of 0.124 au, with a period of 17.515472 days and an equilibrium temperature of ∼570 K. The host star has a clean, single-lined IRTF/SpeX spectrum. Heller et al. (2019) validated EPIC 206317286 b in part by using Pan-STARRS imaging (with a resolution down to 200 mas pixel^{-1}) to eliminate background flux contaminants; we therefore did not obtain additional high-resolution imaging. The vespa FPP value of EPIC 206317286 c is 8.16×10^{-5} using the Campaign 3 multiplicity boost. The centroid p-value is 0.1811, which is consistent with the source of the transiting signal being on the target star. Using the Chen & Kipping (2017) mass–radius relation predicts a mass of planet c of ∼5.4 $M_\oplus$. This would result in a challenging RV semiamplitude ($K \sim 1.5\,\mathrm{m\,s^{-1}}$), and predicts TSM (∼8.0) and ESM (∼0.3) values that indicate atmospheric

follow-up would be challenging, compared to the thresholds recommended by Kempton et al. (2018).

A.6. EPIC 211490999

K2-372 is a moderately faint ($V = 13.60$ mag, $K_s = 11.87$ mag) G5V star (0.92 $R_\odot$, 0.85 $M_\odot$) that was observed in Campaigns 5, 16, and 18. It is orbited by a sub-Neptune-sized planet, K2-372 b, previously noted as EPIC 211490999.01 by Pope et al. (2016), Petigura et al. (2018), Kruse et al. (2019), and de Leon et al. (2021). It is a 2.945 $R_\oplus$ planet, orbiting at a distance of 0.085 au, with a period of 9.844077 days and an equilibrium temperature of ∼870 K. The host star has clean, single-lined Keck/HIRES and McDonald/TS23 spectra, and Gemini/NIRI AO and WIYN/NESSI speckle imaging at 562 nm and 832 nm that show no contaminating stellar companions. The vespa FPP value is 3.39×10^{-3}, using the available contrast curves. The centroid p-value is 0.4752, which is consistent with the source of the transiting signal being on the target star. Using the Chen & Kipping (2017) mass–radius relation predicts a mass of ∼9.2 $M_\oplus$. This would result in a measurable RV semiamplitude ($K \sim 3.1\,\mathrm{m\,s^{-1}}$), but predicts TSM (∼13) and ESM (∼1.0) values that indicate atmospheric follow-up would be challenging, compared to the thresholds recommended by Kempton et al. (2018).

A.7. EPIC 211539054

K2-373 is a bright ($V = 10.47$ mag, $K_s = 9.16$ mag) G1V star (1.49 $R_\odot$, 1.16 $M_\odot$) that was observed in Campaign 5. It is orbited by a sub-Neptune-sized planet, K2-373 b, which was first noted by Kruse et al. (2019) as EPIC 211539054.01. It is a 2.061 $R_\oplus$ planet, orbiting at a distance of 0.102 au, with a period of 11.020660 days and an equilibrium temperature of ∼1130 K. The host star has a clean, single-lined FLWO/TRES spectra, and Palomar/PHARO AO imaging that shows no contaminating stellar companions. The vespa FPP value is 0.00213, using the available contrast curve. The centroid p-value is 0.3779, which is consistent with the source of the transiting signal being on the target star. Using the Chen & Kipping (2017) mass–radius relation predicts a mass of ∼5.2 $M_\oplus$. This would result in a challenging RV semiamplitude ($K \sim 1.3\,\mathrm{m\,s^{-1}}$), and predicts TSM (∼14) and ESM (∼1.0) values that indicate atmospheric follow-up would be challenging, compared to the thresholds recommended by Kempton et al. (2018).

A.8. EPIC 211732116

K2-374 is a moderately bright ($V = 12.80$ mag, $K_s = 11.29$ mag) G3V star (0.91 $R_\odot$, 0.73 $M_\odot$) that was observed in Campaign 16. It is orbited by a super-Earth and a sub-Neptune, which were first noted in Paper IV. K2-374 b (EPIC 211732116.01) is a 2.597 $R_\oplus$ planet, orbiting at a distance of 0.055 au, with a period of 4.521953 days and a high equilibrium temperature of ∼1210 K. K2-374 c (EPIC 211732116.02) is a 2.213 $R_\oplus$ planet, orbiting at a distance of 0.114 au, with a period of 16.434450 days and an equilibrium temperature of ∼790 K. The host star has a clean, single-lined FLWO/TRES spectrum, and Keck/NIRC2 AO imaging that shows no contaminating stellar companions. The vespa FPP values of planets b and c are 6.80×10^{-5} and 2.42×10^{-3}, respectively, using the available contrast curve and the multiplicity boost. The centroid p-values are 0.5403 and

0.5749, respectively, consistent with the source of the transiting signals being on the target star. Using the Chen & Kipping (2017) mass–radius relation predicts masses of $\sim 3.6 \, M_\oplus$ and $\sim 5.7 \, M_\oplus$ for planets b and c, respectively. These mass estimates for the two planets result in challenging RV semiamplitudes ($K = 1.7 \, \mathrm{m \, s^{-1}}$, and $1.8 \, \mathrm{m \, s^{-1}}$), and TSM ($\sim 10$, ~ 11) and ESM (~ 0.7, ~ 0.6) values below the thresholds of interest recommended by Kempton et al. (2018).

A.9. EPIC 212006318

K2-375 is a moderately faint ($V = 13.04$ mag, $K_s = 11.56$ mag) G2V star ($1.54 \, R_\odot$, $1.12 \, M_\odot$) that was observed in Campaign 3. It is orbited by a sub-Neptune-sized planet, K2-375 b, which was previously noted as EPIC 212006318.01 by Pope et al. (2016), Mayo et al. (2018), Kruse et al. (2019), and de Leon et al. (2021). K2-375 b is a $2.243 \, R_\oplus$ planet, orbiting at a distance of 0.121 au, with a period of 14.453895 days and an equilibrium temperature of ~ 1000 K. The host star has clean, single-lined Keck/HIRES and FLWO/TRES spectra, and Palomar/PHARO AO and WIYN/NESSI speckle imaging at 562 nm and 832 nm that show no contaminating stellar companions. The vespa FPP value is 4.11×10^{-3}, without using the available contrast curves. The centroid p-value is 0.1458, which is consistent with the source of the transiting signal being on the target star. Using the Chen & Kipping (2017) mass–radius relation predicts a mass of $\sim 5.8 \, M_\oplus$. This would result in a challenging RV semiamplitude ($K \sim 1.4 \, \mathrm{m \, s^{-1}}$), and predicts TSM ($\sim 4.3$) and ESM ($\sim 0.31$) values that indicate atmospheric follow-up would be challenging, compared to the thresholds recommended by Kempton et al. (2018).

A.10. EPIC 212222383

K2-376 is a bright ($V = 10.42$ mag, $K_s = 9.01$ mag) G1V star ($1.15 \, R_\odot$, $0.91 \, M_\odot$) that was observed in Campaign 16. It is orbited by a super-Earth-sized planet that was first noted in Paper IV as EPIC 212222383.01. K2-376 b is a $1.736 \, R_\oplus$ planet, orbiting at a distance of 0.061 au, with a period of 5.776475 days and an equilibrium temperature of ~ 1240 K. The host star has a clean, single-lined FLWO/TRES spectrum, and Palomar/PHARO AO imaging that shows no contaminating stellar companions. The vespa FPP value is 0.00170, using the available contrast curve. The centroid p-value is 0.6183, which is consistent with the source of the transiting signal being on the target star. Using the Chen & Kipping (2017) mass–radius relation predicts a mass of $\sim 4.1 \, M_\oplus$. This would result in a challenging RV semiamplitude ($K \sim 1.6 \, \mathrm{m \, s^{-1}}$), and predicts TSM ($\sim 21$) and ESM ($\sim 1.6$) values that indicate atmospheric follow-up would be challenging, compared to the thresholds recommended by Kempton et al. (2018).

A.11. EPIC 212530118

K2-377 is a moderately faint ($V = 14.05$ mag, $K_s = 10.99$ mag) K7V star ($0.69 \, R_\odot$, $0.82 \, M_\odot$) that was observed in Campaign 6. It is orbited by a super-Earth-sized planet that was previously noted as EPIC 212530118.01 by Barros et al. (2016) and Kruse et al. (2019). K2-377 b is a $1.693 \, R_\oplus$ planet, orbiting at a distance of 0.100 au, with a period of 12.932235 days and an equilibrium temperature of ~ 530 K. The host star has a clean, single-lined IRTF/SpeX spectrum, and WIYN/NESSI

speckle imaging at 692 nm and 880 nm that show no contaminating stellar companions. The vespa FPP value is 1.14×10^{-3}, using the available contrast curves. The centroid p-value is 0.5774, which is consistent with the source of the transiting signal being on the target star. Using the Chen & Kipping (2017) mass–radius relation predicts a mass of $\sim 3.9 \, M_\oplus$. This would result in a challenging RV semiamplitude ($K \sim 1.2 \, \mathrm{m \, s^{-1}}$), and predicts TSM ($\sim 7.7$) and ESM ($\sim 0.3$) values that indicate atmospheric follow-up would be challenging, compared to the thresholds recommended by Kempton et al. (2018).

A.12. EPIC 212575828

K2-378 is a faint ($V = 15.79$ mag, $K_s = 13.39$ mag) K3V star ($0.73 \, R_\odot$, $0.92 \, M_\odot$), observed in Campaign 6, that is orbited by a sub-Neptune-sized planet. K2-389 b, previously noted by Pope et al. (2016), Crossfield et al. (2016), and Kruse et al. (2019) as EPIC 212575828.01, is a $2.060 \, R_\oplus$ planet, orbiting at a distance of 0.031 au, with a period of 6.293099 days and an equilibrium temperature of ~ 1135 K. The host star has a clean, single-lined Hale/TripleSpec spectrum, and Gemini/DSSI speckle imaging at both 692 nm and 880 nm that show no contaminating stellar companions. The vespa FPP value is 3.78×10^{-3}, using the available contrast curves. The centroid p-value is 0.4968, which is consistent with the source of the transiting signal being on the target star. Using the Chen & Kipping (2017) mass–radius relation predicts a mass of $\sim 9.0 \, M_\oplus$. This would result in a measurable RV semiamplitude ($K \sim 4.5 \, \mathrm{m \, s^{-1}}$), albeit around a faint target, but predicts TSM (~ 12) and ESM (~ 1.6) values that indicate atmospheric follow-up would be challenging, compared to the thresholds recommended by Kempton et al. (2018).

A.13. EPIC 214173069

K2-379 is a moderately faint ($V = 13.21$ mag, $K_s = 10.51$ mag) K3V star ($0.75 \, R_\odot$, $0.86 \, M_\odot$) that was observed in Campaign 7. It is orbited by a sub-Neptune-sized planet, K2-379 b, which was first noted as EPIC 214173069.01 by Kruse et al. (2019). It is a $2.181 \, R_\oplus$ planet, orbiting at a distance of 0.079 au, with a period of 8.777247 days and an equilibrium temperature of ~ 680 K. The host star has clean, single-lined IRTF/SpeX and FLWO/TRES spectra, and Gemini/DSSI speckle imaging at 692 nm and 880 nm that show no contaminating stellar companions. The vespa FPP value is 5.38×10^{-3}, using the available contrast curves. The centroid p-value is 0.8487, which is consistent with the source of the transiting signal being on the target star. Using the Chen & Kipping (2017) mass–radius relation predicts a mass of $\sim 5.6 \, M_\oplus$. This would result in a challenging RV semiamplitude ($K \sim 1.9 \, \mathrm{m \, s^{-1}}$), and predicts TSM ($\sim 17$) and ESM ($\sim 0.8$) values that indicate atmospheric follow-up would be challenging, compared to the thresholds recommended by Kempton et al. (2018). We note that our pipeline did not recover the smaller ($1.4 \, R_\oplus$), longer-period (14.1297 days) candidate, EPIC 214173069.02, reported by Kruse et al. (2019).

A.14. EPIC 214419545

K2-380 is a bright ($V = 11.65$ mag, $K_s = 9.68$ mag) F8V star ($1.32 \, R_\odot$, $0.99 \, M_\odot$) that was observed in Campaign 7. It is orbited by a sub-Neptune-sized planet, K2-380 b, which was first noted as EPIC 214419545.01 by Kruse et al. (2019). It is a

2.729 $R_\oplus$ planet, orbiting at a distance of 0.087 au, with a period of 9.401312 days and an equilibrium temperature of ~1110 K. The host star has a clean, single-lined FLWO/TRES spectrum, and Keck/NIRC2 AO imaging that show no contaminating stellar companions. The vespa FPP value is 8.82×10^{-3}, without using the available contrast curves. The centroid p-value is 0.6540, which is consistent with the source of the transiting signal being on the target star. Using the Chen & Kipping (2017) mass–radius relation predicts a mass of ~8.0 $M_\oplus$. This would result in a measurable RV semiamplitude ($K \sim 2.4\,\mathrm{m\,s^{-1}}$), but predicts TSM (~19) and ESM (~1.8) values that indicate atmospheric follow-up would be challenging, compared to the thresholds recommended by Kempton et al. (2018).

A.15. EPIC 217977895

K2-382 b is a sub-Neptune (2.072 $R_\oplus$) planet in the small planet radius valley, orbiting a moderately faint ($V = 12.98$ mag, $K_s = 11.05$ mag) G8V star (0.81 $R_\odot$, 0.92 $M_\odot$). It was observed in Campaign 7, and was first noted in Mayo et al. (2018) and Kruse et al. (2019) as EPIC 217977895.01. It orbits the star at a distance of 0.148 au, with a period of 21.700156 days and an equilibrium temperature of 615 K. The host star has a clean, single-lined FLWO/TRES spectrum, and Gemini/DSSI speckle imaging at 692 nm and 880 nm which show no contaminating stellar companions. The vespa FPP value is 2.62×10^{-3} using the available contrast curves. The centroid p-value is 0.3721, which is consistent with the source of the transiting signal being on the target star. Using the Chen & Kipping (2017) mass–radius relation predicts a mass of ~5.2 $M_\oplus$. This would result in a challenging RV semiamplitude ($K \sim 1.3\,\mathrm{m\,s^{-1}}$), and predicts TSM (~10) and ESM (~0.4) values that indicate atmospheric follow-up would be challenging, compared to the thresholds recommended by Kempton et al. (2018).

A.16. EPIC 218668602

K2-383 is a moderately bright ($V = 12.68$ mag, $K_s = 10.46$ mag) K0V star (0.80 $R_\odot$, 1.06 $M_\odot$) that was observed in Campaign 7. It is orbited by a super-Earth-sized planet, K2-383 b, which was previously noted by Mayo et al. (2018) and Kruse et al. (2019) as EPIC 218668602.01. It is a 1.564 $R_\oplus$ planet, orbiting at a distance of 0.030 au, with a period of 1.865962 days and an equilibrium temperature of ~1270 K. The host star has a clean, single-lined FLWO/TRES spectrum, and Keck/NIRC2 AO imaging that show no contaminating stellar companions. The vespa FPP value is 2.12×10^{-3}, without using the available contrast curves. The centroid p-value is 0.1391, which is consistent with the source of the transiting signal being on the target star. Using the Chen & Kipping (2017) mass–radius relation predicts a mass of ~3.3 $M_\oplus$. This would result in a challenging RV semiamplitude ($K \sim 1.6\,\mathrm{m\,s^{-1}}$), but predicts TSM (~18) and ESM (~1.7) values that indicate atmospheric follow-up would be challenging, compared to the thresholds recommended by Kempton et al. (2018).

A.17. EPIC 220459477

K2-385 b is a super-Earth (1.539 $R_\oplus$) planet orbiting a moderately faint ($V = 14.65$ mag, $K_s = 12.24$ mag) K3V star that was observed in Campaign 8. It was first noted as EPIC

220459477.01 by Kruse et al. (2019). It orbits the star at a distance of 0.034 au, with a period of 2.380867 days and an equilibrium temperature of ~1100 K. The host star has a clean, single-lined TripleSpec spectrum, and WIYN/NESSI speckle imaging at both 562 nm and 832 nm that show no contaminating stellar companions. The vespa FPP value is 1.09×10^{-5} using the available contrast curves. The centroid p-value is 0.1107, which is consistent with the source of the transiting signal being on the target star. Using the Chen & Kipping (2017) mass–radius relation predicts a mass of ~3.2 $M_\oplus$. This would result in a challenging RV semiamplitude ($K \sim 1.6\,\mathrm{m\,s^{-1}}$), especially given the faintness of the target, and predicts TSM (~8) and ESM (~0.7) values that indicate atmospheric follow-up would be challenging, compared to the thresholds recommended by Kempton et al. (2018).

A.18. EPIC 220510874

K2-386 is a moderately faint ($V = 13.17$ mag, $K_s = 11.52$ mag) F9V star (0.97 $R_\odot$, 0.91 $M_\odot$) that was observed in Campaign 8. It is orbited by a sub-Neptune-sized planet, K2-386 b, which was previously noted as EPIC 220510874.01 by Kruse et al. (2019) and Zink et al. (2019). K2-386 b is a 2.320 $R_\oplus$ planet, orbiting at a distance of 0.073 au, with a period of 7.473223 days and an equilibrium temperature of ~1010 K. The host star has a clean, single-lined McDonald TS23 spectrum, and WIYN/NESSI speckle imaging at 562 nm and 832 nm that show no contaminating stellar companions. The vespa FPP value is 3.34×10^{-5}, using the available contrast curves. The centroid p-value is 0.6971, which is consistent with the source of the transiting signal being on the target star. Using the Chen & Kipping (2017) mass–radius relation predicts a mass of ~6.2 $M_\oplus$. This would result in a measurable RV semiamplitude ($K \sim 2.2\,\mathrm{m\,s^{-1}}$), but predicts TSM (~12) and ESM (~0.9) values that indicate atmospheric follow-up would be challenging, compared to the thresholds recommended by Kempton et al. (2018).

A.19. EPIC 245943455

K2-388 b is a sub-Neptune (3.660 $R_\oplus$) planet orbiting a moderately bright ($V = 12.82$ mag, $K_s = 10.93$ mag) G8V star (0.90 $R_\odot$, 0.84 $M_\odot$). The target was observed in Campaign 12, and the transiting signal was previously noted in Dattilo et al. (2019). The planet orbits the star at a distance of 0.063 au, with a period of 6.339069 days and an equilibrium temperature of ~970 K. The host star has a clean, single-lined Keck/HIRES spectrum, and Palomar/PHARO, Gemini/NIRI, and WIYN/NESSI imaging which all show no contaminating stellar companions. The vespa FPP value is 8.02×10^{-8}, using the available contrast curves. The centroid p-value is 0.0938, which is moderately inconsistent with the source of the transiting signal being on the target star at the ~2σ level, but does not fall below our $p = 0.05$ threshold for revoking a planet's validation status. In Dattilo et al. (2019), they note that transit depth changes as a function of aperture size for this signal, which may indicate a contaminating background star. Although this planet passes our statistical thresholds for validation, it may warrant additional ground-based time-series photometry to confirm the transit is indeed on the target star. Using the Chen & Kipping (2017) mass–radius relation predicts a mass of ~13.1 $M_\oplus$. This would result in a measurable RV semiamplitude ($K \sim 5.1\,\mathrm{m\,s^{-1}}$), but predicts

TSM ($\sim$30a) and ESM ($\sim$3.4) values that indicate atmospheric follow-up would be challenging, compared to the thresholds recommended by Kempton et al. (2018).

A.20. EPIC 245991048

K2-389 is a moderately bright ($V = 12.30$ mag, $K_s = 10.18$ mag) G3V star ($1.08\,R_\odot$, $0.80\,M_\odot$). It was observed in Campaign 12 and is orbited by two sub-Neptunes, which were first noted Paper IV. K2-389 b is a $2.118\,R_\oplus$ planet, orbiting at a distance of 0.076 au, with a period of 8.583566 days and an equilibrium temperature of $\sim$1050 K. Using the Chen & Kipping (2017) mass–radius relation predicts a mass of $\sim$5.7 $M_\oplus$. This would result in a measurable RV semiamplitude ($K \sim 2.0\,\mathrm{m\,s^{-1}}$), but predicts TSM ($\sim$16) and ESM ($\sim$1.3) values that indicate atmospheric follow-up would be challenging, compared to the thresholds recommended by Kempton et al. (2018). K2-389 c is a $2.040\,R_\oplus$ planet, orbiting at a distance of 0.138 au, with a period of 20.851337 days and an equilibrium temperature of $\sim$780 K. Using the Chen & Kipping (2017) mass–radius relation predicts a mass of $\sim$5.3 $M_\oplus$. This would result in a challenging RV semiamplitude ($K \sim 1.4\,\mathrm{m\,s^{-1}}$), and predicts TSM ($\sim$11) and ESM ($\sim$0.6) values that indicate atmospheric follow-up would be challenging, compared to the thresholds recommended by Kempton et al. (2018). The host star has a clean, single-lined FLWO/TRES spectrum, as well as Gemini/NIRI and Palomar/PHARO AO imaging and WIYN/NESSI speckle imaging that show no contaminating stellar companions. The vespa FPP value for planet b is 6.41×10^{-5} using the available contrast curves and the application of the Campaign 12 multiplicity boost. The centroid p-value for planet b of is 0.2457, which is consistent with the source of the transiting signal being on the target star. The vespa FPP value for planet c is 5.75×10^{-5} using the available contrast curves and the application of the Campaign 12 multiplicity boost. The centroid p-value for planet c is 0.2053, which is consistent with the source of the transiting signal being on the target star.

A.21. EPIC 246074314

K2-391 b is a near-Earth-sized ($1.371\,R_\oplus$) planet orbiting a moderately faint (Kep = 12.36 mag, $K_s = 10.71$ mag) G7V star ($0.57\,R_\odot$, $0.76\,M_\odot$), observed in Campaign 12. It was first noted in Paper IV; it orbits the star at a distance of 0.049 au, with a period of 4.622654 days and an equilibrium temperature of $\sim$900 K. The host star has a clean, single-lined FLWO/TRES spectrum, and WIYN/NESSI speckle imaging at 562 nm and 832 nm which show no contaminating stellar companions. The vespa FPP value is 9.87×10^{-5} using the available contrast curves. The centroid p-value is 0.3581, which is consistent with the source of the transiting signal being on the target star. Using the Chen & Kipping (2017) mass–radius relation predicts a mass of $\sim$2.5 $M_\oplus$. This would result in a challenging RV semiamplitude ($K \sim 1.2\,\mathrm{m\,s^{-1}}$), and predicts TSM ($\sim$3.3) and ESM ($\sim$1.1) values that indicate atmospheric follow-up would be challenging, compared to the thresholds recommended by Kempton et al. (2018).

A.22. EPIC 246084398

K2-392 b is a super-Earth ($1.850\,R_\oplus$) planet orbiting a moderately bright ($V = 12.82$ mag, $K_s = 11.24$ mag) G3V star ($1.06\,R_\odot$, $0.84\,M_\odot$), observed in Campaign 12. It was first noted in Paper IV; it orbits the star at a distance of 0.063 au, with a period of 15.399 days and an equilibrium temperature of $\sim$840 K. The host star has a clean, single-lined FLWO/TRES spectrum, and WIYN/NESSI speckle imaging at 562 nm and 832 nm which show no contaminating stellar companions. The vespa FPP value is 2.12×10^{-3}, using the available contrast curves. The centroid p-value is 0.5614, which is consistent with the source of the transiting signal being on the target star. Using the Chen & Kipping (2017) mass–radius relation predicts a mass of $\sim$4.5 $M_\oplus$. This would result in a challenging RV semiamplitude ($K \sim 1.3\,\mathrm{m\,s^{-1}}$), and predicts TSM ($\sim$6.4) and ESM ($\sim$0.4) values that indicate atmospheric follow-up would be challenging, compared to the thresholds recommended by Kempton et al. (2018).

A.23. EPIC 246429049

K2-393 is a bright ($V = 11.84$ mag, $K_s = 10.28$ mag) F9V star ($1.07\,R_\odot$, $0.88\,M_\odot$) that was observed in Campaign 12. It is orbited by a sub-Neptune-sized planet, K2-393 b, which was previously noted by Zink et al. (2019) as EPIC 246429049.01. It is a $2.352\,R_\oplus$ planet, orbiting at a distance of 0.089 au, with a period of 10.413181 days and an equilibrium temperature of $\sim$950 K. The host star has a clean, single-lined FLWO/TRES spectrum, and WIYN/NESSI speckle imaging at 562 nm and 832 nm that show no contaminating stellar companions. The vespa FPP value is 9.00×10^{-3}, using the available contrast curves. The centroid p-value is 0.3512, which is consistent with the source of the transiting signal being on the target star. Using the Chen & Kipping (2017) mass–radius relation predicts a mass of $\sim$6.3 $M_\oplus$. This would result in a measurable RV semiamplitude ($K \sim 2.0\,\mathrm{m\,s^{-1}}$), but predicts TSM ($\sim$16) and ESM ($\sim$1.1) values that indicate atmospheric follow-up would be challenging, compared to the thresholds recommended by Kempton et al. (2018).

A.24. EPIC 246891819

K2-395 is a moderately faint ($V = 14.67$ mag, $K_s = 11.37$ mag) K0V star ($0.78\,R_\odot$, $0.95\,M_\odot$) observed in Campaign 13, that is orbited by two close-in sub-Neptune planets, which were first noted in Paper IV. K2-395 b is a $2.597\,R_\oplus$ planet, orbiting at a distance of 0.055 au, with a period of 4.803352 days and an equilibrium temperature of $\sim$910 K. K2-395 c is a $3.395\,R_\oplus$ planet, orbiting at a distance of 0.080 au, with a period of 8.491282 days and an equilibrium temperature of $\sim$750 K. The host star has a clean, single-lined TripleSpec spectrum, and Keck/NIRC2 AO imaging that shows no contaminating stellar companions. The vespa FPP values of planets b and c are 6.35×10^{-10} and 1.74×10^{-5}, respectively, using the available contrast curve and the Campaign 13 multiplicity boost. The centroid p-values are 0.4413 and 0.4640, respectively, consistent with the source of the transiting signals being on the target star. Using the Chen & Kipping (2017) mass–radius relation predicts masses of $\sim$7.6 $M_\oplus$ and $\sim$11.8 $M_\oplus$ for planets b and c, respectively. These mass estimates for the two planets result in potentially measurable RV semiamplitudes ($K = 3.0\,\mathrm{m\,s^{-1}}$, and $3.8\,\mathrm{m\,s^{-1}}$), but TSM ($\sim$16, $\sim$20) and ESM ($\sim$1.7, $\sim$1.9) values below the thresholds of interest recommended by Kempton et al. (2018).

A.25. EPIC 246953392

K2-396 is a moderately faint ($V = 13.24$ mag, $K_s = 10.81$ mag) G9V star ($0.92 R_\odot$, $0.95 M_\odot$) observed in Campaign 13. It is orbited by an USP super-Earth, K2-396 b, first reported in Paper IV as EPIC 246953392.01, and a longer-period sub-Neptune, K2-396 c(EPIC 246953392.02), reported here for the first time. K2-396 b orbits the star at a distance of 0.015 au, with an USP of 0.673862 days. With a high equilibrium temperature of ~1990 K, it is the second hottest of the validated planets in this analysis. K2-396 c orbits the star at a distance of 0.168 au, with a period of 25.760509 days, and an equilibrium temperature of ~590 K. The host star has a clean, single-lined FLWO/TRES spectrum, and WIYN/NESSI speckle imaging at both 562 nm and 832 nm that show no contaminating stellar companions. The `vespa` FPP values of planets b and c are 4.16×10^{-4} and 1.07×10^{-5} using the available contrast curves and Campaign 13 multiplicity boost. The `centroid` p-values are 0.4124 and 0.3421, which is consistent with the sources of the transiting signals being on the target star. Using the Chen & Kipping (2017) mass–radius relation predicts masses of ~$3.4 M_\oplus$ and ~$10.0 M_\oplus$ for planets b and c, respectively. This would result in measurable RV semiamplitudes ($K \sim 2.6$ m s^{-1} and ~2.2 m s^{-1}), but predicts TSM (~18, ~15) and ESM (~2.3, ~0.7) values that indicate atmospheric follow-up would be challenging, compared to the thresholds recommended by Kempton et al. (2018).

A.26. EPIC 247383003

K2-397 is a bright ($V = 11.83$ mag, $K_s = 9.95$ mag) G7V star ($0.97 R_\odot$, $0.94 M_\odot$) that was observed in Campaign 13. It is orbited by a sub-Neptune-sized planet that was first noted in Paper IV. K2-397 b is a $2.417 R_\oplus$ planet, orbiting at a distance of 0.045 au, with a period of 3.572326 days and an equilibrium temperature of ~1210 K. The host star has a clean, single-lined FLWO/TRES spectrum, and Keck/NIRC2 AO imaging and WIYN/NESSI speckle imaging at 562 nm and 832 nm that show no contaminating stellar companions. The `vespa` FPP value is 0.00799, using the available contrast curves. The `centroid` p-value is 0.5226, which is consistent with the source of the transiting signal being on the target star. Using the Chen & Kipping (2017) mass–radius relation predicts a mass of ~$6.7 M_\oplus$. This would result in a measurable RV semiamplitude ($K \sim 2.9$ m s^{-1}), but predicts TSM (~28) and ESM (~3.0) values that indicate atmospheric follow-up would be challenging, compared to the thresholds recommended by Kempton et al. (2018).

A.27. EPIC 248518307

K2-400 is a faint ($V = 15.13$ mag, $K_s = 10.41$ mag) M3V star ($0.38 R_\odot$, $0.37 M_\odot$) that was observed in Campaign 14. It is orbited by an Earth-sized planet that was first noted in Paper IV as EPIC 248518307.01. K2-400 b is a $1.163 R_\oplus$ planet, orbiting at a distance of 0.035 au, with a period of 3.865053 days and an equilibrium temperature of ~570 K. The host star has a clean, single-lined Hale/TripleSpec spectrum, and WIYN/NESSI speckle imaging at 562 nm and 832 nm that shows no contaminating stellar companions. The `vespa` FPP value is 1.35×10^{-3}, using the available contrast curve. The `centroid` p-value is 0.5332, which is consistent with the source of the transiting signal being on the target star. Using the Chen & Kipping (2017) mass–radius relation predicts a mass of ~1.7

$M_\oplus$. This would result in a challenging RV semiamplitude ($K \sim 1.3$ m s^{-1}), and predicts TSM (~4.0) and ESM (~1.0) values that indicate atmospheric follow-up would be challenging, compared to the thresholds recommended by Kempton et al. (2018).
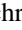
A.28. EPIC 248527514

K2-401 is a moderately faint ($V = 13.72$ mag, $K_s = 11.11$ mag) K5V star ($0.68 R_\odot$, $0.87 M_\odot$) that was observed in Campaign 14. It is orbited by a sub-Neptune that was first noted in Paper IV. K2-401 b is a $2.262 R_\oplus$ planet, orbiting at a distance of 0.064 au, with a period of 6.293099 days and an equilibrium temperature of ~660 K. The host star has a clean, single-lined TripleSpec spectrum, and WIYN/NESSI speckle imaging at both 562 nm and 832 nm that show no contaminating stellar companions. We note that Dressing et al. (2019) found that K2-401 lies above the main sequence and may therefore be an unresolved eclipsing binary; however, the clean spectrum and high-resolution imaging, as well as the low Gaia RUWE value of 1.09, all point to a single host star. The `vespa` FPP value is 3.78×10^{-3}, using the available contrast curves. The `centroid` p-value is 0.3051, which is consistent with the source of the transiting signal being on the target star. Using the Chen & Kipping (2017) mass–radius relation predicts a mass of ~$5.8 M_\oplus$. This would result in a measurable RV semiamplitude ($K \sim 2.2$ m s^{-1}), but predicts TSM (~15) and ESM (~1.1) values that indicate atmospheric follow-up would be challenging, compared to the thresholds recommended by Kempton et al. (2018).

A.29. EPIC 248621597

K2-402 b is a sub-Neptune ($2.678 R_\oplus$) planet orbiting a moderately faint ($V = 13.03$ mag, $K_s = 11.38$ mag) G2V star ($1.28 R_\odot$, $0.94 M_\odot$), observed in Campaign 14. It was first noted in Paper IV; it orbits the star at a distance of 0.128 au, with a period of 17.274740 days and an equilibrium temperature of ~870 K. The host star has a clean, single-lined FLWO/TRES spectrum, and WIYN/NESSI speckle imaging at 562 nm and 832 nm which show no contaminating stellar companions. The `vespa` FPP value is 2.07×10^{-4} using the available contrast curves. The `centroid` p-value is 0.4934, which is consistent with the source of the transiting signal being on the target star. Using the Chen & Kipping (2017) mass–radius relation predicts a mass of ~$7.8 M_\oplus$. This would result in a measurable RV semiamplitude ($K \sim 2.0$ m s^{-1}), and predicts TSM (~7.4) and ESM (~0.5) values that indicate atmospheric follow-up would be challenging, compared to the thresholds recommended by Kempton et al. (2018).

A.30. EPIC 248861279

K2-404 b is a sub-Neptune ($2.530 R_\oplus$) planet orbiting a moderately faint ($V = 14.56$ mag, $K_s = 10.75$ mag) early M dwarf (M1V, $0.55 R_\odot$, $0.55 M_\odot$), observed in Campaign 14. It was first noted in Paper IV; it orbits the star at a distance of 0.089 au, with a period of 13.115365 days. With a relatively low equilibrium temperature of ~450 K, it is one of the coolest validated planets in this analysis. The host star has a clean, single-lined TripleSpec spectrum, and both Keck/NIRC2 AO imaging and WIYN/NESSI speckle imaging which show no contaminating stellar companions. The `vespa` FPP value is 8.62×10^{-4} using the available contrast curves. The

centroid p-value is 0.4292, which is consistent with the source of the transiting signal being on the target star. Using the Chen & Kipping ([2017]) mass–radius relation predicts a mass of $\sim 7.3\,M_\oplus$. This would result in a measurable RV semiamplitude ($K \sim 3.0\,\mathrm{m\,s^{-1}}$), and predicts TSM ($\sim 20$) and ESM ($\sim 0.8$) values that indicate atmospheric follow-up would be challenging, compared to the thresholds recommended by Kempton et al. ([2018]).

A.31. EPIC 249403651

K2-407 is a bright ($V = 11.97$ mag, $K_s = 10.21$ mag) early G4V star ($0.93\,R_\odot$, $0.88\,M_\odot$) that was observed in Campaign 15 and is orbited by two small, close-in planets. The two candidates were first noted in Paper IV; K2-407 b is a super-Earth ($1.283\,R_\oplus$) planet, orbiting at a distance of 0.054 au, with a period of 4.941907 days and an equilibrium temperature of ~ 1105 K, and K2-407 c is a super-Earth ($1.360\,R_\oplus$) planet, orbiting at a distance of 0.083 au, with a period of 9.224530 days and an equilibrium temperature of ~ 900 K. The host star has a clean, single-lined FLWO/TRES spectrum, and Gemini/DSSI speckle imaging at 692 nm and 880 nm which show no contaminating stellar companions. The vespa FPP values for planets b and c are 3.23×10^{-5} and 1.03×10^{-4}, respectively, incorporating the available contrast curves and Campaign 15 multiplicity boost. The centroid p-value for planet b is 0.0826, which is marginally consistent with the source of the transiting signal being on the target star. The centroid p-value for planet c is 0.0372, which is marginally inconsistent with the source of the transiting signal being on the target star given our threshold of 0.05. However, visual inspection of the centroid plots shows no systematic offset, with the transit cadences that fall outside the significance contours spread around a large fraction of the exterior of the contours, and the presence of multiple signals in the same light curve gives credence to their planetary nature. We consider planet c to be validated, but note that additional ground-based time-series photometry, while challenging given the shallow depths of these transits, would provide additional assurance. From the Chen & Kipping ([2017]) mass–radius relation, we estimate masses of $\sim 2.1\,M_\oplus$ and $\sim 2.5\,M_\oplus$ for planets b and c, respectively, leading to very low RV semiamplitude estimates and atmospheric spectroscopy metrics.

A.32. EPIC 249924395

K2-409 b is a sub-Neptune ($2.482\,R_\oplus$) planet orbiting a moderately faint ($V = 12.76$ mag, $K_s = 11.04$ mag) G4V star ($1.23\,R_\odot$, $0.89\,M_\odot$), observed in Campaign 15. It was first noted in Paper IV; it orbits the star at a distance of 0.029 au, with a period of 1.908084 days and a very high equilibrium temperature of ~ 1800 K. The host star has a clean, single-lined FLWO/TRES spectrum, and Gemini/DSSI speckle imaging which shows no contaminating stellar companions. Ground-based time-series photometry of K2-409 during a predicted transit with the 0.6 m University of Louisville Manner Telescope found no detectable event on the target star (consistent with the shallow K2 detection) and no nearby binaries eclipsing at the predicted transit time within $\sim 120''$ down to $\Delta\mathrm{mag} = 6.5$, eliminating many blended eclipsing binary scenarios. The vespa FPP value is 3.92×10^{-5} using the available contrast curves. The centroid p-value is 0.4360, which is consistent with the source

of the transiting signal being on the target star. Using the Chen & Kipping ([2017]) mass–radius relation predicts a mass of $\sim 6.7\,M_\oplus$. This would result in a measurable RV semiamplitude ($K \sim 3.8\,\mathrm{m\,s^{-1}}$) but, given the relative faintness of the target, predicts TSM (~ 18) and ESM (~ 2.2) values that indicate atmospheric follow-up would be challenging, compared to the thresholds recommended by Kempton et al. ([2018]).

ORCID iDs

Jessie L. Christiansen ● https://orcid.org/0000-0002-8035-4778
Sakhee Bhure ● https://orcid.org/0000-0002-6673-8206
Jon K. Zink ● https://orcid.org/0000-0003-1848-2063
Kevin K. Hardegree-Ullman ● https://orcid.org/0000-0003-3702-0382
Christina Hedges ● https://orcid.org/0000-0002-3385-8391
Timothy D. Morton ● https://orcid.org/0000-0002-8537-5711
Allyson Bieryla ● https://orcid.org/0000-0001-6637-5401
David R. Ciardi ● https://orcid.org/0000-0002-5741-3047
William D. Cochran ● https://orcid.org/0000-0001-9662-3496
Courtney D. Dressing ● https://orcid.org/0000-0001-8189-0233
Mark E. Everett ● https://orcid.org/0000-0002-0885-7215
Howard Isaacson ● https://orcid.org/0000-0002-0531-1073
John H. Livingston ● https://orcid.org/0000-0002-4881-3620
Carl Ziegler ● https://orcid.org/0000-0002-0619-7639
Michael L. Calkins ● https://orcid.org/0000-0002-2830-5661
Gilbert A. Esquerdo ● https://orcid.org/0000-0002-9789-5474
David W. Latham ● https://orcid.org/0000-0001-9911-7388
Michael Endl ● https://orcid.org/0000-0002-7714-6310
Benjamin J. Fulton ● https://orcid.org/0000-0003-3504-5316
Lea A. Hirsch ● https://orcid.org/0000-0001-8058-7443
Andrew W. Howard ● https://orcid.org/0000-0001-8638-0320
Lauren M. Weiss ● https://orcid.org/0000-0002-3725-3058
Fei Dai ● https://orcid.org/0000-0002-8958-0683
Teruyuki Hirano ● https://orcid.org/0000-0003-3618-7535
Motohide Tamura ● https://orcid.org/0000-0002-6510-0681
Joshua E. Schlieder ● https://orcid.org/0000-0001-5347-7062
Thomas Barclay ● https://orcid.org/0000-0001-7139-2724
Ian J. M. Crossfield ● https://orcid.org/0000-0002-1835-1891
Emily A. Gilbert ● https://orcid.org/0000-0002-0388-8004
Steven Giacalone ● https://orcid.org/0000-0002-8965-3969
Erik A. Petigura ● https://orcid.org/0000-0003-0967-2893

References

Agol, E., & Deck, K. 2016, ApJ, 818, 177
Aigrain, S., Parviainen, H., & Pope, B. J. S. 2016, MNRAS, 459, 2408
Barclay, T., Quintana, E. V., Adams, F. C., et al. 2015, ApJ, 809, 7
Barros, S. C. C., Demangeon, O., & Deleuil, M. 2016, A&A, 594, A100
Broeg, C., Fortier, A., Ehrenreich, D., et al. 2013, in EPJ Web of Conf. 47 (Les Ules: EDP Sciences), 03005
Bryson, S. T., Jenkins, J. M., Gilliland, R. L., et al. 2013, PASP, 125, 889
Buchhave, L. A., Bakos, G. Á., Hartman, J. D., et al. 2010, ApJ, 720, 1118
Cabrera, J., Barros, S. C. C., Armstrong, D., et al. 2017, A&A, 606, A75
Castro González, A., Díez Alonso, E., Menéndez Blanco, J., et al. 2020, MNRAS, 499, 5416
Chen, J., & Kipping, D. 2017, ApJ, 834, 17
Christiansen, J. L., Crossfield, I. J. M., Barentsen, G., et al. 2018, AJ, 155, 57
Claret, A., & Bloemen, S. 2011, A&A, 529, A75
Crossfield, I. J. M., Ciardi, D. R., Petigura, E. A., et al. 2016, ApJS, 226, 7

Cushing, M. C., Vacca, W. D., & Rayner, J. T. 2004, PASP, 116, 362
Dai, F., Howard, A. W., Batalha, N. M., et al. 2021, AJ, 162, 62
Dattilo, A., Vanderburg, A., Shallue, C. J., et al. 2019, AJ, 157, 169
Dawson, R. I., Chiang, E., & Lee, E. J. 2015, MNRAS, 453, 1471
de Leon, J. P., Livingston, J., Endl, M., et al. 2021, MNRAS, 508, 195
Dekany, R., Roberts, J., Burruss, R., et al. 2013, ApJ, 776, 130
Demangeon, O. D. S., Zapatero Osorio, M. R., Alibert, Y., et al. 2021, A&A, 653, A41
Díaz, R. F., Almenara, J. M., Santerne, A., et al. 2014, MNRAS, 441, 983
Dressing, C. D., Vanderburg, A., Schlieder, J. E., et al. 2017, AJ, 154, 207
Dressing, C. D., Hardegree-Ullman, K., Schlieder, J. E., et al. 2019, AJ, 158, 87
Foreman-Mackey, D., Barentsen, G., & Barclay, T. 2019, dfm/exoplanet: exoplanet v0.1.5, Zenodo doi: 10.5281/zenodo.2587222
Foreman-Mackey, D., Hogg, D. W., Lang, D., & Goodman, J. 2013, PASP, 125, 306
Fulton, B. J., Petigura, E. A., Howard, A. W., et al. 2017, AJ, 154, 109
Gaia Collaboration, Brown, A. G. A., Vallenari, A., et al. 2021, A&A, 649, A1
Gillon, M., Triaud, A. H. M. J., Demory, B.-O., et al. 2017, Natur, 542, 456
Goodman, J., & Weare, J. 2010, Commun. Appl. Math. Comput., 5, 65
Haas, M. R., Batalha, N. M., Bryson, S. T., et al. 2010, ApJL, 713, L115
Hardegree-Ullman, K. K., Zink, J. K., Christiansen, J. L., et al. 2020, ApJS, 247, 28
Hardegree-Ullman, K. K., Christiansen, J. L., Ciardi, D. R., et al. 2021, AJ, 161, 219
Hayward, T. L., Brandl, B., Pirger, B., et al. 2001, PASP, 113, 105
Hedges, C. 2021, RNAAS, 5, 262
Heller, R., Hippke, M., & Rodenbeck, K. 2019, A&A, 627, A66
Howard, A. W., Johnson, J. A., Marcy, G. W., et al. 2010, ApJ, 721, 1467
Howell, S. B., Everett, M. E., Sherry, W., Horch, E., & Ciardi, D. R. 2011, AJ, 142, 19
Howell, S. B., Sobeck, C., Haas, M., et al. 2014, PASP, 126, 398
Huber, D., Bryson, S. T., Haas, M. R., et al. 2016, ApJS, 224, 2
Kempton, E. M. R., Bean, J. L., Louie, D. R., et al. 2018, PASP, 130, 114401
Kostov, V. B., Mullally, S. E., Quintana, E. V., et al. 2019, AJ, 157, 124
Kreidberg, L. 2015, PASP, 127, 1161
Kruse, E., Agol, E., Luger, R., & Foreman-Mackey, D. 2019, ApJS, 244, 11
Lee, E. J., & Chiang, E. 2015, ApJ, 811, 41
Lissauer, J. J., Marcy, G. W., Rowe, J. F., et al. 2012, ApJ, 750, 112

Livingston, J. H., Crossfield, I. J. M., Petigura, E. A., et al. 2018, AJ, 156, 277
Luger, R., Agol, E., Kruse, E., et al. 2016, AJ, 152, 100
Luger, R., Kruse, E., Foreman-Mackey, D., Agol, E., & Saunders, N. 2018, AJ, 156, 99
Mayo, A. W., Vanderburg, A., Latham, D. W., et al. 2018, AJ, 155, 136
Montet, B. T., Morton, T. D., Foreman-Mackey, D., et al. 2015, ApJ, 809, 25
Morton, T. D., Bryson, S. T., Coughlin, J. L., et al. 2016, ApJ, 822, 86
Nowak, G., Palle, E., Gandolfi, D., et al. 2017, AJ, 153, 131
Petigura, E. A., Howard, A. W., & Marcy, G. W. 2013, PNAS, 110, 19273
Petigura, E. A., Crossfield, I. J. M., Isaacson, H., et al. 2018, AJ, 155, 21
Pope, B. J. S., Parviainen, H., & Aigrain, S. 2016, MNRAS, 461, 3399
Quintana, E. V., Barclay, T., Raymond, S. N., et al. 2014, Sci, 344, 277
Ricker, G. R., Winn, J. N., Vanderspek, R., et al. 2015, JATIS, 1, 014003
Rizzuto, A. C., Vanderburg, A., Mann, A. W., et al. 2018, AJ, 156, 195
Rodríguez Martínez, R., Ballard, S., Mayo, A., et al. 2019, AJ, 158, 135
Salvatier, J., Wiecki, T., & Fonnesbeck, C. 2015, arXiv:1507.08050
Saunders, N., Luger, R., & Barnes, R. 2019, AJ, 157, 197
Schlieder, J. E., Gonzales, E. J., Ciardi, D. R., et al. 2021, FrASS, 8, 63
Scott, N. J., Howell, S. B., Horch, E. P., & Everett, M. E. 2018, PASP, 130, 054502
Sinukoff, E., Howard, A. W., Petigura, E. A., et al. 2016, ApJ, 827, 78
Thompson, S. E., Coughlin, J. L., Hoffman, K., et al. 2018, ApJS, 235, 38
Tokovinin, A. 2018, PASP, 130, 035002
Torres, G., Fressin, F., Batalha, N. M., et al. 2011, ApJ, 727, 24
Tull, R. G., MacQueen, P. J., Sneden, C., & Lambert, D. L. 1995, PASP, 107, 251
Vanderburg, A., & Johnson, J. A. 2014, PASP, 126, 948
Vanderburg, A., Latham, D. W., Buchhave, L. A., et al. 2016, ApJS, 222, 14
Vissapragada, S., Jontof-Hutter, D., Shporer, A., et al. 2020, AJ, 159, 108
Volk, K., & Malhotra, R. 2020, AJ, 160, 98
Winters, J. G., Medina, A. A., Irwin, J. M., et al. 2019, AJ, 158, 152
Zink, J. K., Hardegree-Ullman, K. K., Christiansen, J. L., et al. 2020a, AJ, 159, 154
Zink, J. K., Hardegree-Ullman, K. K., Christiansen, J. L., et al. 2020b, AJ, 160, 94
Zink, J. K., Hardegree-Ullman, K. K., Christiansen, J. L., et al. 2019, RNAAS, 3, 43
Zink, J. K., Hardegree-Ullman, K. K., Christiansen, J. L., et al. 2021, AJ, 162, 259